Copyright Warning & Restrictions

The copyright law of the United States (Title 17, United States Code) governs the making of photocopies or other reproductions of copyrighted material.

Under certain conditions specified in the law, libraries and archives are authorized to furnish a photocopy or other reproduction. One of these specified conditions is that the photocopy or reproduction is not to be "used for any purpose other than private study, scholarship, or research." If a, user makes a request for, or later uses, a photocopy or reproduction for purposes in excess of "fair use" that user may be liable for copyright infringement,

This institution reserves the right to refuse to accept a copying order if, in its judgment, fulfillment of the order would involve violation of copyright law.

Please Note: The author retains the copyright while the New Jersey Institute of Technology reserves the right to distribute this thesis or dissertation

Printing note: If you do not wish to print this page, then select "Pages from: first page # to: last page #" on the print dialog screen

ABSTRACT

THE EFFECT OF NANOCLAYS ON THE PROPERTIES OF ASPIRIN MODIFIED ENTERIC POLYMER PREPARED BY HOT-MELT MIXING

by
Nonjaros Chomcharn

Melt mixing in batch equipment or continuous extruders is a technique that recently gained the attention of the pharmaceutical industry. This dissertation investigates two controlled-release drug delivery systems. The first system, namely the enteric matrix, contains an active pharmaceutical ingredient (API) and plasticizer in an enteric polymer while in the second system a nanoclay is added to the enteric matrix, to produce a polymer nanocomposite. The first system employs hot-melt mixing to prepare a modified enteric matrix, as a delayed-release dosage form. Different concentrations of aspirin (ASP) ranging from 10 – 30% w/w are melt-mixed with a plasticized Eudragit® L100-55 in a batch mixer for 5 minutes at 100°C which is above the plasticized polymer's glass transition temperature (T_g) and below the ASP's melting point. Processing ASP with Eudragit® L100-55 under these conditions does not promote hydrolysis of ASP. X-ray diffraction spectra obtained at room temperature reveal that the aspirin is present in a crystalline state. However, at elevated temperatures the dissolved aspirin displays a plasticizing effect by reducing the glass transition temperature (T_g) and lowering the viscosity of the polymer in proportion to its increasing concentration. The amount of ASP loading has no significant impact on the dissolution profiles. The samples meet USP delayed-release requirements and the API release mechanism is non-Fickian.

In the second system, polymer nanocomposites are produced by incorporating a nanoclay, hydrotalcite (HT). The morphology of HT in the nanocomposites, originally a

multilayer structure, is significantly changed with increasing ASP loading. ASP shows affinity to the Al and Mg ions of the HT layers, resulting in a change of the HT morphology in the composites. The polymer chain of Eudragit® L100-55 is also expected to be intercalated into HT layers but to a lesser extent. At low concentrations of ASP (5% and 10%w/w), ASP molecules penetrate the HT's interlayers causing an expansion of its basal spacing (intercalation). The delamination (exfoliation) of HT in which the multilayer structure collapses and separates to individual platelets occurs at high ASP loading (30%w/w) with the formation of ASP metal salt. The dispersion of HT reduces the nanocomposites' permeability and increases tortuosity as evidence by the significantly prolonged release of ASP with its release rate greatly depending on the HT morphology.

In the third system, 10%-30%w/w of CAF was processed with plasticized Eudragit® L100-55 under identical conditions as for the first system. CAF in crystalline form is observed in the API/polymer blends after cooling. The release rate of CAF (CAF/Eudragit® L100-55) in pH 7.4 medium is slightly faster than ASP (ASP/Eudragit® L100-55) due its higher aqueous solubility. The fourth system is classified as polymer nanocomposites with a cationic API and an anionic nanoclay. MMT is present in an agglomerated phase in all nanocomposites. The CAF release in the pH 7.4 medium from CAF/MMT/Eudragit® L100-55 is slightly slower compared to CAF/Eudragit® L100-55. Therefore, the agglomeration of MMT does not significantly retard the release rate of CAF from the CAF/MMT/Eudragit® L100-55. The lack of change of MMT morphology could be due to the low affinity of CAF to MMT since CAF is a weak base.

THE EFFECT OF NANOCLAYS ON THE PROPERTIES OF ASPIRIN MODIFIED ENTERIC POLYMER PREPARED BY HOT-MELT MIXING

by
Nonjaros Chomcharn

A Dissertation
Submitted to the Faculty of
New Jersey Institute of Technology
in Partial Fulfillment of the Requirements for the Degree of
Doctor of Philosophy in Chemical Engineering

Department of Chemical, Biological and Pharmaceutical Engineering

May 2013

.

APPROVAL PAGE

THE EFFECT OF NANOCLAYS ON THE PROPERTIES OF ASPIRIN MODIFIED ENTERIC POLYMER PREPARED BY HOT-MELT MIXING

Nonjaros Chomcharn

Dr. Marino Xanthos, Dissertation Advisor — Date
Professor of Chemical, Biological and Pharmaceutical Engineering, NJIT

Dr. Costas C. Gogos, Committee Member — Date
Distinguished Research Professor of Chemical, Biological and Pharmaceutical Engineering, NJIT

Dr. Piero M. Armenante, Committee Member — Date
Distinguished Professor of Chemical, Biological and Pharmaceutical Engineering, NJIT

Dr. Laurent Simon, Committee Member — Date
Associate Professor of Chemical, Biological and Pharmaceutical Engineering, NJIT

Dr. Craig McKelvey, Committee Member — Date
Senior Investigator of Global Solubilization Center of Excellence Leader
Formulation Development, Merck & Co., Inc.

BIOGRAPHICAL SKETCH

Author: Nonjaros Chomcharn

Degree: Doctor of Philosophy

Date: May 2013

Undergraduate and Graduate Education:

- Doctor of Philosophy in Chemical Engineering,
  New Jersey Institute of Technology, Newark, NJ, 2013
- Master of Science in Pharmaceutical Engineering,
  New Jersey Institute of Technology, Newark, NJ, 2009
- Bachelor of Science in Pharmaceutical Science,
  Chulalongkorn University, Bangkok, Thailand, 2003

Major: Chemical Engineering

Publications:

Nonjaros Chomcharn and Marino Xanthos, "Properties of aspirin modified enteric polymer prepared by hot-melt mixing", International Journal of Pharmaceutics, in press.

Presentations:

Nonjaros Chomcharn and Marino Xanthos, "Controlled release of polymer matrix containing aspirin and nanoclays prepared by hot-melt mixing", Proceedings of the International Society for Pharmaceutical Engineering (ISPE) Annual Meeting 2012, San Francisco, CA, November 2012.

Nonjaros Chomcharn and Marino Xanthos, "Applications of nanoclays in controlled release of API-Polymer matrix prepared by hot-melt mixing", Proceedings of the American Institute of Chemical Engineers (AIChE) Annual Meeting 2012, Pittsburgh, PA, October 2012.

Nonjaros Chomcharn and Marino Xanthos, “Controlled release of polymer matrix containing aspirin and nanoclays”, Proceedings of the Society of Plastics Engineers (SPE) ANTEC 2012, Orlando, FL, April 2012.

Nonjaros Chomcharn and Marino Xanthos, “Study of controlled release of aspirin and caffeine modified by anionic and cationic clays”, Proceedings of the American Association of Pharmaceutical Scientists (AAPS) Annual Meeting 2011, Washington, DC, October 2011.

To my parents for their love and greatest support since 2:45 pm on Monday, July 7, 1980.

ACKNOWLEDGMENT

I owe my deepest gratitude to my advisor, Professor Marino Xanthos, who has been mentoring me since 2010. I consider “mentoring” is the best word describing the relationship between Dr. Xanthos and me since not only academic perspective he taught me but also life beyond the classroom. I could never be me today without the support from Dr. Xanthos. Thank you for having me as your students; it is an honor to work with you.

I am also indebted to Professor Costas C. Gogos, one the committee members. Every time Dr.Gogos saw me, he always stopped by to talk and encouraged me for my research. I have learned so many aspects from Dr. Gogos and the credit of this work is shared to Dr. Gogos as well.

This dissertation would not been possible without the valuable feedbacks from committee members: Dr. Piero M. Armenante, Dr. Laurent Simon and Dr. Craig McKelvey (Merck & Co.).

I would like express my gratitude to NJIT Residence Life especially Mrs. Sanjeannetta Worley, my supervisor, for the scholarship I am awarded since 2009.

I would like to thank you current and former Polymer Processing Institute (PPI) staffs for their advice and technical support for equipment/instrument: Dr. Herman Suwardie, Dr. Nikolaos Ioannidis, Dr. Huiju Liu and Mr. Michael Zawisa.

Two persons who guided me when I started my research are Dr. Jin Uk Ha and Dr. Graciela Terife. I really appreciate their time and support.

Lastly, I wish to thank my friends at NJIT: Dr. Suarwee Snitsiriwat, Dr. Patchara Suttiwan, Dr. Min Yang, Dr. Itsaso Murua Auzmendi, Jia Fan, Meng Li and Na Yao.

TABLE OF CONTENTS

TABLE OF CONTENTS
(Continued)

Chapter **Page**

TABLE OF CONTENTS
(Continued)

TABLE OF CONTENTS
(Continued)

Chapter **Page**

LIST OF TABLES

LIST OF FIGURES

LIST OF FIGURES
(Continued)

LIST OF FIGURES
(Continued)

Figure **Page**

LIST OF FIGURES
(Continued)

LIST OF ACRONYMS/ABBREVIATIONS

API	Active Pharmaceutical Ingredient
ASP	Aspirin
ASP/Eudragit® L100-55	Eudragit® L100-55 mixed with triethyl citrate and aspirin
ASP/HT/Eudragit® L100-55	Eudragit® L100-55 mixed with triethyl citrate, hydrotalcite and aspirin
ASP/MMT/Eudragit® L100-55	Eudragit® L100-55 mixed with triethyl citrate, montmorillonite and aspirin
CAF	Caffeine
CAF/Eudragit® L100-55	Eudragit® L100-55 mixed with triethyl citrate and caffeine
CAF/MMT/Eudragit® L100-55	Eudragit® L100-55 mixed with triethyl citrate, montmorillonite and caffeine
DSC	Differential scanning calorimetry
EDX	Energy dispersive X-ray analysis
FTIR	Fourier transform infrared spectroscopy
HPLC	High liquid performance chromatography
HT	Hydrotalcite
MMT	Montmorillonite
SEM	Scanning electron microscopy
TEC	Triethyl citrate
TEM	Transmission electron microscopy
T_g	Glass transition temperature

TGA	Thermogravimetric analysis
WVT	Water vapor transmission
WVTR	Water vapor transmission rate
XRD	Wide-angle X-ray diffraction

CHAPTER 1

INTRODUCTION

Polymer processing parameters are continuously studied in the plastics and related industries since polymers are the most common materials used in daily life applications; for instance, food containers, clothes, mobile phone cases, automotive tires and even airplane's wings. Polymers are extensively employed due to a wide range of properties obtained by structure modification. Polymers are also of extreme importance in the pharmaceutical industry as excipients in different dosage forms which are, but not limited to tablets, capsules, creams and solutions. The use of polymers in film-coating processes demands a better understanding of their properties compared to plain tablet manufacturing. For such applications, this is similar to the requirements of the plastics industry where comprehensive polymer properties (melt viscosity, molecular weight, glass transition temperature, modulus, etc.) are fully evaluated before processing.

In 2000, Abbott Laboratories adopted one polymer processing technique namely, hot-melt extrusion (HME) to prepare an amorphous solid dispersion, Kaletra® which is a combination product containing lopinavir and ritonavir. Since the Active Pharmaceutical Ingredient (API) ritonavir exhibits low aqueous solubility, utilizing the SOLIQS Meltrex® formulation technology, an amorphous solid dispersion of ritonavir in a matrix of Kollidon® VA 64 and surfactants was designed to prepare a matrix with enhanced API solubility (Breitenbach, 2006). HME can solve several problems in pharmaceutical formulations such as enhancing solubility of poorly water-soluble APIs, modifying the

release of APIs and masking their unpleasant taste. It has been almost 20 years since the very first commercial product was manufactured by HME. However, very few products have been commercialized. One reason is that HME requires a high level of polymer processing and polymer property understanding which is developed by limited groups of researchers in the pharmaceutical industry. HME in pharmaceutics becomes more complicated due to the fact that a number of APIs are sensitive to elevated temperatures, resulting in more constrained process conditions (lower temperature and shorter residence time). Therefore, the fundamentals of polymer processing for pharmaceutical applications should be extensively addressed in order to achieve the full benefits of HME.

The use of HME or hot melt mixing (HMM) to prepare a controlled-release polymer matrix is the focus of this dissertation. HMM is also a term involving materials mixing at elevated temperatures in a batch mixer. The APIs used in the present work have not been previously processed, to our knowledge by HMM or HME. In Chapter 2 of the dissertation, a review of available important literature on HME and modification of APIs for controlled release is discussed. Chapter 3 summarizes experimental methods that are used in this work. Two systems are investigated in Chapters 4 and 5: an enteric matrix and polymer nanocomposites based on anionic API.

The first system (Chapter 4) investigates the feasibility of enteric matrix manufacturing prepared by HMM. The selected API is aspirin (ASP) since it is normally available as enteric-coated tablets. ASP's initial degradation temperature is 150°C and becomes even lower in the presence of moisture. Therefore, ASP is an appropriate candidate API for incorporation in an enteric matrix preparation. ASP is processed with an enteric polymer, Eudragit® L100-55 under predetermined conditions using the batch

mixer. Dissolution analysis using mathematical models are also employed in this Chapter. In Chapter 5, the second system which is an extension of work from the first system is reported. The enteric matrix properties are examined when an additional excipient, nanoclays, is added. In general, polymer permeability can be reduced by the dispersed platelets of nanoclays. The reduced permeability could lead to a modified-release or to be more specific, a prolonged-release profile. Hydrotalcite (HT) nanoclay is chosen since it is used as API itself and as a carrier for controlled-release systems. Therefore, HT would be very compatible with drug delivery systems.

Chapter 7 and 8 describe the initial experiments involving polymer nanocomposites in a cationic system. Caffeine (CAF) and montmorillonite (MMT) are used as API and nanoclays, respectively while the polymer base is still Eudragit® L100-55. The purpose of the cationic system is to compare the nanoclay's morphology and dissolution profile with anionic system. Hence, materials characterization is not fully conducted as anionic system. The developed data are summarized along with future work in Chapter 8.

CHAPTER 2

LITERATURE REVIEW

2.1 Solid Dispersions and Limit of Miscibility/Solubility

It is estimated that about 40% of the new chemical entities (NCE) being discovered are poorly water-soluble (Lipinski, 2001). Solubility, especially in aqueous systems is an important physicochemical property of API's. To enter the human body's blood circulation, the API has to be dissolved and absorbed through the gastrointestinal tract. Improving API's solubility is a critical key to promote API dissolution and therefore, its therapeutic efficacy. Solid dispersions are known as an effective method enhancing dissolution of hydrophobic API's

Solid dispersions are defined as a group of solid products consisting of at least two different components, generally a hydrophilic matrix and a hydrophobic drug. (Dhirendra et al., 2009) The matrix can be either crystalline or amorphous. The drug can be dispersed molecularly, as amorphous particles (clusters) or as crystalline particles. Different types of solid dispersions based on their molecular arrangement are presented in Table 2.1.

Table 2.1 Types of Solid Dispersions (Dhirendra et al., 2009)

Solid dispersion types		Matrix *	API **	Remarks	No. phases
I	Eutectics	C	C	The first type of solid dispersion prepared	2
II	Amorphous precipitations in crystalline matrix	C	A	Rarely encountered	2
III	Solid solutions				
	Continuous solid solutions	C	M	Miscible at all compositions	1
	Discontinuous solid solutions	C	M	Partially miscible, 2 phases even though drug is molecularly dispersed	2
	Substitutional solid solutions	C	M	Molecular diameter of drug (solute) differs less than 15% from the matrix (solvent) diameter. In that case the drug and matrix are substitutional. Can be continuous or discontinuous. When discontinuous: 2 phases even though drug is molecularly dispersed.	1 or 2
	Interstitial solid solutions	C	M	Drug (solute) molecular diameter less than 59% of matrix (solvent) diameter. Usually limited miscibility, discontinuous.	2
IV	Glass suspension	A	C	Particle size of dispersed phase dependent on cooling/evaporation rate. Obtained after crystallization of drug in amorphous matrix.	2
V	Glass suspension	A	A	Particle size of dispersed phase dependent on cooling/evaporation rate; many solid dispersions are of this type.	2
VI	Glass solution	A	M	Requires miscibility OR solid solubility, complex formation or upon fast cooling OR evaporation during preparation.	1

*A: matrix in an amorphous state, C: matrix in a crystalline state

**: A: drug dispersed as amorphous clusters in the matrix, C: drug dispersed as crystalline particles in the matrix, M: drug molecularly dispersed throughout the matrix

The ultimate solubility enhancement can be achieved when the API is molecularly dispersed in the polymer chosen as a carrier, which can be obtained in two solid dispersion types: type III (solid solution) and type VI (glass solution). It has been suggested that a thermodynamically stable formulation is obtained when the drug is completely dissolved below its saturation solubility in the polymer, resulting in solid solution and glass solution (Kolter et al., 2010). When the drug concentration exceeds the saturation level, the whole system is only kinetically controlled since the API may crystallize or precipitate out of the polymer during storage. Glass suspensions in which both API and polymer are in amorphous phase are also kinetically controlled because the API is dispersed in an amorphous polymer and may crystallize whereas the polymer matrix containing crystalline API is quite stable. Therefore, the solubility limit of API in the selected polymer is a strong factor determining solid dispersion type and its stability (Kolter et al., 2010).

Hildebrand and Scott established fundamental solubility parameters which can be used as a tool predicting the miscibility of the components of the formulations (Hansen 2007). The Hildebrand solubility parameter is defined as the square root of cohesive energy density:

$$\delta = (\frac{E}{V})^{1/2} \tag{2.1}$$

Where V is the molar volume of the pure solvent and E is its (measurable) energy of vaporization. The total E of a liquid consists of several individual parts. These arise from

(atomic) dispersion forces, (molecular) permanent dipole-permanent dipole forces, and (molecular) hydrogen bonding (electron exchange) (Hansen, 2007).

Hansen has proposed the calculation of solubility parameters based on the total cohesion energy (Hansen, 2007). The total cohesion energy, E, must be the sum of the individual energies (dispersion, polar, H-bonding) that make it up.

$$E = E_D + E_p + E_H \tag{2.2}$$

Dividing this by the molar volume gives the square of the total (or Hildebrand) solubility parameter as the sum of the squares of the Hansen D, P and H components.

$$E/V = E_D/V + E_p/V + E_H/V \tag{2.3}$$

$$\delta^2 = \delta^2_D + \delta^2_p + \delta^2_H \tag{2.4}$$

The solubility parameters can also be determined by other experimental methods, for instance, inverse gas chromatography and calorimetry (Egawa et al., 1992; Rey-Mermet et al., 1991, Huu-Phuoc et al., 1987). Regardless of methods used to measure solubility parameters, predictions of solubility are similar. If the difference in solubility parameters between polymer and plasticizer, or polymer and API is <7.0 $MPa^{1/2}$, the two components are likely to be miscible and form a solid glassy solution; if >10 $MPa^{1/2}$, they are likely to be immiscible, and the formation of a solid glassy solution is unlikely (Greenhalgh et al., 1999; Forster et al., 2001). It is understood that these parameters are

particularly dependent on properties such as water activity, polydispersity, molecular weight, temperature, etc. Nonetheless, the listed values may be used as a screening tool for solubility estimation.

2.2 Hot-melt Extrusion (HME)

Hot-melt extrusion (HME) has gained interest in the pharmaceutical industry due to its potential to resolve the issue of limited solubility of many nominally water-soluble APIs. HME is a process where API and polymer are melted/ softened, followed by kneading under elevated temperatures and pressures and then forcing through an orifice by screw action (Kolter et al., 2010). Since the process involves the melting of different thermoplastic materials with API in the barrel of the extruder, HME can deliver a polymer matrix with different properties for various applications. Wide range advantages of HME are listed in Table 2.2.

Table 2.2 Advantages of HME (Kolter et al., 2010)

Problem	Solution by HME
Poor bioavailability due to poor API solubility	Use of HME to prepare solid solution/ dispersion
Poor API stability during processing caused by hydrolysis	Use of HME as alternative to wet agglomeration (no hydrolytic stress)
Unreliable sustained release action	Use of HME to prepare sustained release dosage forms (single/ multiple units)
Poor stability or tolerability of API in the stomach	Use of HME to prepare enteric release dosage forms
Poor taste of API	Use of HME to prepare taste-masked dosage forms
Manufacturing of films	Use of HME to prepare oral strips or dermal patches

The effect of three process parameters associated with HME, i.e., mixing temperatures, screw rotational speeds, and residence times on indomethacin (INM)-Eudragit® EPO extrudate was investigated (Huiju et al., 2010). From the system's dynamic dissolution behavior, increasing set temperature and screw speed enhanced dissolution rate of indomethacin in the batch mixer and in the co-rotating twin-screw extrusion studies. It was concluded that the dissolution of APIs in a polymeric excipient melt is a laminar forced convective diffusion process, and that laminar distributive mixing can significantly enhance the dissolution process. In addition, it was concluded that the kneading blocks may be the most important equipment design parameter during co-rotating twin-screw extrusion controlling the full dissolution of the drug in the polymer melt. The release of INM from the Eudragit® EPO extrudate in pH 1.2 medium was significantly improved compared to pristine INM due to the amorphous state of INM in the extrudate samples.

The downstream operations can modify the properties of the extrudate prepared by HMM and HME. The impact of foaming on dissolution of Soluplus® containing 30%w/w INM, which was obtained by HMM was studied (Terife et al., 2012). INM found in amorphous form in unfoamed HMM samples had faster release rate in pH 7.4 medium compared to pure INM. With the foaming process using supercritical CO_2 as the physical blowing agent (PBA) at 100°C and 9.65 MPa the release of INM from foamed samples was even faster. The improved release rate suggested by the authors was caused by enhanced solvent absorption rate through the foamed disks due to higher surface area as well as very short diffusional lengths through each of the walls of the cells.

2.3 HME Using Enteric Polymers (Eudragit® L100-55)

Enhancing solubility is not the only advantage of HME; HME can also prepare sustained release and enteric dosage forms by dispersing the API in a suitable polymer matrix. Enteric properties of tablets/ pellets are conventionally obtained by film-coating with a pH-dependent polymer such as the copolymer of methacrylic acid and ethyl acrylate available as Kollicoat® MAE 100P (BASF) or Eudragit® L100-55 (Evonik). HME can provide an enteric matrix with substantially lower manufacturing time and cost since fewer unit operations and no solvents are required.

Andrews et al., prepared hot-melt extruded enteric tablets using a single-screw Randcastle Microtruder extruder (model RCP-0750) fitted with an 8 mm die (Andrews et al., 2008). 5-aminosalicylic acid was processed with Eudragit® L100-55 and the temperatures of the four heating zones were maintained at 95, 105, 110 and 115°C. Triethyl citrate (TEC) and citric acid were employed as liquid and solid plasticizers, respectively. The effects of gelling agent, polyvinylpyrrolidone (PVP K30) and polyacrylic acid (Carbopol 971P NF) were also investigated. HME tablets showed excellent gastro-resistance. Drug release from HME tablets was dependent on the concentration of TEC, citric acid, PVP K30 and Carbopol 971P NF. The incorporation of the gelling agent significantly reduced the erosion of the matrix and drug release rate at pH 6.8, resulting in slower release rate. However, the gastro-resistant property was lost due to the formation of channels within the tablets.

Bruce et al. reported that hot-melt extruded guaifenesin tablets showed crystal growth on the surface of the extrudate (Bruce et al., 2007). Eudragit® L100-55, TEC and guaifenesin were extruded at temperatures ranging from 60 to 115°C. The limit of

guaifenesin solubility in Eudragit® L100-55 was found to be 25%w/w. Hydrophilic polymeric additives including PVP K25, polycarbophil, PEG 3350, poloxamer 188 were added as crystal growth inhibitors; the extent of crystal growth was reduced for all additives. The addition of hydrophilic additives was expected to alter the dissolution of Eudragit® L100-55 from only erosion to swelling/erosion. However, the formulations containing 10%w/w hydrophilic additive did not swell during dissolution and therefore has no effect on the API release compared to formulations without hydrophilic additives.

Hughey et al. developed dissolution-enhanced solid dispersions of Roche Research Compound A (ROA) using a HAAKE Minilab II Microcompounder equipped with 5/14-mm conical screws (Hughey et al., 2010). The compound classified as BCS class II was chemically unstable at elevated temperatures and acidic pH values. Eudragit® L100-55 dispersions prepared by HME at 140°C required the use of micronized ROA and reduced residence times in order to render ROA amorphous. The dissolution of ROA was significantly increased in neutral pH compared to crystalline ROA.

The preparation of theophylline (water soluble API) enteric matrix systems with different plasticizers including TEC, acetyltributyl citrate (ATBC), citric acid monohydrate, polyethylene glycol 8000 and methyl paraben was examined by Schilling and coworkers (Schilling et al., 2010). The investigated polymers were cellulosic polymers (Aqoat® LF and HF) and acrylic polymers (Eudragit® S100, L100 and L100-55). A mini extruder equipped with two co-rotating screws was used. Cellulosic polymers demonstrated lower melt viscosities during extrusion compared to polymethacrylate polymers due their lower molecular weight and lower T_g. A cellulosic extrudate plasticized with TEC exhibited a higher burst effect and faster drug diffusion rates in the

acid stage than the extrudate prepared with polymethacrylates with more than 20% drug released after 2 hours. The use of a less soluble plasticizer such as ATBC was suggested to reduce drug release. Cellulosic polymers are more hydrophilic than polymethacrylates enhancing faster water penetration and more extensive hydration. This could lead to increased matrix permeability and drug diffusion rates even in the acid stage. In the buffer phase, the polymethacrylate pellets exhibited a more sustained-release profile; this behavior was attributed to the larger molecular weight and slower hydration and erosion characteristics.

2.4 Aspirin and Caffeine

Aspirin (ASP) is widely used for multiple indications depending on the dosage regimen. High-dose ASP (325 – 500 mg) is prescribed for pain relief whilst low-dose ASP (60 – 81 mg) is intended to prevent cardiovascular events (Angiolillo et al., 2008). Both strengths are currently available as enteric-coated tablets due to their common side effect, i.e., gastric irritation. Literature studies of HME with ASP are very limited since ASP has relatively high water solubility. ASP is sensitive to moisture and gradually decomposes in aqueous solution through hydrolysis to salicylic acid and acetic acid (Florey, 1979; Lund, 1994). Therefore, dry granulation is commonly used to prepare ASP tablets to avoid exposure to moisture (Erum et al., 2011; Troy, 2006).

The hydrolysis of ASP can occur due to the incompatibility with other excipients. El-Banna et al. reported that when ASP was incorporated in physical mixture with polyvinylpyrrolidone (PVC), it exhibited enhanced decomposition rate under accelerated

storage conditions (El-Banna et at., 1978). The authors suggested that the acceleration rate may be due to the hygroscopic character of the PVP.

The interactions between the amino groups of cationic methylmethacrylate polymers, generally used as enteric coating materials and ASP should be considered. Note that ASP has undergone hydrolysis when processing with Eudragit® RL and RS100, a cationic polymer containing quaternary ammonium groups (Petereit et al., 1999).

Caffeine (CAF) is available in tablets ranging from 65-200 mg. It is used as stimulant for central nervous system from the group of xanthine derivatives and can be used to impart a desired level of increased alertness (McLellan et al., 2005). The sustained-release of CAF from a polymeric tablet matrix using poly(ethylene oxide) was developed by Tan and coworkers (Tan et al., 2006). The CAF-poly(ethylene oxide) tablet exhibited less burst release in simulated intestinal fluid compared to other polymers. McGinity and Lach studied the adsorption of CAF to MMT prepared by ion-exchange (McGinity and Lach, 1976). CAF was bounded moderately to MMT and the 1:5 complex of CAF and MMT released 42% of the drug into the dissolution 0.1 N HCl medium.

2.5 Clays in the Pharmaceutical Industry

Clays are used as APIs for a wide range of indications. For oral administration, their remedies are but not limited to antacids, gastrointestinal protectors, antidiarrhoeaics, osmotic oral laxatives, homeostatics, direct emetics, antianemics and mineral supplements. They may also be used topically as antiseptics, disinfectants, dermatological protectors, anti-inflammatories, local anesthetics, keratolytic reducers and decongestive eye drops (Carretero and Pozo, 2010).

Clays are also employed as pharmaceutical excipients playing several roles according to their structural and physico-chemical properties. Carretero and Pozo (2009) summarized the clay properties and their use as follows:

(1) High adsorption capacity and specific surface area for use as carriers and releasers of API and flavor correctors

(2) Propensity to take up water and decompose in acid media, for use as disintegrants and desiccants

(3) Unctuousness for use as lubricants

(4) Thixotropic and colloidal properties for use as emulsifying, thickening and anticaking agents

(5) Slight alkaline reaction (pH) and plasticity for use as diluents and binders

(6) Solubility in water, giving solutions with osmotic pressure similar to that of corporal liquids, for use as isotonic agents

(7) Opaqueness and color for use as opacifiers and pigments

2.6 Hydrotalcite and Montmorillonite

Hydrotalcite (HT) is one of several layered-double hydroxide (LDH) materials designating synthetic or natural layer/lamellar hydroxides with two kinds of metallic cations in the main layers and interlayer domains containing anionic species (Roy et al., 2001). HT is the LDH consisting of Mg as divalent and Al as trivalent cations. The positive charge of the main layers counterbalanced by the negative charge of interlayered anions is the key in maintaining the LDH structure; therefore, LDHs are classified as anionic clays due to the presence of anionic species kept between the cationic main

layers. One major characteristic of LDHs is their ability to exchange interlayered anions with guest anions if the latter have higher affinity to the cationic main layers. This phenomenon is called intercalation; cationic clays such as montmorillonite also possess similar ion exchange characteristics but with opposite charge. Having this property, HT and other anionic clays in the LDH family are finding applications in the removal of acid dyes, HPO_4^{2-}, CN^-, CrO_4^{2-}, AsO_4^{3-}, etc. from waste water as well as in the neutralization and thermal stabilization of halogen-containing polymers (Mitaya, 1983).

In another application taking advantage of the HT's ion exchange property and its multilayer structure, several researchers investigated API/nanoclay hybrids by employing LDH as a carrier intercalated by API; in these systems the API release profile and API solubility were modified. Different methods have been suggested to prepare LDH and API/ nanoclay hybrids (Costantino et al., 2008). They can be summarized as follows (Arco et al., 2007; Roy et al., 2001):

(1) Co-precipitation – it is based on the slow addition of a mix solution of divalent and trivalent metal salts in adequate proportion into a reactor containing water or other appropriate solvents. To prepare API/ nanoclay hybrids, the API can be added in the reactor and become the intercalated species. An optional solution is added in the reactor in order to maintain the pH at a selected value leading to the co-precipitation.

(2) Calcination and reconstruction – by heating the LDH in the furnace at approximately 500°C, surface water is first lost, then the interlamellar water molecules and finally, roughly in the 200-350°C range, water corresponding to the dehydroxylation of the main layers, leading to the collapse of the

structure. Carbon dioxide may also be removed if carbonate anions were initially present. The entire process is named calcination and the consequent product is called calcined LDH. The reconstruction can take place in a solution containing new ions, such as dissolved API to be intercalated under controlled conditions.

(3) Ion exchange – exchange in LDH depends mainly on the electrostatic interaction between the positively charged hydroxylate sheets and the exchange anions, and to a lesser extent, on the free energy involved in the changes of hydration. Exchange is therefore favored for in-going anions with a higher charge density. The rate limiting step for this method is the diffusion of the in-going anions within the interlayer which could also be prevented by a too small basal spacing. Hence, the selected in-going anions/ API must possess high charge density and adequate molecular size.

Carja et al. have intercalated ASP to LDH by two methods (Carja et al., 2007). The first method is based on direct co-precipitation synthesis of ASP-HT nano-hybrids in aqueous solution of Mg and Al salts. An ethanol-aqueous solution of ASP was added drop-wise at a constant pH of 8.5. The second method is based on the reconstruction method in which calcined LDH was added to a water-ethanol ASP solution. Both methods successfully delivered ASP-intercalated LDH but the sample obtained by co-precipitation appeared to be more crystalline than the sample prepared by reconstruction according to XRD results. The asymmetric stretching of interlayer carbonate (COO^-) of ASP was found in FTIR spectra, further indicating the intercalation of ASP in a salt form.

Hong and Weng-gong prepared drug-containing LDH (MgAlZn-Asp-LDH) by the co-precipitation method with ASP (Hong and Weng-gong, 2010). Magnesium (II) was partially replaced by zinc (II) in the hydrotalcite-like layers, and ASP was dispersed into the interlayer region. Due to the increase of HT basal spacing to 1.32 nm, the authors suggested the conformation of intercalated ASP as vertically-arranged monolayer ASP. ASP was present as ionized form (COO^-) and this carboxylate group was bound to the Zn^{2+} through oxygen atoms. In dissolution under pH 7.4 medium, it showed biphasic release pattern, with an early burst release of ASP (48.3% of ASP released after the first 1.2 hours) followed by a relatively slower release (46.8% of ASP released after 51 hours). The initial burst release may be attributed to the ASP being weakly adsorbed on the outer surface of LDH; the slow release of the rest of ASP can be due to the strong interaction between aspirin molecules and the lamella host.

Ambrogi et al. synthesized HT in chloride form by co-precipitation method and performed intercalation reaction with ibuprofen (Ambrogi et al., 2001). The reaction took place in a Gallen Kamp orbital incubator type INR2000 at 60°C for 3 days. The ibuprofen-intercalated HT was successfully produced and this was confirmed by the increase of the interlayer spacing from 0.78 nm to 2.17 nm. The authors suggested that the ibuprofen ions were accommodated in the interlayer as a monolayer. The drug release profile in simulated intestinal fluid showed that 60% of the API was released after 20 minutes and 100% after 100 minutes. The rapid release during the first 20 minutes could be the free ibuprofen while the latter sustained-release was due to intercalated ibuprofen in the HT interlayer. The phosphate buffer generated a mixture of two anions, $H_2PO_4^-$ and

HPO_4^{2-} which both are able to intercalate into HT. Therefore, the intercalated ibuprofen was gradually replaced by phosphate anions and dissolved in the buffer.

Mefenamic and meclofenamic have been intercalated into HT by three different methods: (1) coprecipitation (2) reconstruction (3) ion exchange from HT in the chloride form (Arco et al., 2007). Intercalation has been achieved by all three methods and the gallery height was expanded to approximately 2.20 nm in most cases. Elemental analysis determined the drug loading which ranged from 42% to 54% for mefenamic and 39% to 54% for meclofenamic. According to FTIR spectra, mefenamic was in intercalated anionic forms in which the carboxylate groups were oriented towards the brucite-type layers to enhance the electrostatic interaction. The use of LDH enhanced the apparent solubility of mefenamic in mefenamic-LHD hybrid at three pH values tested, 1.2, 4.5 and 6.8. The mefenamic-LDH hybrid had a slower release rate compared to pure API and a physical mixture with LDH at all pH values tested (Arco et al., 2008).

Montmorillonite (MMT) is one of the most widely used species in the smectite group of clays (Carretero and Pozo, 2009). Various grades of MMT were studied for use as disintegrants, binders and lubricants for solid dosage forms (Wai et al., 1966) while it is commonly used in suspensions as thickening agent/suspending agents in liquid dosage forms. The use of MMT to modify the release of API is reported.

The adsorption of various APIs to MMT was investigated by McGinity and Lach (McGinity and Lach, 1976). The studied APIs were cationic APIs (chlorpheniramine maleate, amphetamine sulfate, propoxyphene HCl), anionic APIs (sodium salicylate and sulfanilamide), amphoteric APIs or nonionic APIs (theophylline and CAF). Dissolution tests showed that cationic APIs and nonionic APIs bind strongly to MMT. The quantity

of API bound by one unit of MMT varied considerably. Anionic APIs, on the contrary, were bound weakly. The authors suggested the binding mechanism of cationic APIs to MMT as a two-step process: a cationic-exchange reaction followed by strong surface chemisorption.

Dapsone-intercalated MMT was successfully prepared by ion exchange at room temperature (Fan, 2011). MMT-Na^+ (Closite® Na^+) was employed as a carrier for the API. The loading of intercalated dapsone in MMT was found to be approximately 10%. Two phases of dapsone release profile were obtained in the dissolution test under pH 7.4 medium. In the first 30 minutes, fast release rate was observed due to the dapsone adhered/coated on the MMT's surface. After that, the release was slowed down indicating the release of dapsone from the MMT interspacing.

MMT was used to modify the release rate of acetaminophen-poly(ethylene oxide) solid dispersion prepared by HMM (Yang et al., 2010). Two types of MMT (Cloisite® 15A and 30B) were added to the binary mixture of API and polymer at the ratio of 10%w/w. The presence of either nanoclay dramatically accelerates the drug's recrystallization rate and slows down the drug's releasing rate. The drop of the releasing rate is mainly due to the decrease of wettability, as supported by the contact angle data. Data analysis of the dissolution results suggests that the addition of nanoclays changes the drug's release mechanism from erosion dominant to diffusion dominant.

2.7 Polymer Nanocomposites

Polymer nanocomposites are one of the breakthrough materials used in plastic-based components such as automotive, electronics, biomedical devices and safety equipment (Jeon and Baek, 2010; Paul and Robeson, 2008). In general, the addition of fillers to the polymer base affects numerous properties, for example, stiffness, toughness, flexural modulus, permeability and heat resistance (Xanthos, 2010). Nanocomposites are the particle-filled composites in which at least one dimension of the dispersed particles is in the nanometer range (Alexandre and Dubois, 2000).

Toyota researchers were the first group that successfully developed clay-polymer composite materials such as a nylon 6-clay hybrids using in situ polymerization (Kojima et al., 1993; Usuki et al., 1993). The nylon polymer chain was intercalated into montmorillonite, resulting in increased basal spacing. The authors suggested that the ammonium cations ($-NH_3^+$) in nylon 6 interact with the anions in montmorillonite. The new composites of nylon 6 and silicate layers of montmorillonite developed were found superior in strength, modulus and heat distortion to pure nylon 6. This achievement has led to an extension of research in clay-based nanocomposites due to significant mechanical property advantages (Paul and Robeson, 2008; Fornes, 2002).

Nylon 6-clay hybrids can also be prepared by direct melt compounding of polymers with clays. Cho and Paul prepared Nylon 6-organoclay nanocomposites using a conventional single and a twin screw extruder (Cho and Paul, 2001). To achieve a better interaction with the organic polymers, the cations (typically sodium) present in montmorillonite to balance the net negative charge of aluminum/magnesium silicate layers were exchanged with long chain C15 – C18 molecules with a cationic group, such

as quaternary ammonium salts to produce an organoclay. Then, the organoclay was melt compounded with nylon 6. The single screw extrusion could not deliver full exfoliation because the amount of shear is insufficient and the residence time is too short. Consequently, the final product is a mixture of exfoliated and unchanged clay. A high degree of exfoliation was obtained by twin screw extrusion. The authors reported continuous improvement in strength and modulus relatively to the neat nylon 6 matrix as more organoclay was added. It was suggested by Durmus and coworkers that the high degree of exfoliation of nylon 6/clay composites is due to the strong interactions, specifically hydrogen bonds, between the polar polymer chains and the organically modified clay (organoclay) layers (Durmus et al., 2007).

Generally, the clay structure can be present in the polymer nanocomposites in three phases: agglomeration, intercalation, and exfoliation as shown in Figure 2.1 (Paul and Robeson, 2008). The agglomeration state is the original structure in which the entire structure is constituted by the stacking of layers, forming aggregates of tactoids. The XRD of the polymer nanocomposites would show unchanged spectra compared to pure clays whilst large tactoids are depicted in Transmission Electron Microscopy (TEM). In the intercalation state the basal spacing of the clay is expanded by the guest species which can be ions or polymer chains. The XRD peak of clays in the nanocomposites is shifted to lower angle, indicating an increased basal spacing between the main layers. For exfoliation, the stacks of layers are completely separated and dispersed individually as a sheet/ platelet in the nanocomposites. Therefore, no XRD spectra are shown since there is no crystal structure formed by layers of clays anymore. The final structure of clays in the nanocomposites depends on the interfacial interactions between polymer chain,

compatibilizer (if needed), and clay platelets. To maximize a particular property by adding selected nanoclays, several researchers proposed that an exfoliated state of the nanoclays should be achieved due to the substantially high surface area of clay platelets dispersed in the polymer matrix (Paul and Robeson, 2008; Marchant and Jayaraman, 2002). Figure 2.2 is the schematic of a polymer-clay nanocompoistes with completely exfoliated (molecularly dispersed) clay sheets within the polymer matrix material (Fisher, 2003).

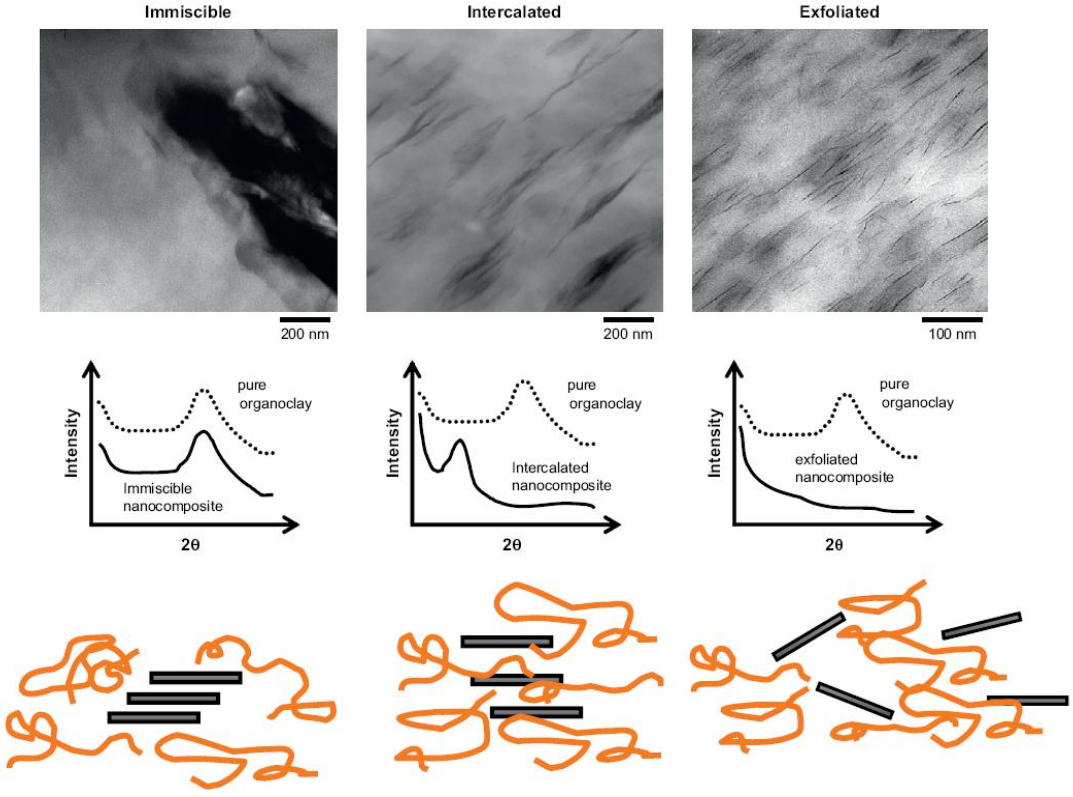

Figure 2.1 Illustration of different state of nanoclays in polymers and the corresponding morphology, XRD spectra and TEM images (Paul and Robeson, 2008).

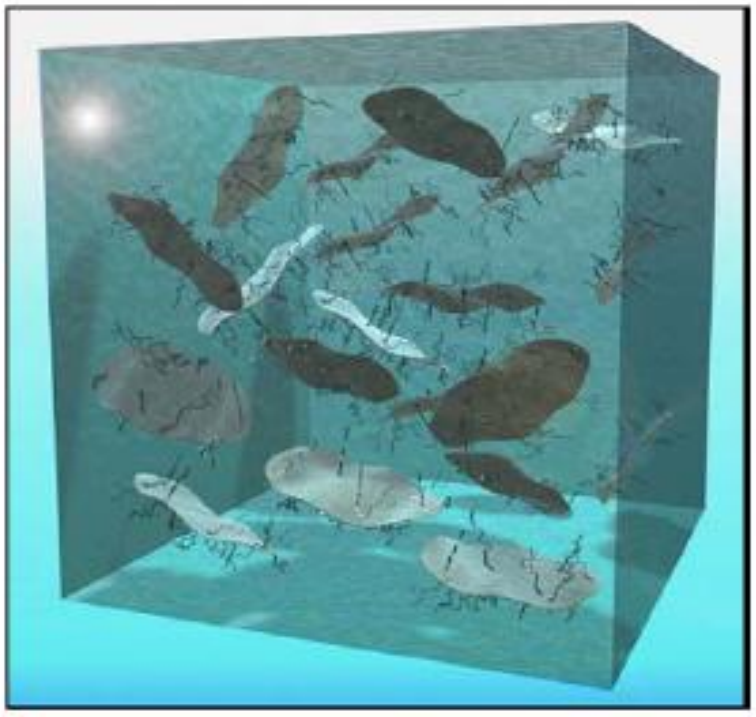

Figure 2.2 Illustration of polymer-clay nanocomposites with completely exfoliated clay sheets (Fischer, 2003).

In the polymer nanocomposites field, HT was employed as filler in several polymers to modify their original properties for particular applications, for example, poly(vinyl chloride), polypropylene, poly(methyl methacrylate) (Ardanuy et al., 2010; Manzi-Nshuti et al., 2009; Huang and Wang, 2009; Bao et al., 2006).

Nogueira et al. synthesized poly(methyl methacrylate) (PMMA)/ LDH nanocomposites by in situ polymerization (Nogueira et al., 2012; Nogueira et al., 2011). The LDH was synthesized by co-precipitation varying the divalent/ trivalent compositions. Since the LDH's surface is hydrophilic, it was intercalated by two different anions, dodecyl sulfate and lauric acid to enhance hydrophobicity and facilitate dispersion (exfoliation) in the polymer matrix. The advantages of organic modified LDH

are (1) an appropriate organic species reduces the hydrophilicity of the clay layers and promote compatibility between the layer and the polymer matrix; (2) larger basal spacing hinders electrostatic interactions between the layers and makes it easier to achieve exfoliation of the layered crystal into single layers. The anion intercalation is important because HT presents a small interlayer distance which prevents the intercalation. The exfoliation phase of HT was confirmed by XRD results. Thermal degradation temperature of nanocomposites was higher than PMMA. The authors explained this enhancement as follows: (1) the LDH layers have a much higher thermal resistance than organic PMMA molecules, (2) the excellent barrier property of homogeneously dispersed LDH single layers prevented the migration of some small volatile molecules from the inner matrix to the surface. Other properties of nanocomposites were also improved. Elastic modulus tested below the glass transition temperature was increased compared to PMMA. The glass transition temperature was also increased due to the decrease in the chain mobility; the maximum T_g increase was found to be 17°C. This is supported by Marangoni and coworkers who claim that chemical bonding, weak as hydrogen bonding or strong as covalent bonding is increasing between the filler and polymer chain when intercalated or exfoliated clays are present in the polymer matrix (Marangoni et al., 2008). Furthermore, the exfoliation of LDH in poly(methyl methacrylate) prepared by in situ polymerization results in enhanced thermal stability caused by the prevention of out-diffusion of the volatile gas from the thermally decomposing composites. Since exfoliated LDH sheets are well-dispersed, they act as a gas barrier, reducing permeability of the volatile gas (Nogueira et al., 2011; Wang, 2006).

PMMA nanocomposites were also investigated by Manzi-Nshuti and coworkers (Manzi-Nshuti et al., 2009). PMMA is an optically clear amorphous thermoplastic used as a substitute for inorganic glass due to higher impact strength and undergoes ductile rather than brittle fracture. The authors incorporated undecenoate-intercalated LDH in PMMA by in situ polymerization and obtained exfoliated HT in PMMA. T_g was not significantly increased while the molecular weight determined by viscosity measurement indicated the increase of molecular weight of the PMMA nanocomposites. The fire-resistant property was improved since a reduction up to 36% in peak heat release rate (PHRR) was found in all PMMA nanocomposites.

With adequate polymer processing, the desired exfoliation phase can be obtained; shear intensity and residence time must be optimized to achieve a high degree of exfoliation during extrusion (Dennis et al., 2001). In addition, the incorporation of compatibilizers might be necessary to facilitate the exfoliation.

2.8 Polymer Nanocomposites in Pharmaceutical Applications

There are very limited studies on polymer nanocomposites in oral solid dosage forms. Ha and Xanthos investigated the release characteristics of diclofenac from two carriers (Ha and Xanthos, 2011). The first carrier system was obtained by intercalating diclofenac into HT to produce a nanoclay hybrid. Then, the nanoclay hybrid was dispersed in an acrylic polymer by melt mixing. The polymer used was Eudragit® E100 (soluble in pH < 5.0) and S100 (soluble in pH > 7.0). The intercalation was performed by adding calcined LDH in the hydroalcoholic solution containing diclofenac. The solution pH was adjusted to 6.0 and the reaction was carried out at 60°C for 2 days in a closed system. The API was

successfully intercalated in its amorphous state in the clay. As a result, the API showed increased apparent solubility vs. its crystalline form in simulated gastric fluid (pH 1.2). The API release was very rapid in pH 1.2 due to the dissolution of HT in acidic medium. The dissolution profile of nanoclay hybrid in simulated intestinal fluid (pH 7.4) showed a slower release rate since HT did not dissolve in the neutral pH medium and the intercalated diclofenac anions had to be ion exchanged with the phosphate ions of the medium in order to diffuse out from the clay interlayer. The nanoclay hybrid was hot-melt mixed with Eudragit® in the batch mixer at a given temperature to prepare nanoclay hybrid/ Eudragit® composites. The dissolution results in pH 7.4 showed slower release than polymer systems that contained only API as a result of an additional diffusional step due to the presence of nanoplatelets.

Some researchers have reported applications in the biomedical field. Chung et al. investigated the release of dexamethasone acetate (DexA) from polyurethane organosilicate nanocomposites using APIs of different size and polarity (Chung et al., 2013). MMT (Closite Na^+) was modified with organic modifiers before processing with polyurethane and API. The nanocomposites containing DexA, a neutral molecule, did not dissociate into ions, resulting in unchanged MMT morphology. The API release was performed in a sink volume of 50 mL phosphate buffer saline (pH 7.4) placed in a 37°C incubator. The presence of clay not only decreased the permeability of the nanocomposites due to the impermeable silicate but also the attractive interactions between MMT-DexA and PU-DexA.

CHAPTER 3

EXPERIMENTAL

3.1 Materials

3.1.1 Active Pharmaceutical Ingredients

3.1.1.1 Anionic API: Acetyl salicylic Acid/ aspirin (ASP). ASP was purchased from Sigma-Aldrich (St. Louis, USA). It has a melting point of 135°C and its pKa is 3.5 (25°C). At 25°C, 3 mg of ASP are soluble in 1 ml water while 10 mg of ASP are soluble in 1 ml water at 37°C (Sigma-Aldrich). Its structure is shown in Figure 3.1. The solubility of ASP in aqueous buffer solutions with pH 1.2 and 7.2 at 25°C is 0.061 mg/ml (Rasool et al., 2010) and 2.7 mg/ml (Cayman Chemical, 2012), respectively. ASP is considered as anionic API due to the presence of carboxylic group. Therefore, ASP can be intercalated into the interlayer of anionic clays. The hydrolysis caused by the breaking of esterified functional groups can result in the formation of salicylic acid and acetic acid. Reported density is 1.40 g/cm^3 (Budavari et al., 1996).

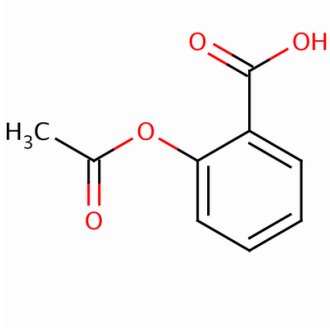

Figure 3.1 Chemical structure of ASP.

3.1.1.2 Cationic API: Caffeine (CAF). CAF is purchased from Sigma-Aldrich Co. (St. Louis, USA) and is a white powder with a molecular weight of 194.2 mg/mol. It melts in the range of 234-236.5°C (Sigma-Aldrich). CAF's solubility in water (25°C) is 16.7 mg/ml, 200 mg/ml at 80°C, and 666 mg/ml in boiling water (Sigma-Aldrich). The reported pKa is 14.0 (Lund, 1994) and density is 1.23 g/cm^3 (Budavari et al., 1996). CAF can form salts with acids and is decomposed by strong bases (Clarke and Moffatt, 1986). CAF is considered as a cationic API due to the presence of ternary amine groups.

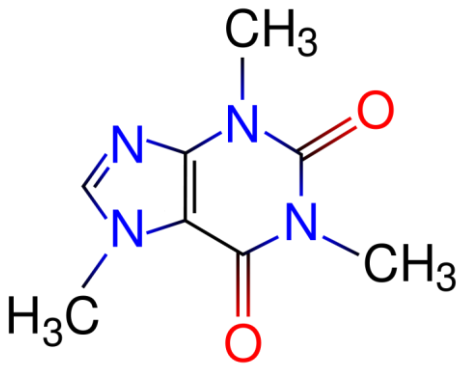

Figure 3.2 Chemical structure of CAF.

3.1.2 Polymers

An anionic copolymer based on methacrylic acid and ethyl acrylate (Eudragit® L100-55) shown in Figure 3.3 was kindly provided by Evonik (Piscataway, NJ). Eudragit® L100-55, with T_g of 110°C is classified as a pH-dependent polymer and is water soluble at pH above 5.5 as per supplier's literature (Evonik Industries, 2011). The reported density is 1.21 g/cm^3 (Yap et al., 2008). The weight average molar mass is approximately 320,000 g/mol.

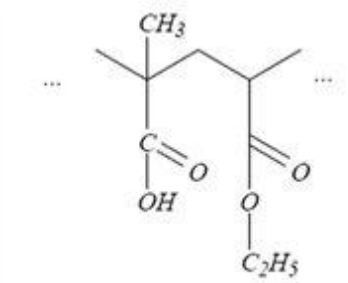

Figure 3.3 Chemical structure of Eudragit® L100-55.

3.1.3 Plasticizers

The triethyl citrate (TEC) plasticizer shown in Figure 3.4 was purchased from Sigma-Aldrich (St. Louis, USA). TEC is a colorless and odorless oily liquid with molecular weight 276.2 g/mol and density of 1.137 g/mL. Its reported melting point is -55°C and its boiling points are 127°C at 1 mm Hg and 294°C at 760 mm Hg. The solubility in water is 62 g/L (Budavari et al., 1996).

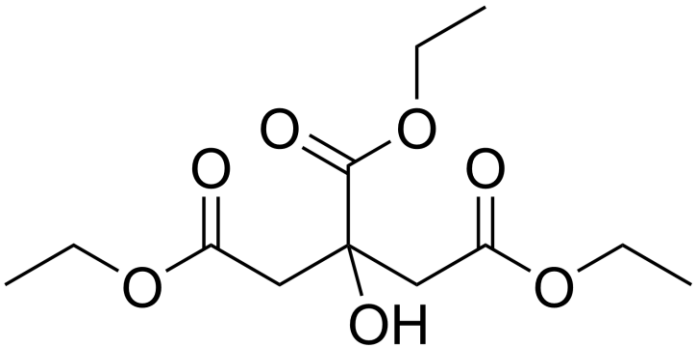

Figure 3.4 Chemical structure of TEC.

3.1.4 Nanoclays

3.1.4.1 Anionic nanoclays: Hydrotalcite. Hydrotalcite (HT) (Pural® HT 63) is kindly donated from SASOL Germany GmbH (Hamburg, Germany). It is a layered double hydroxide containing carbonate anions between the layers to neutralize the positive charge of divalent (Magnesium) and trivalent (Aluminum) metallic cations forming brucite-like layers on the surface (Rives, 2001). The manufacturer's reported weight ratio of Al_2O_3: MgO is 38:62 and the d-spacing between each layer due to the presence of carbonate anions and water is 7.7 Å. The chemical formula is $Mg_4Al_2(OH)_{12}CO_3 \cdot nH_2O$ and the anionic exchange capacity is approximately 3.4 meq/g (Toraishi et al., 2002).

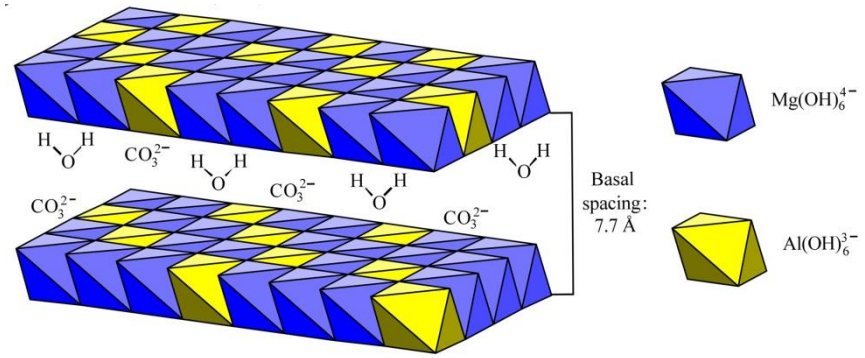

Figure 3.5 Molecular structure of Pural® HT 63. (adapted from Pural® product information: http://www.sasoltechdata.com/tds/PURAL-MG.pdf)

3.1.4.2 Cationic nanoclays: Montmorillonite. Cloisite® Na^+ was obtained from Southern Clay Products Inc. It is a hydrated aluminum silicate with sodium ions kept in the interlayer as the predominant exchange cation (Cationic Exchange Capacity = 92.6 meq/100g). The chemical formula is $Na_{0.33}Al_2Si_4O_{10}(OH)_2.nH_2O$ with a d-spacing value of 11.7 Å.

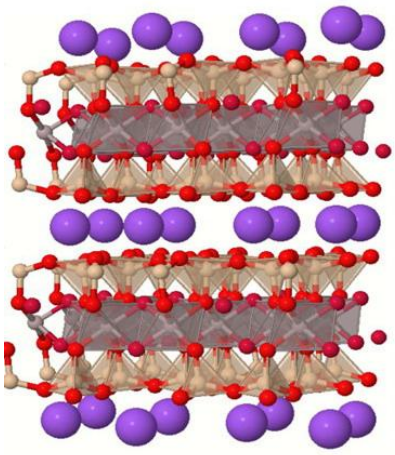

Figure 3.6 Molecular structure of Cloisite® Na^+; purple spheres represent Na^+ ions (source: http://education.mrsec.wisc.edu/Edetc/pmk/pages/montmorillonite.html).

3.2 Sample Preparation

3.2.1 Preparation of API/Polymer

Eudragit® L100-55 was predried in the oven at 70°C for 2 hours to eliminate moisture which could promote the hydrolysis of ASP. Eudragit® L100-55 was pre-plasticized with TEC in a mortar and pestle. Then, ASP or CAF was added and premixed with the pre-plasticized polymer until homogeneous powder was obtained. Hot-melt mixed samples were prepared in a Brabender FE-2000 batch mixer (C.W. Brabender Instruments Inc.,

South Hackensack, NJ). The batch mixer, depicted in Figure 3.7 consists primarily of a central bowl section equipped with rotor blades rotating in opposing directions and at varying speeds (Martin, 2007). The processing temperature was 100°C with a mixing time of 5 minutes at a rotational speed of 50 rpm. After mixing was completed, the samples were removed from the mixer and cooled down to room temperature. Thin discs were prepared by compressing at 100°C for 1 minute to obtain samples 25 mm in diameter and 1.0-1.4 mm in thickness for further analysis.

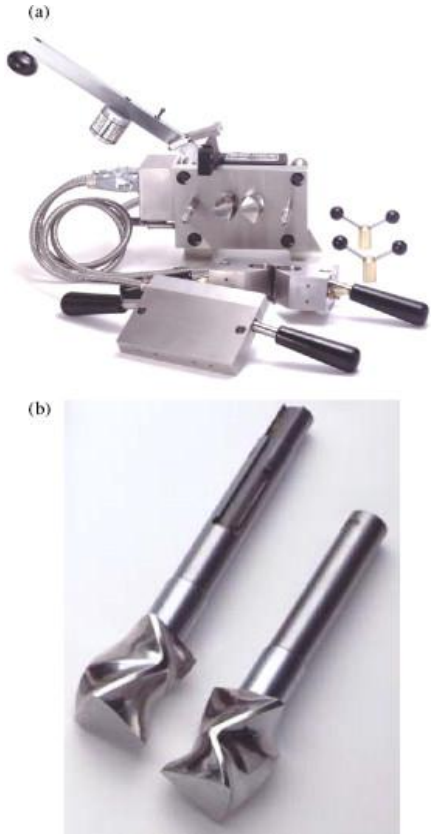

Figure 3.7 Brabender batch mixer (a) frontal view of all components (b) mixing screw. Source: http://www.brabender.com

3.2.2 Preparation of API/Nanoclay/Polymer Composites

3.2.2.1 ASP/HT/Eudragit® L100-55. Predried Eudragit® L100-55 was mixed with ASP and HT in a mortar and pestle for 5 minutes. Then TEC was added and kneaded with the pre-mixed polymer for another 5 minutes until homogeneous powder was obtained. Hot-melt mixed samples were prepared in the Brabender FE-2000 batch mixer. The processing temperature was 90°C with a predetermined mixing time at a rotational speed of 50 rpm. Preliminary runs indicated strong interactions associated with rapidly increasing torque, resembling to crosslinking event after a certain mixing time. To minimize the torque increase, triplicate runs for each formulation were conducted to determine the optimum mixing time as follows: 3 minutes for 5ASP10HT and 10ASP10HT, and 1 minute for 30ASP10HT. After the mixing was completed, the samples were removed from the mixer and cooled down to room temperature. Thin discs were prepared by compressing at 100°C for 1 minute to obtain samples 25 mm in diameter and 1.0-1.4 mm in thickness for further analysis.

3.2.2.1 CAF/MMT/Eudragit® L100-55. The pre-blend preparation of the three components was similar to that of ASP/HT/ Eudragit® L100-55. Predried Eudragit® L100-55 was mixed with CAF and MMT in a mortar and pestle for 5 minutes. Then TEC was added and kneaded with the pre-mixed polymer for another 5 minutes until homogeneous powder was obtained. The hot-melt mixed samples were prepared in the Brabender FE-2000 batch mixer. The processing temperature was 100°C at a rotational speed of 50 rpm. The mixing time was 5 minutes since no torque increase was earlier observed in all formulations due to strong interactions as in the ASP/HT/Eudragit® L100-

55 system. After mixing was completed, the samples were removed from the mixer and cooled down to room temperature. Thin discs were prepared by compressing at 100°C for 1 minute to obtain samples 25 mm in diameter and 1.0-1.4 mm in thickness for further analysis.

3.3 Materials Characterization

3.3.1 Fourier Transform Infrared (FTIR) Spectrophotometry

FTIR spectra were obtained using a Spectrum One FTIR Spectrophotometer (Perkin-Elmer® Instruments, Waltham, MA, USA). KBr pellets containing 1.2-1.5 wt% samples were used in the mid-infrared range (400 – 4000 cm^{-1}). The normalized % Transmittance is plotted vs. wavenumber to represent the FTIR spectra.

3.3.2 Wide-angle X-ray Diffraction (XRD)

X-ray diffraction spectra were taken with a Philips PW3040 diffractometer (Cu K_a radiation, λ= 154 nm), operating at a voltage of 45 kV and current of 40 mA. The samples were scanned over the 2θ range of 2-70° at the step size of 0.02 and scan rate of 2.25 s per step. The slit configurations were 0.5°, 0.5°, and 10 mm for divergence, anti-divergence, and receiving slit, respectively.

3.3.3 Differential Scanning Calorimetry (DSC)

Measurements of melting point and T_g were carried out by a DSC Q100 (TA Instruments, New Castle, DE, USA) under a constant flow of nitrogen at 40 mL/min. Approximately 5-10 mg samples were weighed and placed in an aluminum pan. Heat rate used in the melting point analysis was 10°C/min. To determine the T_g, samples were equilibrated at

-20°C for 5 minutes and then ramped to 180°C at 2°C/min with a modulation of 0.2°C every 40s. The T_g determination was conducted in triplicate and values were measured at the midpoint of the transition step of the reverse heat-flow versus temperature curve.

3.3.4 Thermogravimetric Analysis (TGA)

(TGA) was performed using TGA-7 (Perkin-Elmer® Instruments, Waltham, MA, USA). Samples were placed in an open aluminum pan and heated at a rate of 10°C/min in air atmosphere (flow rate 20 mL/min) for dynamic TGA and at temperatures ranging from 80°C to 120°C over 10 minutes for isothermal TGA. All tests were performed in duplicate.

3.3.5 Scanning Electron Microscopy (SEM)

The samples (surface and cross-section) were examined with a LEO 1530 VP Emission SEM at 3-5 keV working voltage. After the discs were cooled down to room temperature, the cross-section was created by gently bending and breaking the sample with a tweezer to minimize the effect on morphology. The samples were coated with carbon using a Bal-Tee Med 020 Sputter Coater.

3.3.6 Dissolution Test and UV-Vis Analysis

APIs' release rate and amounts were investigated by a Distek dissolution system 2100A (Distek Inc., North Brunswick, NJ). Dissolution was studied according to USP 32 using apparatus II (paddle) at 37°C ± 0.1°C with a rotational paddle speed of 50 rpm in triplicate for both immediate-release and delayed release tests. For immediate release, the dissolution medium was 1 L of pH 7.4 phosphate buffer solution representing a simulated intestinal fluid whilst for delayed-release the sample was placed in 750 mL of 0.1 N HCl,

referred to as acid stage. After 2 hours of operation in the HCl solution, 250 mL of 0.20 M tribasic sodium phosphate that has been equilibrated at 37°C was added to the vessel. The resulting medium's pH was 7.4±0.1, referred to as buffer stage, and the operation was continued. An aliquot of the fluid was withdrawn at predetermined intervals for analysis.

To establish the calibration curve, the ASP standard solution prepared by dissolving ASP in the same solvent as in the dissolution test was transferred and diluted to obtain the set of calibration solutions ranging in ASP concentration from 20 to 300 mg/L. The concentration of ASP (calibration solutions and withdrawn samples) was measured by UV-vis Spectrophotometer at λ_{max} = 280 nm in the acid stage and λ_{max} = 265 nm in the buffer stage. For CAF the calibration curve was established similarly to that of ASP and the absorbance was measured at λ_{max} = 275 nm in phosphate medium solvent (pH 7.4). The presence of Eudragit® L100-55, TEC, HT and MMT was confirmed in an additional study as not interfering with the ASP and CAF absorbance at the selected wavelengths.

3.3.7 ASP Quantitative Determination Using High Performance Liquid Chromatography (HPLC)

ASP assay determination followed the USP 32 procedure for aspirin delayed-release tablets. The sample discs were cut/ground, and an equivalent amount to 100 mg of ASP was weighed and diluted with 20 ml of a diluting solution (mixture of acetonitrile and formic acid 99:1) in a 50 ml volumetric flask. The flask was shaken vigorously for about 10 minutes and centrifuged to prepare a stock solution which was then diluted with the diluting solution. An aliquot of diluted stock solution was then injected into a high performance liquid chromatograph (Hewlett Packard HPLC-1050) with a detector set at

280 nm and C_{18} column (3.9 mm x 150 mm). Three injections were carried out for each sample; the % Assay was the average of 3 injections in which the relative standard deviation was < 2.0%.

3.3.8 Rheometry

Rotational shear rheological characterization was performed using a Rheometrics Scientific RMS-800 with plate diameter of 25 mm and gap of 0.8 mm (plate-plate configuration). A dynamic frequency sweep was carried out at a strain of 5% within the linear viscoelastic region, predetermined by a dynamic strain sweep. The tests were run on the plate equilibrated at 80°C and 100°C with the frequency ranging from 10^{-1} – 10^{2} rad/s.

3.3.9 Water Vapor Transmission (WVT)

The permeability test was followed ASTM Standard Test Methods for Water Vapor Transmission (WVT) of Materials (E96-05). This test evaluates the amount of water that is absorbed and permeates through the material being tested. The permeability cup is made of stainless steel with 4.80 cm in diameter. The cup was filled with 10 ml of distilled water leaving a small gap of air space between specimen and the water. The cup was sealed to prevent any vapor loss except through the test sample and then placed on the balance. The weight loss was recoded periodically for 7 days in which the cup remained on the balance during the entire testing period to avoid an error from the balance pan.

3.3.10 Polarized Light Microscopy

An optical microscope (Carl Zeiss Universal Research Microscope) was used to characterize the samples' morphology. The Zeiss Axiocam Digital camera has 5MB pixel resolution.

CHAPTER 4

API/ POLYMER MIXTURES: ASP/EUDRAGIT® L100-55

Formulations with various ASP concentrations ranging from 10%-30%w/w are shown in Table 4.1. The TEC to Eudragit® L100-55 weight ratio was fixed at 1:4 in all formulations. Solubility parameter was used as a tool predicting the miscibility of the components of the formulations (Hansen, 2007). Table 4.2 contains values of solubility parameters calculated by the authors as per Hildebrand and Hansen equations (Hansen, 2007) and values taken from published data. The difference of solubility parameters among ASP, TEC and Eudragit® L100-55 shown in Table 4.2 is marginal, suggesting a miscible plasticized matrix/API system.

Table 4.1 Sample Formulations Prepared by Hot-melt Mixing

System	Formulation	Component (%wt)		
		ASP	TEC	Eudragit® L100-55
Plasticizer/polymer	TEC/EUL	-	20	80
API/plasticizer-polymer	10ASP	10	18	72
	15ASP	15	17	68
	20ASP	20	16	64
	30ASP	30	14	56

Table 4.2 Calculated Solubility Parameters ($MPa^{1/2}$) for Components of Formulations

	ASP	TEC	Eudragit® L100-55
Hildebrand	21.4	22.2	21.1
Hansen	23.2	20.9	22.3
Hoftyzer/ Van Krevelen*			23.1
Determined from dispersion and polar surface free energy**	24.1		

* Sauer, 2008
**Samaha and Naggar, 1991

4.1 Preliminary Study

Since elevated temperatures are used in hot-melt mixing, thermal analysis was first conducted to determine optimum processing parameters; this is crucial for ASPs in which the degradation is both dependent on water vapor pressure and temperature (Leeson and Mattocks, 1958). Figure 4.1 shows the ASP's weight loss under dynamic conditions. After 150°C, two weight loss steps are shown as follows: (1) release of salicylic acid and acetic acid with the formation of an intermediary compound (ASP dimmers) and (2) thermal degradation of the intermediary compound (Silva et al., 2004). Eudragit® L100-55 begins to degrade above 150°C due to side chain decomposition (Petereit and Weiabrod, 1999; Hughey et al., 2010). An isothermal study was performed in the range 80-120 °C with 10 minutes of holding time. Approximately 0.2% weight loss was found when ASP was heated at the highest temperature used in this study, i.e., 120°C. (data not shown). This indicates that in the absence of moisture ASP is stable below 120°C. Figure 4.2 shows the results of isothermal TGA performed at 110°C. Eudragit® L100-55's weight loss was found to be approximately 3% due to its moisture content, in agreement with the weight loss on drying reported in the analysis certificate of the as received batch. As a result, Eudragit® L100-55 was predried in the oven at 70°C for 2 hours before

processing to eliminate moisture which could cause hydrolysis of ASP. Physical mixtures of 10ASP and 30ASP showed similar weight losses as the pristine Eudragit® L100-55 suggesting the absence of any additional adverse interactions among the components of the formulations.

Given that Eudragit® L100-55 has a T_g of approximately 110°C, TEC has been shown to be an effective plasticizer by lowering T_g to approximately 95°C when added at 10%w/w (Andrews et al., 2008). The 1:4 ratio of TEC:Eudragit® L100-55 employed in this work should be able to reduce the T_g by at least 20°C according to published work (Ha and Xanthos, 2011; Schilling et at., 2010) . Therefore, the operating temperature in the batch mixer was set at 100°C and a 5-minute mixing time was used to minimize the degradation of ASP and that of the plasticized polymer.

To evaluate the uniformity of mixing, the test run was performed on the study batch having lowest ASP concentration in this work, i.e., 10%w/w. After processing, five samples throughout the batch mixer were examined by DSC and TGA. High consistency results were obtained, indicating homogeneous mixtures.

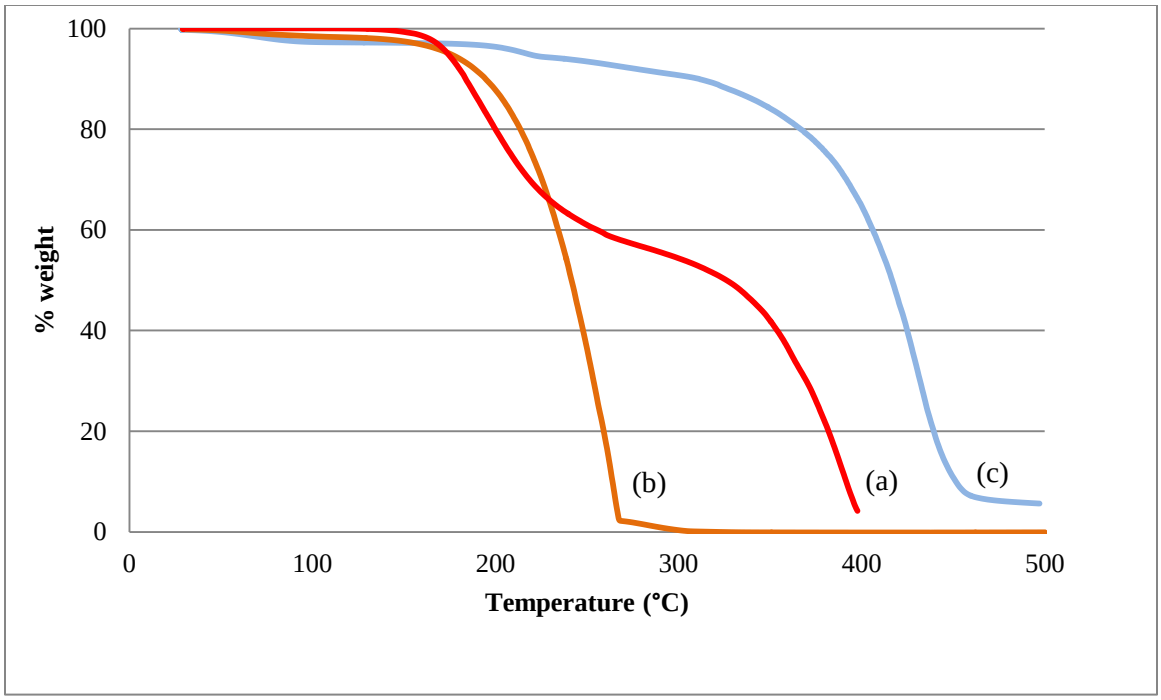

Figure 4.1 TGA results of (a) ASP, (b) pristine Eudragit® L100-55, (c) TEC.

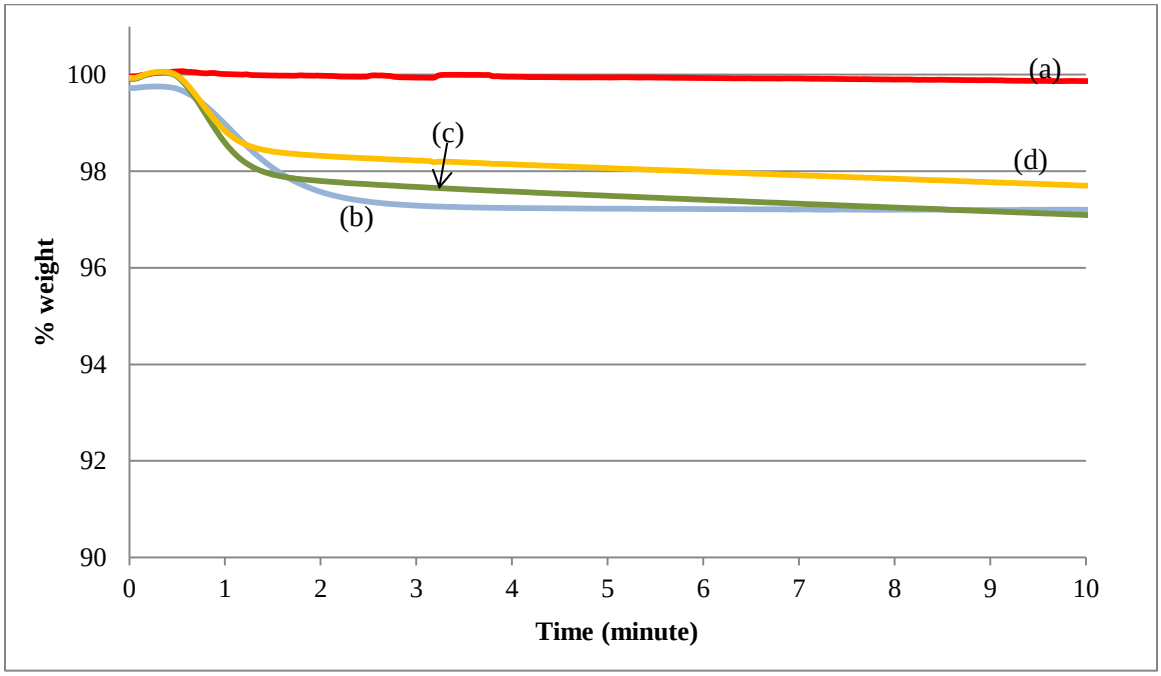

Figure 4.2 Isothermal TGA at 110°C of (a) ASP, (b) pristine :Eudragit® L100-55, (c) physical mixture of 10ASP, (d) physical mixture of 30ASP.

4.2 Mixing Process Monitoring

Torque and temperature were followed during mixing in order to determine physical or chemical state changes. After approximately 45 seconds of fluctuating torque, the torque gradually started decreasing, indicating dissolution of the API in the molten polymer as shown in Figure 4.3 for 10ASP formulation. As the torque was reaching equilibrium, the temperature stabilized at approximately 110°C. No physical and/or chemical changes, corresponding to a rapid drop or rapid increase of torque, were evident until the end of the mixing cycle which suggests the absence of degradation or structural modification under the given mixing conditions

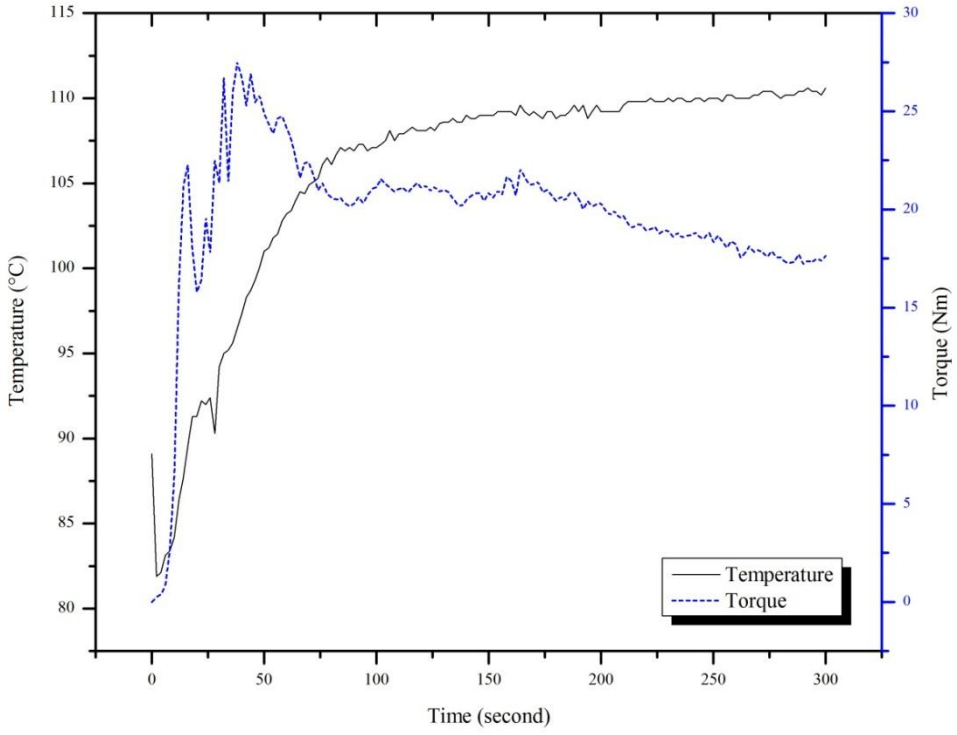

Figure 4.3 Torque and temperature vs. time curves in the batch mixer of 10ASP.

4.3. Determination of % ASP in Polymer Compounds

The amount of ASP in the melt-mixed samples met USP 32 assay requirements for delayed-release tablets (95.0 – 105.0%) as shown in Table 4.3. The limit of free salicylic acid according to UPS 32 in the case of tablets that are coated must not be more than 3.0%. 10ASP showed the highest amount of salicylic acid but still did not fail the USP specification. Thus, mixing of an acidic API such as ASP with the acidic Eudragit® L100-55 does not promote hydrolysis as reported when Eudragit® RL and RS100 were employed in formulations containing ASP due to the presence of quaternary ammonium groups (Petereit and Weiabrod, 1999).

Table 4.3 Nominal and Actual Amounts of ASP in Melt Processed Formulations

Formulations	%ASP in the enteric matrix	Assay	
		%ASP	%Salicylic acid
10ASP	10%	96.3	2.2
20ASP	20%	97.2	1.8
30ASP	30%	97.6	1.5

4.4 FTIR Results

The FTIR spectra in Figure 4.4 show the bands corresponding to ASP, Eudragit® L100-55, and selected melt-mixed samples. For ASP, the peaks at 1755 cm^{-1} and 1692 cm^{-1} correspond to the C=O vibrations of the ester and the carboxylic acid groups, respectively, whereas the peak at 1606 cm^{-1} represents C=C in the benzene ring. The broad band in the range of 2500 – 3200 cm^{-1} is due to the OH vibrations of the carboxylic group (Rasool et al., 2010; Ajun et al., 2009; Olmsted III, 1998). Eudragit® L100-55 contains similar ester and carboxylic functional groups as ASP, found at 1736 cm^{-1} and

1705 cm^{-1}. Additional ester vibration peaks are found at 1269 and 1179 cm^{-1}. The peaks at 1396, 1449, and 1475 cm^{-1} correspond to CH_x vibrations as per Evonik's literature.

For TEC/EUL, 20ASP and 30ASP formulations, there is an overlap of the -OH vibrations associated with the carboxylic group (2500 - 3300 cm^{-1}) and alcohol (2700 – 3500 cm^{-1}), resulting in a very broad range 2500 – 3500 cm^{-1}. Additional evidence suggesting that no significant changes occurred to the samples processed by hot-melt mixing is the presence of the original bands representing esterified carboxylic group at 1753 cm^{-1} as shown in Figure 4.4 (e) – 20ASP and Figure 4.4 (f) – 30ASP. These peaks cannot be detected in Formulations 10ASP and 15ASP, possibly because of the low ASP concentration. However, a new intense peak is observed at 1400 cm^{-1} in all processed formulations. TEC/EUL sample, containing only TEC and Eudragit® L100-55 also shows this strong peak at 1401 cm^{-1}.This peak probably corresponds to the shift of the CH_x vibration of 1396 cm^{-1} of Eudragit® L100-55 after processing by hot-melt mixing.

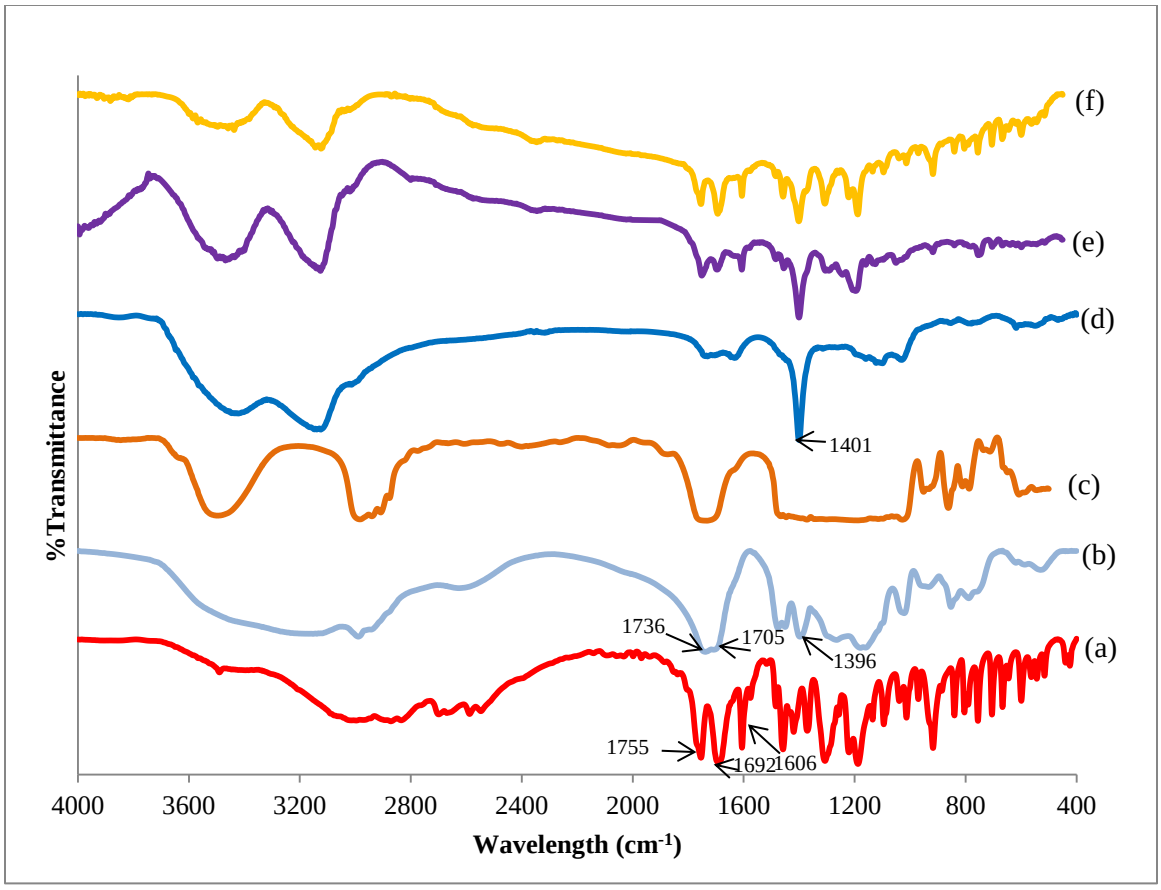

Figure 4.4 FTIR spectra of (a) ASP, (b) pristine Eudragit® L100-55, (c) TEC, (d) TEC/EUL, (e) 20ASP, (f) 30ASP.

4.5 XRD Results

XRD was used to investigate the state of ASP in the hot-melt mixed samples and the possible formation of salicylic acid during melt-mixing. ASP shows a number of sharp peaks, suggesting a highly crystalline structure (Figure 4.5). The two main characteristic XRD peaks of ASP are displayed at 2θ of 7.8° and 15.6° with the latter 2θ angle having apparently a greater intensity. These two distinct peaks are found in all processed samples even at the lowest ASP concentration of 10% (10ASP) whilst 30ASP showed most of the corresponding ASP's XRD peaks due to the high ASP loading. The crystal structure was formed by recrystallization of the ASP as the sample was cooled down to room

temperature; by contrast, Eudragit® L100-55, an amorphous polymer, and its plasticized version (TEC/EUL) do not show any peaks. This indicates that ASP is immiscible with the plasticized polymer, and therefore not molecularly dispersed at room temperature. Unlike ASP, the XRD spectra of salicylic acid, a derivative of ASP, taken from the literature (Turk and Lietzow, 2008; Fukuoka et al., 1987) have two nearly equal intensity peaks at 2θ of 11.0° and 15.6° which do not appear in the melt-mixed samples.

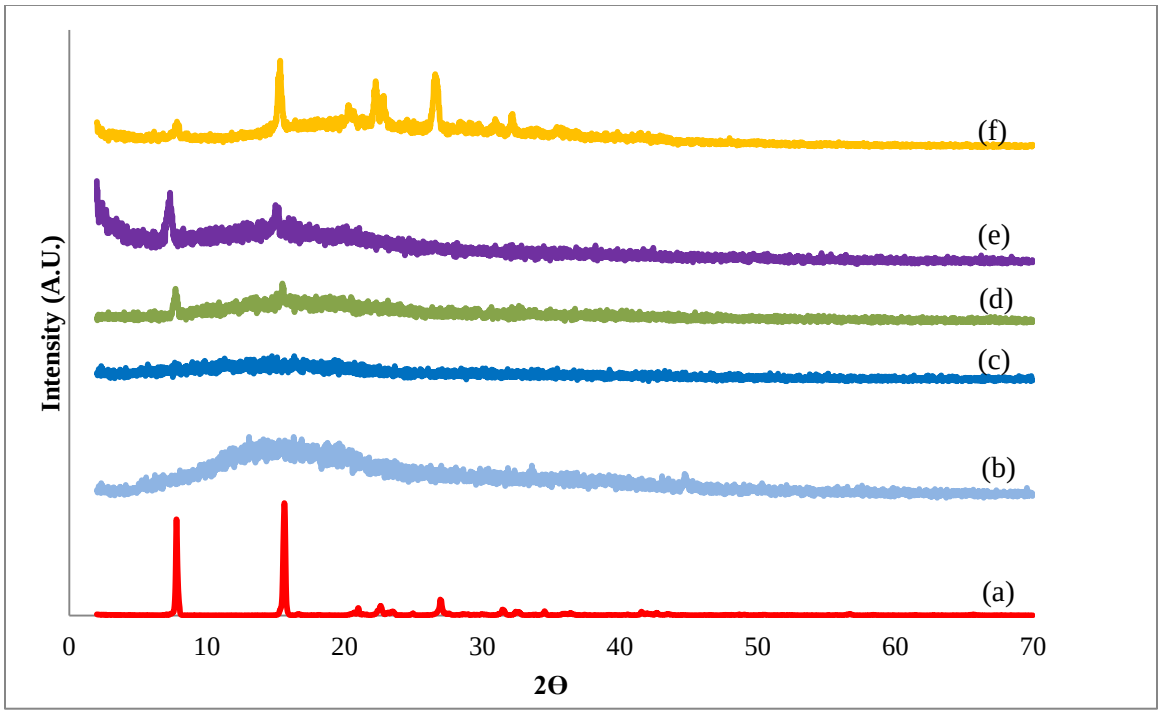

Figure 4.5 XRD spectra of (a) ASP, (b) pristine Eudragit® L100-55, (c) TEC/EUL, (d) 10ASP, (e) 20ASP, (f) 30ASP.

4.6. Glass Transition Temperature (T_g) Determination

To evaluate the effect of API on the polymer T_g, thermal analysis data of the processed samples and the physical mixtures of identical ASP-TEC/Eudragit® L100-55 formulations are shown in Figure 4.6. Pristine Eudragit® L100-55's T_g was determined to be 122°C which is in agreement with Evonik's specifications. At a 1:4 ratio of TEC:Eudragit® L100-55, T_g was reduced by 20°C to 100.5°C. By adding ASP in the polymer matrix, T_g decreases with increasing ASP loading from 0% to 30%, in both physical mixtures and melt mixed samples; this shows the additional plasticizing effect of ASP as a result of its miscibility with Eudragit® L100-55.

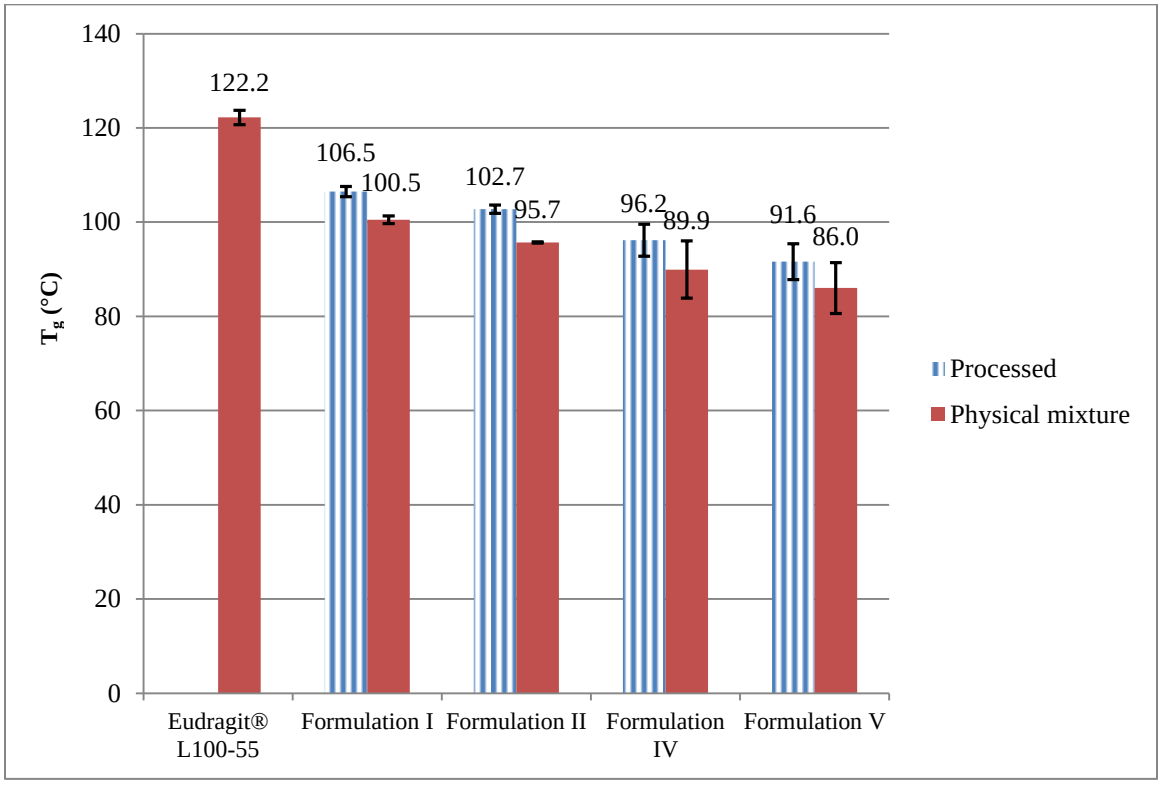

Figure 4.6 T_g of physical mixtures and hot-melt mixed samples. Comparison with pristine polymer.

4.7 Dissolution Tests

The controlled release of ASP from the polymer compounds prepared by hot-melt mixing is shown in Figure 4.7 and Figure 4.9 for immediate-release (pH 7.4) and delayed-release, respectively. The purpose of conducting immediate-release dissolution is two-fold: (1) to examine the difference in the dissolution profiles with and without an acidic stage and (2) to investigate the API release mechanism by curve fitting with modeling equations since the sample is tested under one condition and 100% of API is still present in the sample at time = 0. Note that the API at the surface might be released in the acidic stage, resulting in <100% of API in the sample as the medium's pH is raised to that of the buffer stage. Figure 4.7 shows no significant differences of the ASP release profile among three concentrations in the pH 7.4 medium. In 10ASP, the API was steadily released from the matrix and reached the maximum concentration over a period of 5 hours. Slightly faster release rates were found in 20ASP and 30ASP resulting in complete release within 4 hours. In 30ASP, the initial burst effect is presumably caused by undissolved ASP in Eudragit® L100-55 at the disc's surface since the ASP loading excesses the limit of solubility according to DSC heat flow analysis (data not shown) and rheology results.

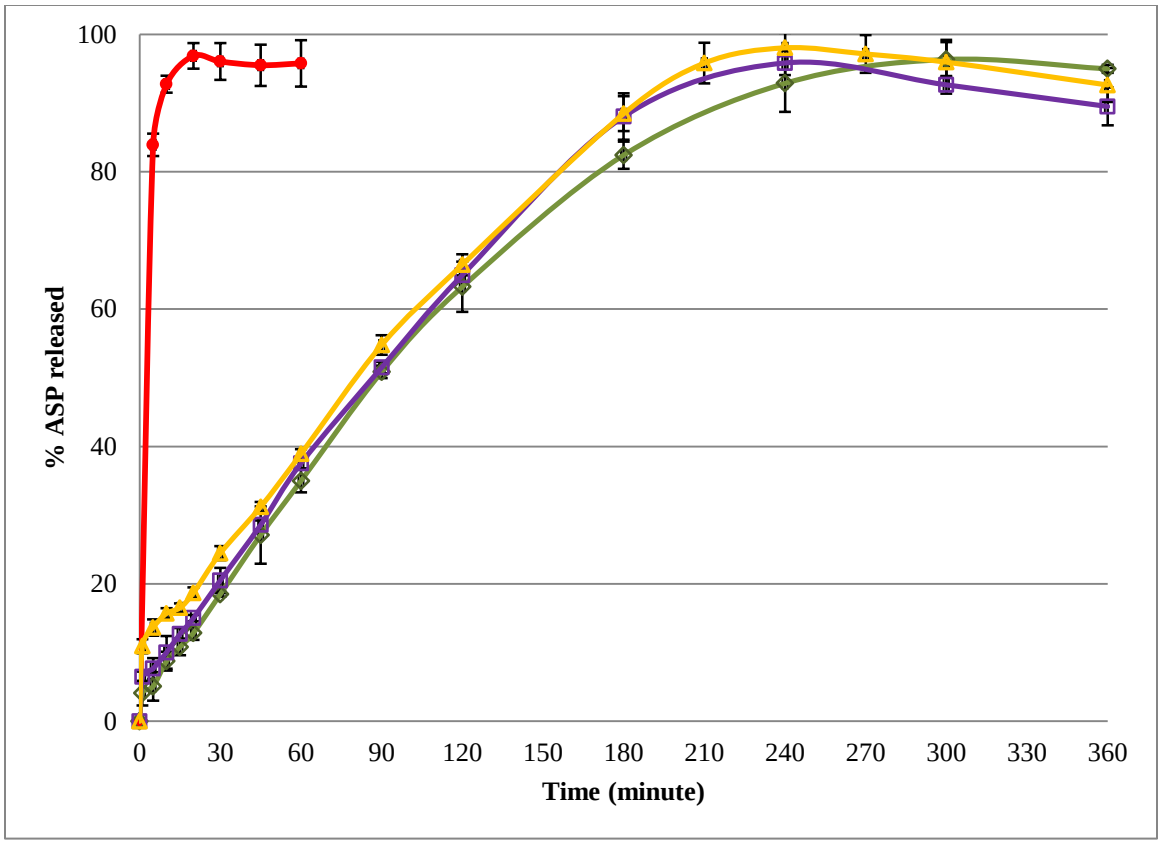

Figure 4.7 Immediate-release dissolution profiles (pH 7.4) of (●) ASP, (◊) 10ASP, (□) 20ASP, (△) 30ASP.

A water-soluble API incorporated in a polymer matrix is mainly released by diffusion, while self-erosion dominates in a low water solubility API (Costa and Lobo, 2001). Eudragit® L100-55 is an erodible pH-dependent solubility polymer which is intended to dissolve in neutral to weakly alkali conditions (Al-Taani and Tashtoush, 2003). Since ASP is a water-soluble API with a pKa 3.5 it is highly soluble in the pH 7.4 medium as depicted in Figure 4.7. Hence, it can be anticipated that the release mechanism of ASP-plasticized Eudragit® L100-55 should be drug diffusion dominating. To investigate the mechanism controlling the release of ASP, statistical analysis and modeling equations can be used. Power law is a simple equation (4.1) describing solute release for different mechanisms i.e., Fickian diffusion, anomalous transport (non-

Fickian), Case-II transport and Super-Case-II transport (Peppas and Sahlin, 1989; Ritger and Peppas, 1987; Peppas, 1985).

$$\frac{M_t}{M_\infty} = kt^n \tag{4.1}$$

$\frac{M_t}{M_\infty}$ is the ratio of the mass of drug released at time t to the mass of drug released at time approaching infinity, *k* is a constant incorporating characteristics of the macromolecular network system and the drug, and n is the diffusional exponent, which is indicative of the transport mechanism. The sample geometry has an effect on the diffusional exponent n. The aspect ratio 2a/L, where a is the sample's radius and L is the thickness, is used to define the geometry. The aspect ratio of the samples in this work is approximately 25 and is, thus, assumed to be the case of a thin film. For such a case, Fickian diffusion is determined by n = 0.5, non-Fickian (Anomalous) by 0.5 < n < 1.0, Case-II transport by n = 1.0 and Super-Case-II transport by n >1.0. For Fickian diffusion (n=0.5), *k* can be defined as:

$$k = 4(\frac{D}{\pi l^2})^{0.5} \tag{4.2}$$

The data shown in Table 4.4 are calculated by using curve fitting tool in MATLAB® version R2011b with 95% confidence interval (CI). R^2 is greater than 0.99 except for 30ASP due to the presence of points at the initial stages of the dissolution

caused by the burst effect. Transport mechanisms for all formulations followed non-Fickian transport since 0.5 < n < 1.0. At low ASP concentration, the n value of 0.86 is close to that of case II transport associated with polymer relaxation, while at ASP loadings up to 30% the n value of 0.59 is close to 0.5, associated with diffusion contribution. Thus, the drug diffusion mechanism predicted earlier for this system should be valid when the ASP loading is higher than 30%w/w.

Table 4.4 Calculated Model Parameters

Sample	Power law[1] $M_t/M_\infty = kt^n$	Peppas and Sahlin[2] $M_t/M_\infty = k_1t^{0.5} + k_2t$	
	n ± 95%CI	k_1 (%min$^{-0.5}$) ± 95%CI	k_2 (%min$^{-0.5}$) ± 95%CI
10ASP	0.86 ± 0.06	1.18 ± 0.44	0.43 ± 0.05
20ASP	0.78 ± 0.08	1.97 ± 0.63	0.36 ± 0.07
30ASP	0.59 ± 0.15	3.78 ± 1.66	0.18 ± 0.22

[1] Ritger and Peppas, 1987
[2] Peppas and Sahlin, 1989

Another equation, Equation (4.3), can be used to differentiate the diffusion and relaxation characteristics of solute release (Peppas and Sahlin, 1989).

$$\frac{M_t}{M_\infty} = kt^m + kt^{2m} \tag{4.3}$$

The first term on the right-hand side represents the Fickian diffusion contribution of the API; the second term is responsible for the relaxational contribution (erosion) of the polymer. The purely Fickian diffusional exponent (m) for different shapes has been derived (Ritger and Peppas, 1987). For thin discs as prepared in this work, m is equal to

0.5. Equation (4.1) and (4.3) are valid for the first 60% of the fraction release ($M_t/M_\infty \leq$ 0.6). The data from curve fitting are shown in Table 4.4.

Equation (4.3) can be written as

$$\frac{M_t}{M_\infty} = k_1 t^m \left[1 + \frac{k_2}{k_1}\right] t^m \tag{4.4}$$

The percentage of API release due to Fickian mechanism (F) is calculated as

$$F = \frac{1}{1 + \frac{k_2}{k_1} t^m} \tag{4.5}$$

With a coupled diffusion/relaxation model for the polymer matrix containing ASP it is shown that diffusion contribution was dominant since the k_1 value was greater than k_2 in all cases. However, the plot of F vs. time according to Equation (4.5) revealed explicitly the degree of API diffusion over time as displayed on Figure 4.8. 30ASP has the highest F among other formulations and its value gradually dropped to roughly 0.5 at the end the test while the F of 10ASP and 20ASP decreased rapidly at the beginning and reached equilibrium at a value below 0.25. It is interesting that the dissolution profile (%ASP released vs. time) of all three formulations did not show significant variation but

the degree of diffusion was dramatically different. The amount of ASP has an impact on the ratio of diffusion to relaxation contribution at a given time.

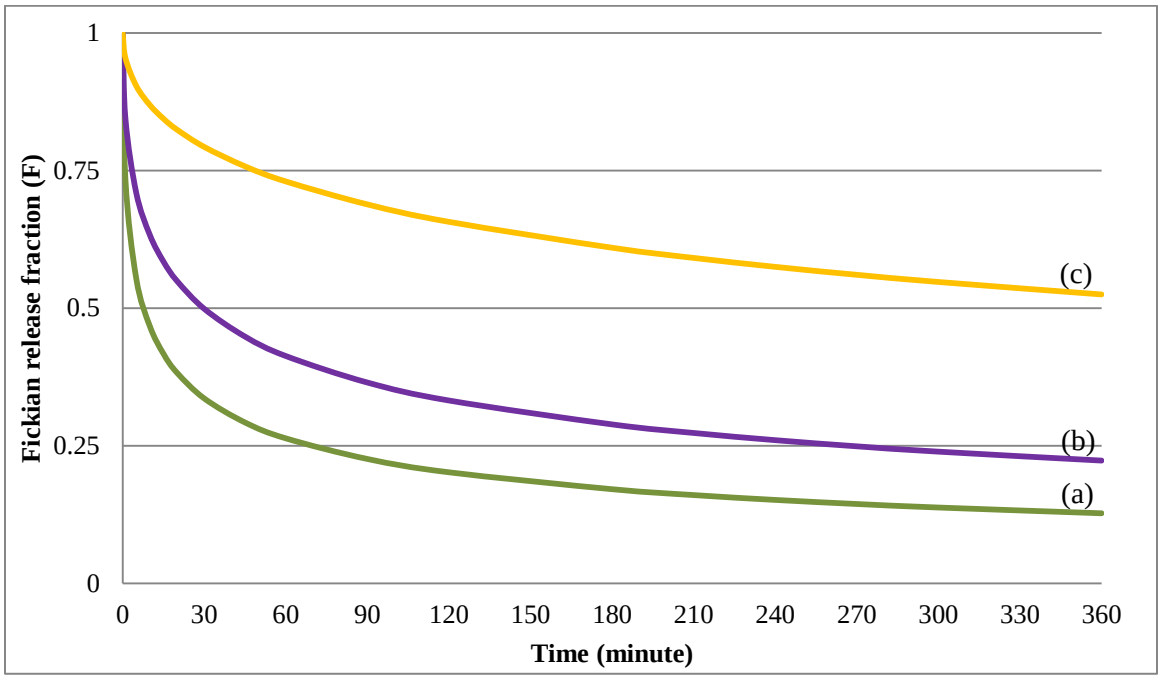

Figure 4.8 Plot of Fickian release fraction (F) vs. time of (a) 10ASP, (b) 20ASP, (c) 30ASP.

Since Eudragit® L100-55 is normally used as enteric coating material, the delayed-release profile was investigated to ensure that the polymer matrix can withstand the acidic stage for 2 hours and can maintain a sustained release profile by slowly releasing ASP after the medium is adjusted to a buffer stage. Figure 4.9 shows the delayed-release profile of formulations 10ASP and 30ASP. According to USP 32 (2009)-section 711-, under delayed-release dosage forms dissolution, no individual sample exceeds 10% release when dissolved in the acid stage. In fact, in the acidic stage (2 hours), 7.4% and 8.8% of ASP were released from 10ASP and 30ASP, respectively. Among the reasons for meeting the requirements for delayed release may be the fact that

the samples processed by HME deliver a lower porosity matrix (Schilling et al., 2010). After the pH was raised to 7.4, sustained release profile was obtained and achieved maximum concentrations at periods similar to those occurring in immediate-release dissolutions (pH 7.4). In both formulations, the release in the buffer stage of the delayed-release was enhanced to some extent due to the fact that the samples were submerged in acidic solution earlier for 2 hours leading to the access of the medium to the enteric matrix. Once the pH was increased to 7.4, the formed porous network during the acid stage promoted ASP release.

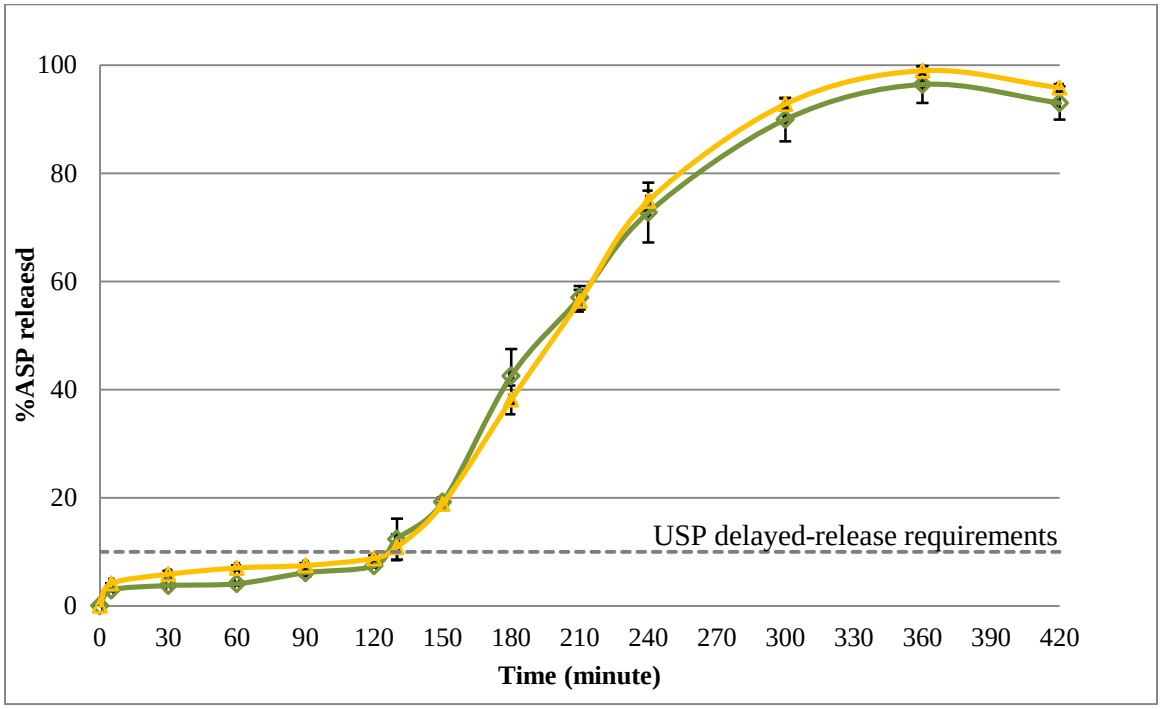

Figure 4.9 Delayed-release dissolution profiles of (◊) 10ASP, (Δ) 30ASP.

The enteric dosage form with prolonged-release in the small intestine obtained by hot-melt mixing in this study could benefit patients as follows: First, if the API is susceptible to attack under acidic conditions it could be protected in the stomach in its

enteric dosage form; this form could also prevent the API to be released in the stomach if it causes stomach irritation. Second, the food residence time in the small intestine (duodenum, jejunum and ileum) is approximately 4-6 hours (Allen et al., 2011). Providing a prolonged release, this would allow the API to be slowly released during the residence time and, therefore, the intake frequency could be reduced.

4.8 Rheology Results

Figure 4.10 shows shear viscosity vs. frequency curves for the five formulations measured at 100°C. The viscosity of the samples decreased with increasing ASP concentration and also with increasing frequency. It was also noted that samples containing ASP appeared to be less brittle than TEC/EUL samples. The curves for 10ASP and 15ASP showed little differences presumably as a result of the small differences in ASP concentrations. However, the curves for formulations 20ASP and 30ASP are nearly identical. This may be related to the fact that ASP loading at 20-30% is approaching the limit of its solubility in Eudragit® L100-55 at 100°C.

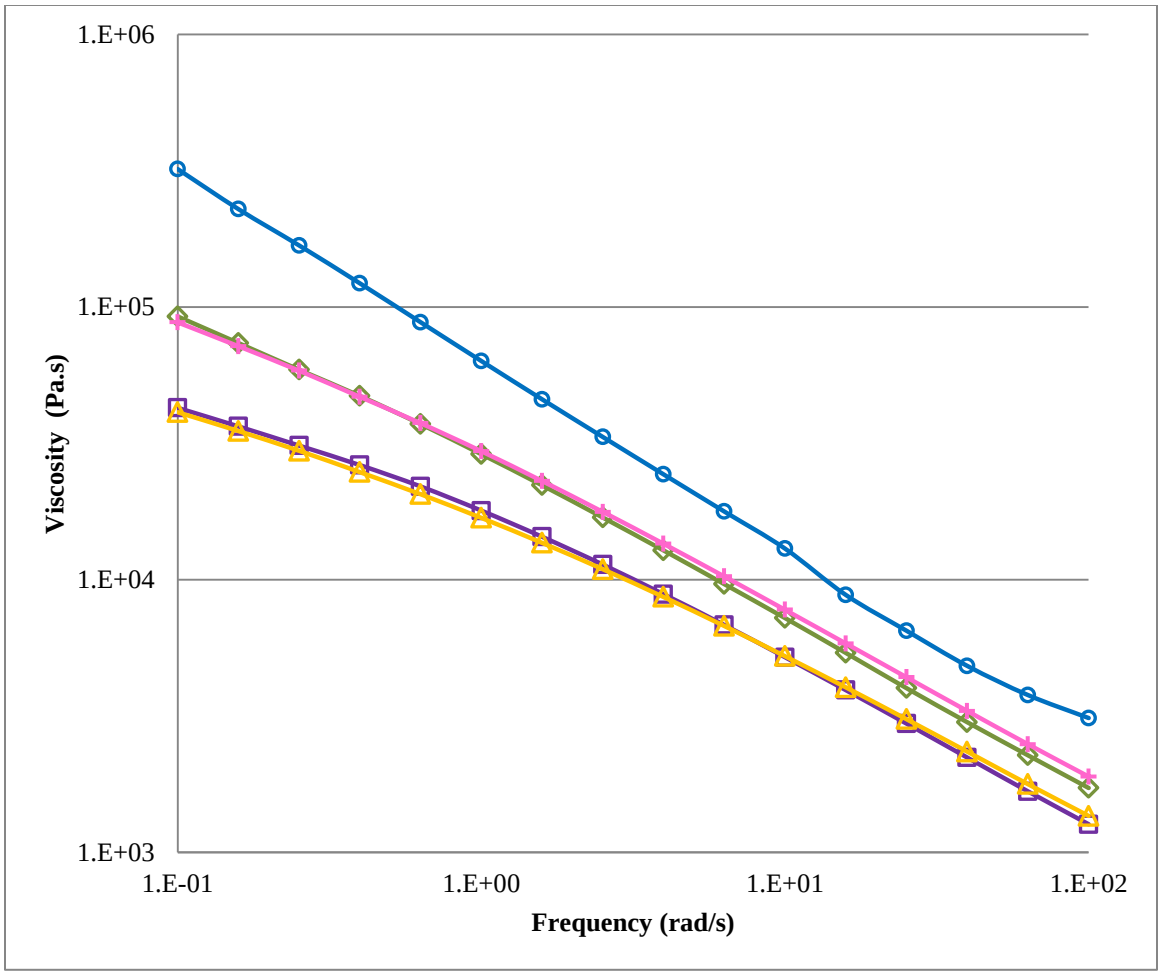

Figure 4.10 Viscosity vs. frequency curves measured at 100°C of (○) TEC/EUL, (◊) 10ASP, (+) 15ASP, (□) 20ASP, (△) 30ASP.

The viscosity data are plotted as viscosity ratios of compound/matrix (η/η_o) vs. %ASP in Figure 4.11. It appears that the ratio starts increasing at some concentrations above 20% in agreement with the interpretation of the data in Figure 4.10 that suggest transition from ASP solution to ASP dispersion at ASP concentrations approaching 20%. The present data are in good agreement with those of the rheological method employed recently to determine the solubility of acetaminophen in polyethylene oxide (Yang et al., 2011).

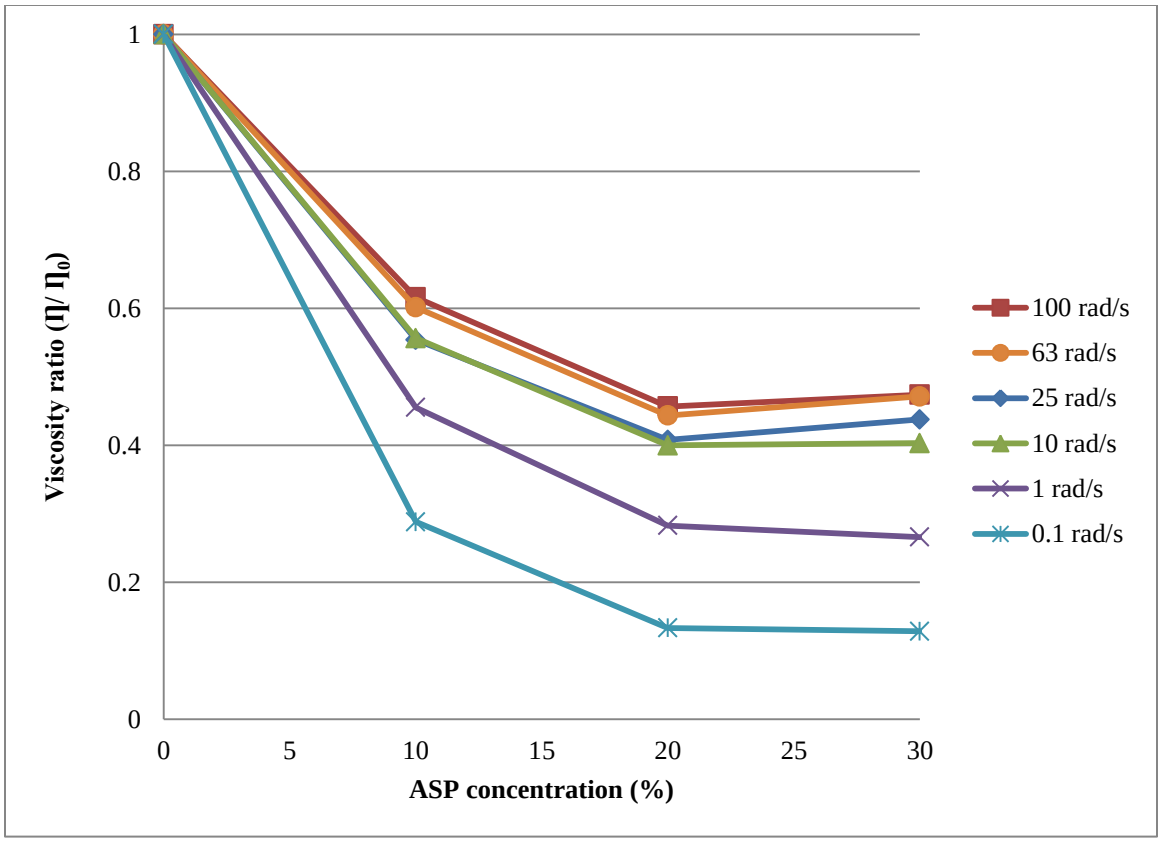

Figure 4.11 Viscosity ratio at different ASP concentrations and different frequencies measured at 100°C.

Oscillatory experiments provide information on the storage (elastic) component (G') and loss (viscous) component (G") of the modulus for a given system at a given temperature. Figure 4.12 shows a plot of G' vs. G" (modified Cole-Cole plot) with interception line and a crossover point. G' = G" for all five formulations. Most points of TEC/EUL fall above the line and this corresponds to a predominant elastic response. In the presence of ASP, the rheological properties are altered and are a function of frequency. Crossover points were found at 0.55, 0.94, 2.27, and 4.92 rad/s for 10ASP, 15ASP, 20ASP, and 30ASP, respectively; in other words more points were obtained under the interception line at greater ASP loadings. This clearly shows a more viscous response with increasing ASP concentration.

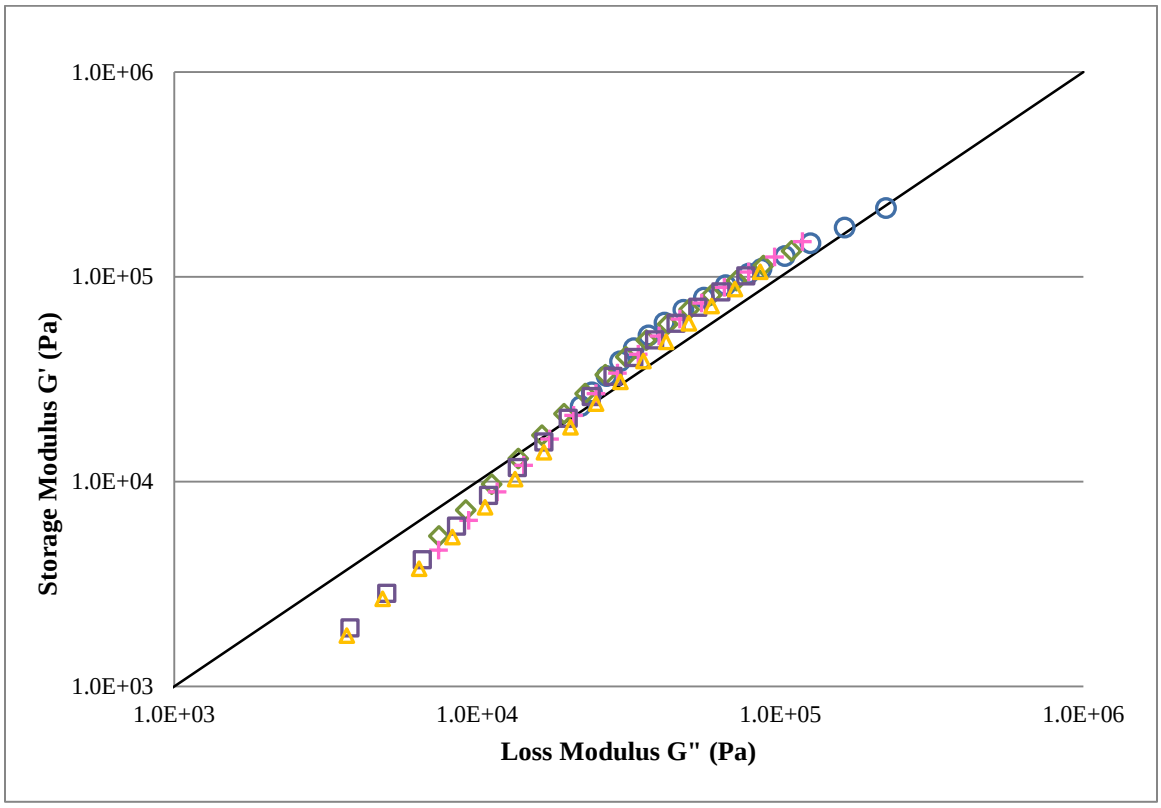

Figure 4.12 Plot of storage modulus (G') vs. loss modulus (G") of (O) TEC/EUL, (◊) 10ASP, (+) 15ASP, (□) 20ASP, (Δ) 30ASP. The solid line represents the case of G' = G".

4.9 SEM Results

Figure 4.13 - 4.16 show pristine ASP crystals and cross-sections of melt-mixed samples. After the melt-mixed samples were pressed and cooled down to room temperature, the discs were dissected and observed immediately. ASP (Figure 4.13) showed oblong-shaped crystals with size ranging from 400 - 1000 μm. ASP crystals were carbon-coated twice due to excessive charging while cross-sectional samples had normally a single-layered coating observed as bright spots in the images. TEC/EUL (a plasticized polymer) has a smooth surface. Crystals of ASP were found as bright spots in Figure 4.15 and 4.16 for 10ASP and 30ASP, respectively with a crystal size less than 200 μm. This is in

agreement with XRD spectra suggesting that recrystallized ASP crystals were present even at the low concentration of 10%ASP.

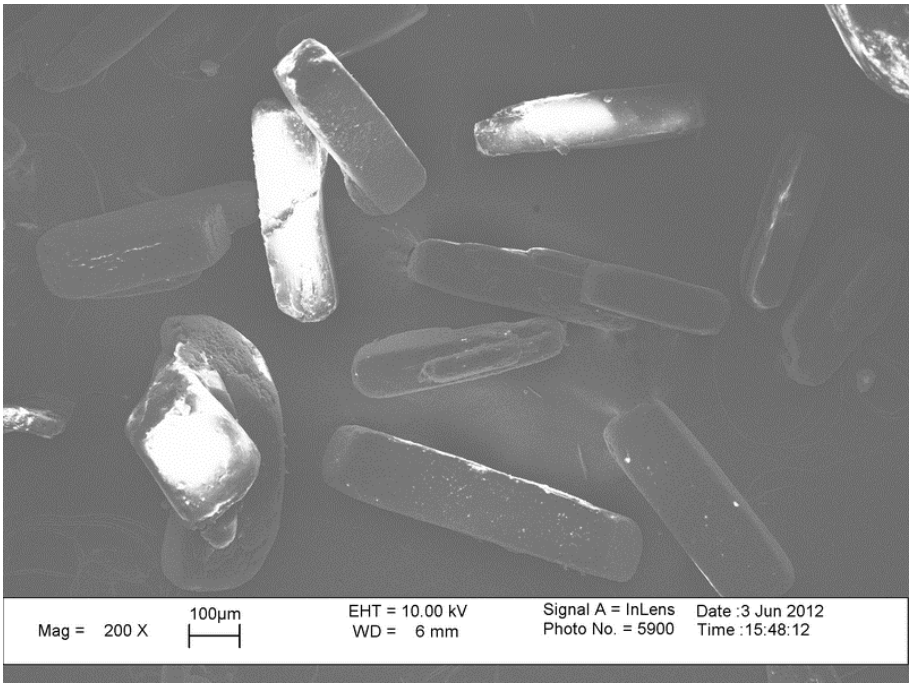

Figure 4.13 SEM of ASP crystals.

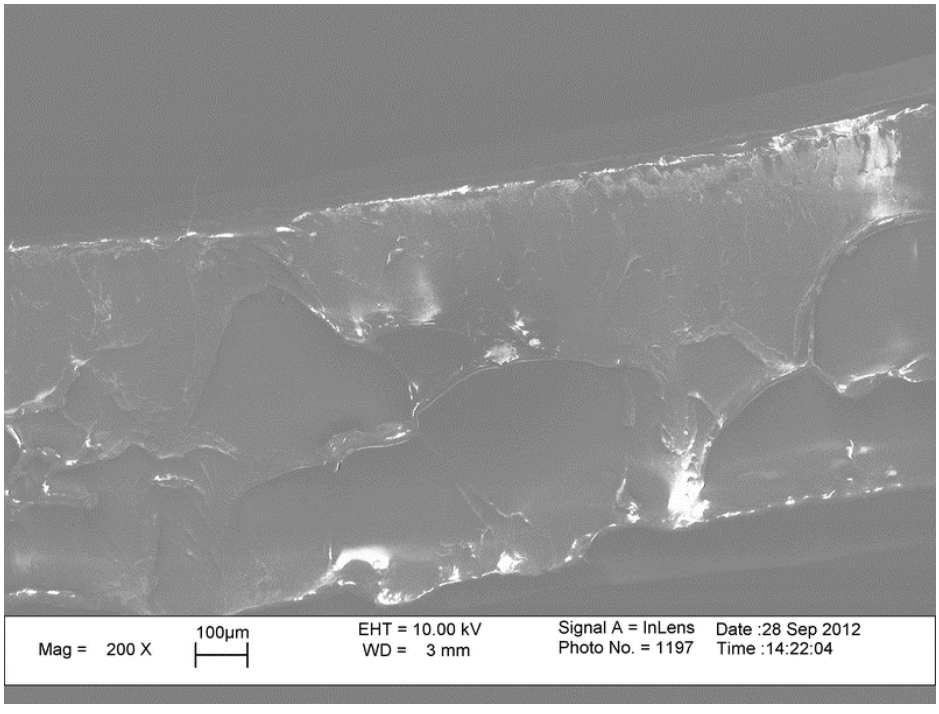

Figure 4.14 SEM of cross-section of TEC/EUL.

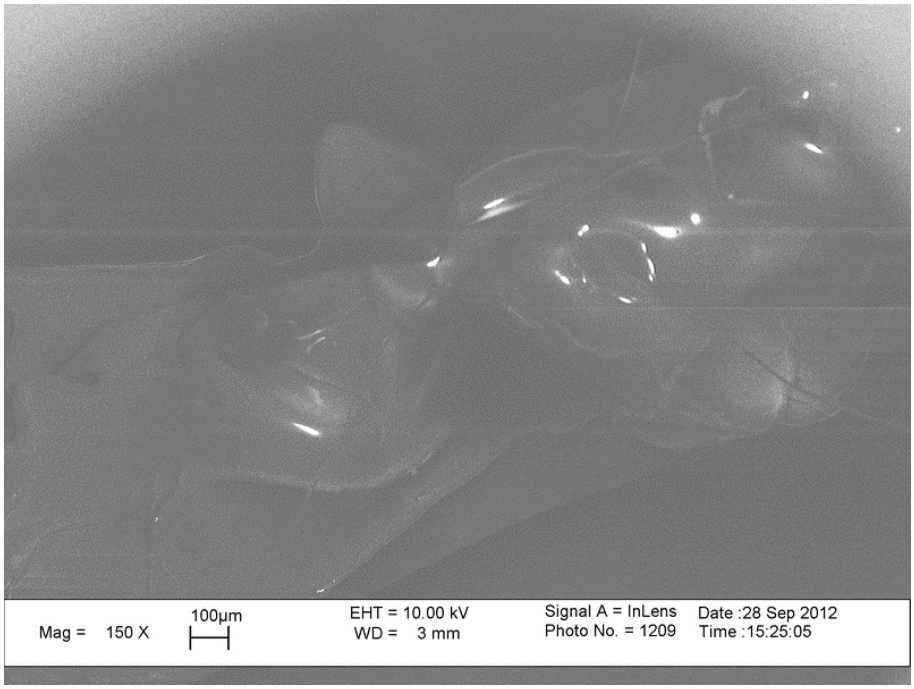

Figure 4.15 SEM of cross-section of 10ASP.

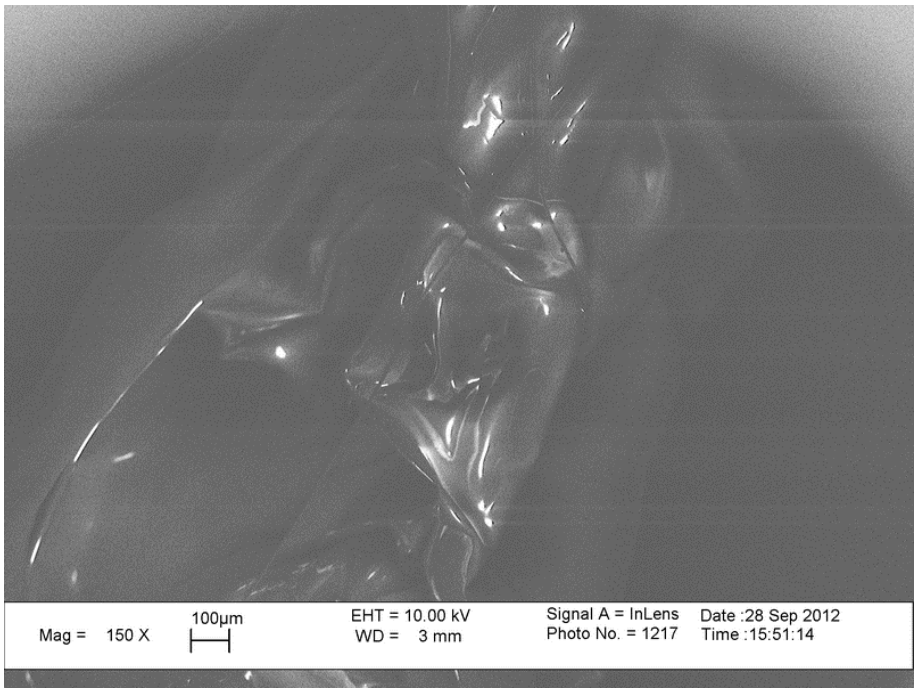

Figure 4.16 SEM of cross-section of 30ASP.

CHAPTER 5

API/NANOCLAY/POLYMER COMPOSITES: ASP/HT/EULDRAGIT® L100-55

HT/Eudragit® L100-55 and ASP/HT/Eudragit® L100-55 formulations are shown in Table 5.1. HT was added at a concentration of 10%w/w in all polymer nanocomposite formulations. Reported AEC of HT is 3.4 meq/g (Toraishi et al., 2002); the maximum amount of ASP which can be exchanged with original anions in HT is 6.13 g per 10 g of HT (see Appendix A). The amount of ASP in the formulations was varied from below AEC to above AEC values of HT.

Table 5.1 Sample Formulations Prepared by Hot Melt Mixing

System	Formulation	Component (%wt)			
		ASP	HT	TEC	Eudragit® L100-55
Nanoclay-plasticizer-polymer	10HT	-	10	18	72
API-nanoclay-plasticizer-polymer	5ASP10HT	5	10	17	68
	10ASP10HT	10	10	16	64
	30ASP10HT	30	10	12	48

5.1 Mixing Process Monitoring

The evolution of torque of sample 10HT during mixing in the batch mixer is shown in Figure 5.1. In the first minute, the torque value increased and remained steady afterwards. The torque did not decrease as previously observed in the ASP/Eudragit® L100-55 samples since HT is not dissolved in the molten Eudragit® L100-55 and remains as suspended particles.

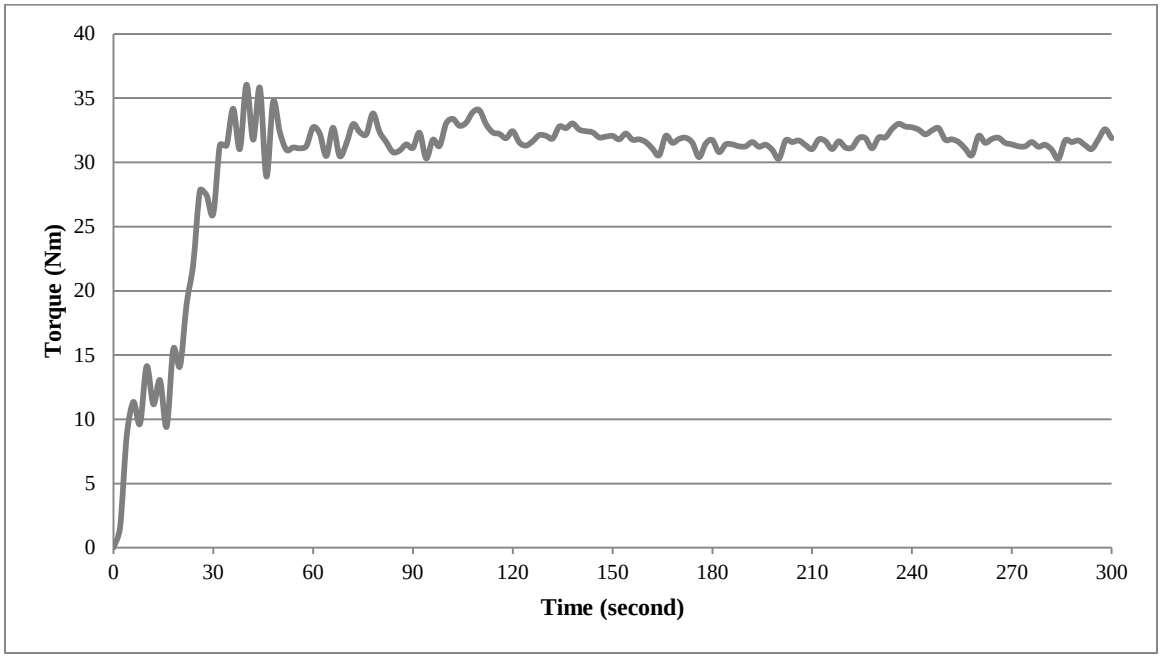

Figure 5.1 The evolution of torque of 10HT during melt mixing.

Systems containing ASP, HT and Eudragit® L100-55 showed, however, a different behavior that was attributed to the presence of strong interactions or occurrence of reactions among the components after a certain period of mixing time. Preliminary runs for all three ASP/HT formulations showed a similar pattern of torque evolution. After the pre-mixed components were fed into the chamber, the torque dramatically rose, followed by a gradual decrease since ASP was dissolved in the molten polymer while HT remained instead in suspension. At this phase, the mixture was in a rubbery state. As mixing proceeded further, the torque (and the corresponding viscosity) increased again as a result of a possible crosslinking reaction and declined towards the end of the run when a dry and bulky powder reminiscent of crosslinked polymer was formed. Three preliminary runs for each formulation were carried out and confirmed that the torque increase took

place repeatedly in the same manner and at the same time and torque levels. Hence, the onset of the torque increase was used as an endpoint of optimum mixing time in the actual runs of all formulations.

During melt mixing, the increase in torque indicating a strong interaction between carboxylic groups of the polymer and Al and/or Mg of the HT has been reported by Pradhan and coworkers (Pradhan et al., 2008). The HT was intercalated with anionic surfactant sodium 1-decanesulfonate in order to enhance its hydrophobic property and expand the HT's basal space, resulting in an ease of polymer chain intercalation. In this dissertation, both ASP and Eudragit® L100-55 contain carboxylic groups which can interact with Al and/or Mg in HT. Therefore, it is possible that the initial portion of decreased torque is due to the dissolution of ASP in the polymer melt and promotion of the intercalation in the HT layers. Then, the HT layers can be sufficiently separated in order to accommodate large species such as carboxylic group bearing polymer chains. A complex between HT and carboxylic groups from both ASP and Eudragit® L100-55 can then be obtained.

The mixing times for 5ASP10HT and 10ASP10HT prior to the torque increase, shown in Figures 5.2 and 5.3, respectively were determined to be approximately 3 minutes. Product appearance and torque evolution were closely monitored during mixing to ensure that the possible crosslinking reaction was not yet initiated. For the 30ASP10HT sample (Figure 5.4), the onset of the torque increase occurred after only 80 seconds in the preliminary run. It is also of interest that the torque level before and after the onset of the torque increase is lower than that in the 5ASP10HT and 10ASP10HT systems that contain lower concentrations of ASP. Hence, the actual mixing time for the

30ASP10HT system was set at 60 seconds. These results confirm that ASP is a critical reactant whose concentration dictates the rate and extent of the possible crosslinking reaction. It should be noted that the majority of melt mixed samples were further heated at 100^{o}C for about a minute to produce films suitable for subsequent characterization by FTIR, XRD and other methods. Thus, it is highly likely that in these samples the reaction responsible for the torque increase has indeed taken place.

The possibility of a crosslinking reaction is discussed further in this dissertation (Sections 5.3 and 5.6) as a reaction that gives rise to aluminum and/or magnesium carboxylate salts derived from the carboxylic groups of aspirin and the multiple sites of metal oxides/hydroxides present in the HT.

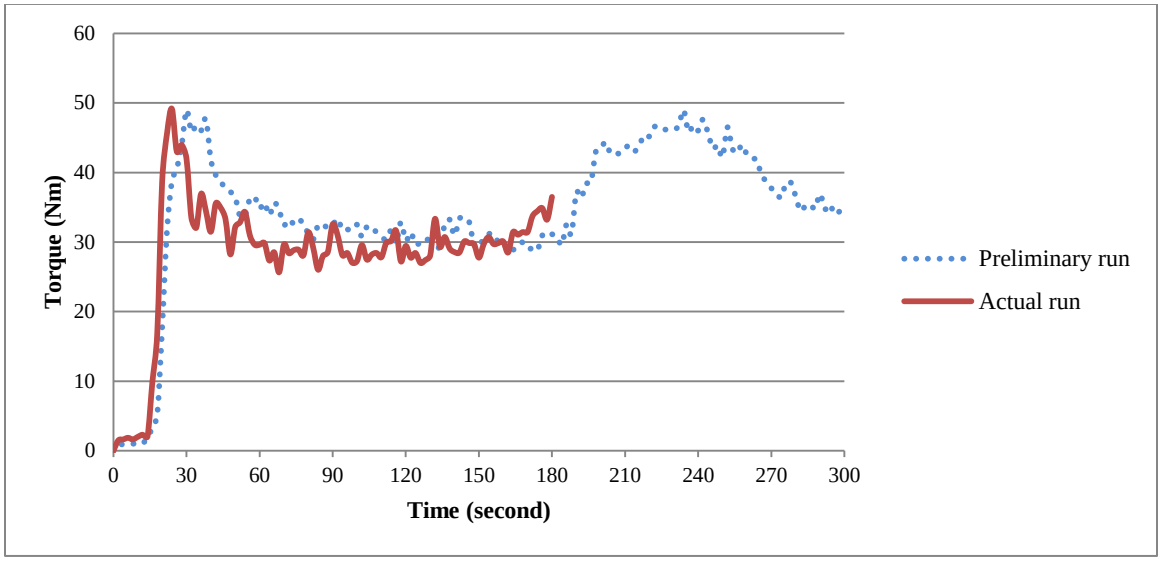

Figure 5.2 The evolution of torque of sample 5ASP10HT during melt mixing.

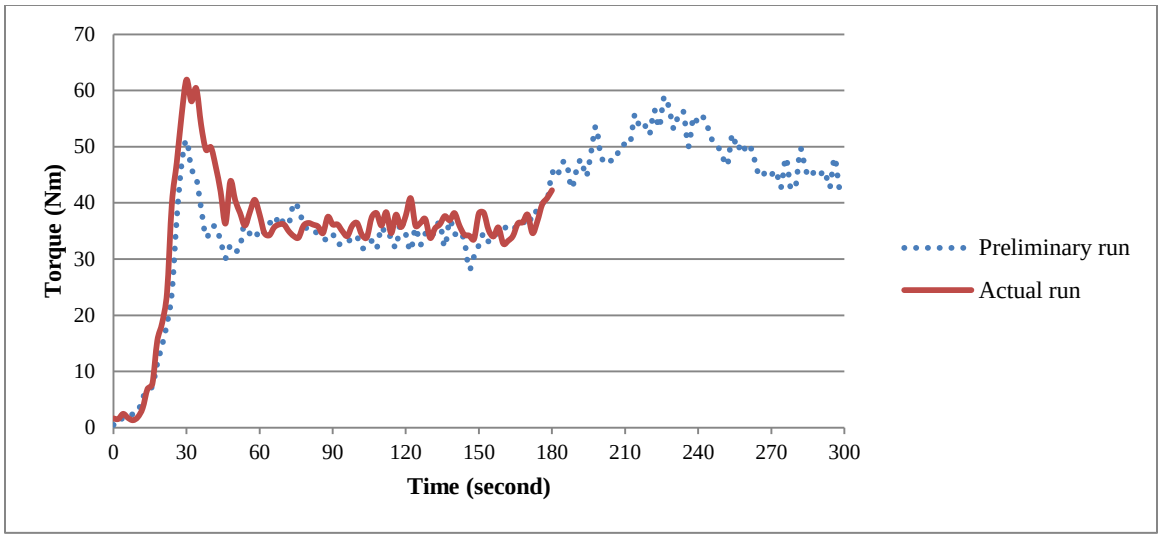

Figure 5.3 The evolution of torque of sample 10ASP10HT during melt mixing.

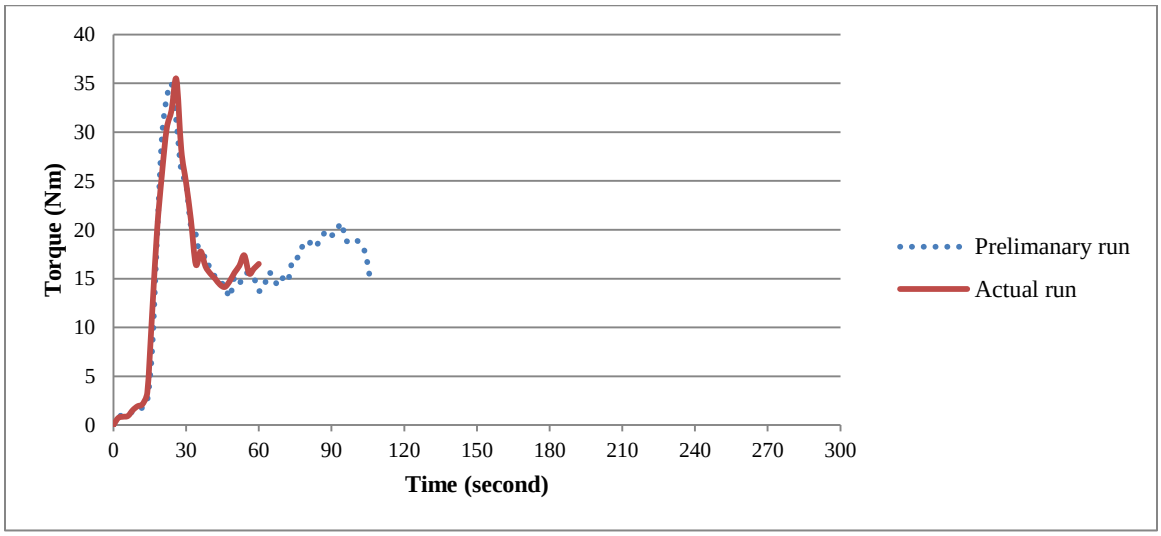

Figure 5.4 The evolution of torque of sample 30ASP10HT during melt mixing.

5.2 XRD Results

Figure 5.5 shows XRD spectra of Eudragit® L100-55, HT and 10HT. Eudragit® L100-55 is an amorphous polymer and, therefore, does not show any peaks. Since HT has a double-layered metal hydroxide structure consisting of magnesium and aluminum hydroxide octahedra interconnected via the edges (Drits and Bookin, 2001; Pural MG

Sasol), strong peaks are found at the 2θ angle of 11.6^{o} and 23.3^{o}, representing d_{001} and d_{002} planes, respectively. According to Bragg's law of diffraction, the corresponding basal spacing of HT at the first angle is 7.8 Å which is in agreement with the supplier's specifications and other authors data (Arco et al., 2007; Crepaldi et al., 2002; Ambrogi et al., 2001). In general, the basal spacing is measured from the bottom to bottom of the two brucite layers which contain intercalated anions (Figure 3.5). The reported thickness of the brucite layer is 4.8 Å (Nalawade et al., 2009; Drezdzon, 1988) while the diameter of the intercalated CO_3^{2-} is 3 Å (Crespo et al., 1997); therefore, the resultant basal spacing is 7.8 Å. The high intensity peaks at the HT's original 2θ angle in the spectrum of 10HT suggest an intact double-layered structure. This also implies that the carbonate anions trapped within the HT's interlayer are not replaced by the polymer chains or, in other words, no intercalation of HT by the Eudragit® L100-55 chains containing methacrylic acid and ethyl acrylate side chains.

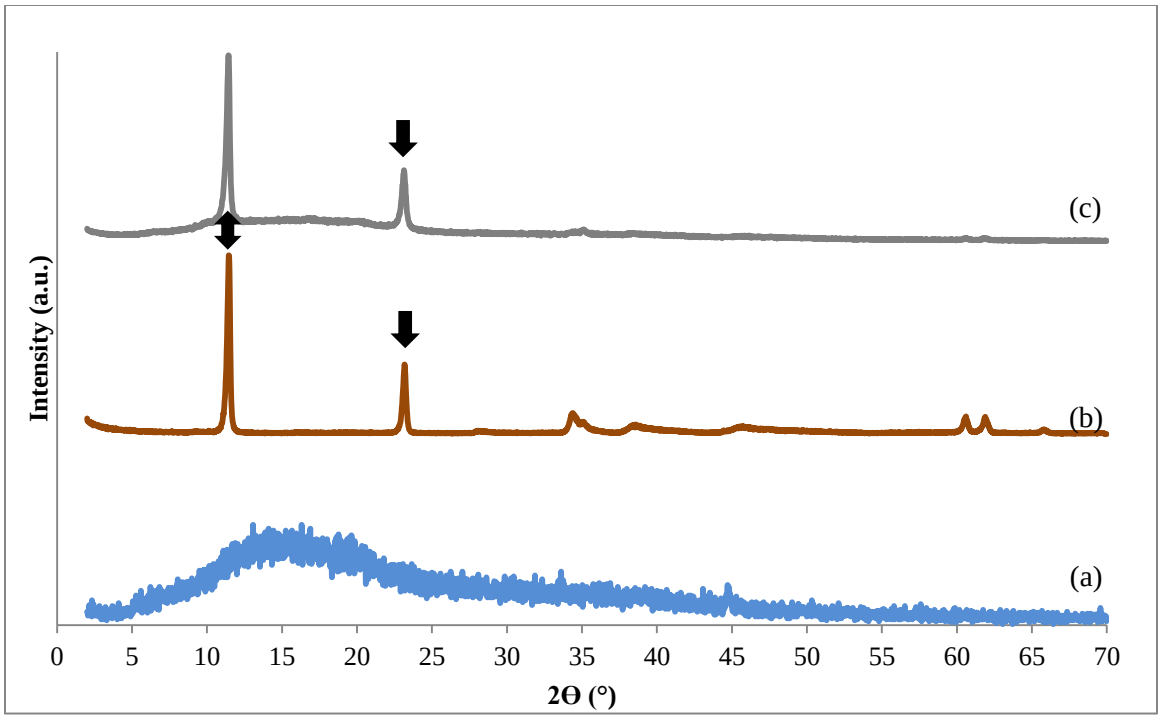

Figure 5.5 XRD spectra of (a) Eudragit® L100-55, (b) HT, (c) 10HT.

ASP and HT have highly ordered crystalline structures, with XRD peaks shown in Figures 5.6 (a) and (b), respectively. It appears that hot melt mixing of ASP with the Eudragit® L100-55 polymer matrix containing HT enhanced the collapse of HT's double-layer structure resulting in partial intercalation and exfoliation. For the sample with the lowest ASP concentration, 5ASP10HT (Figure 5.6 (c)), the d_{001} plane was shifted from the 2θ angle of 11.6° to 4.9° indicating an increase of basal spacing from 7.7 Å to 17.9 Å. The increased basal spacing could be due to the intercalation of both ASP molecules and Eudragit® L100-55 polymer chains. The new corresponding spacing between the two brucite layers was 13.1 Å (after subtracting 4.8 Å from 17.9 Å). ASP's molecular size has been determined by several researchers. ASP's dimensions reported by Hong and Wen-gong are 8.1Å x 7.2Å x 3.6Å (Hong and Wen-gong, 2010) whereas Xu and coworkers

suggested a different largest dimension of ASP of 7.27Å (Xu et al., 1999). Since the expanded basal spacing of the 5ASP10HT composites is larger than the dimension of ASP, the increased basal spacing was possibly responsible for the ASP molecules intercalated into the HT interlayer by replacing the original carbonate anions. The increased basal space caused by the polymer chain is varied based on polymer structure and the basal space is expanded by approximately 10 Å - 20 Å (Ardanuy et al., 2010; Fornes, et al., 2002; Giannelis et al., 1999).

The intercalation of ASP into the LDH layers has been successfully performed under different processing conditions. Hong and Wen-gong intercalated ASP in a MgAlZn layered-double hydroxide by co-precipitation using $ZnCl_2$ and $MgCl_2$ as precursors (Hong and Wen-gong, 2010). In general, carbonate anions entrapped in the layered-double hydroxide are difficult to be replaced by ion exchange. One method to remove carbonate anions is calcination by heating pristine LDH up to approximately 300-500°C for several hours (Ha and Xanthos, 2011; Constantino et al., 2008; Crepaldi et al., 2002). The present study suggests that intercalation can occur rapidly by high shear at elevated temperatures during HMM in the batch mixer within 3 minutes (optimum mixing time for 5ASP10HT). However, the HT's characteristic XRD peaks can still be observed at 11.6° and 23.3°, albeit at lower intensity as compared to pristine HT. This indicates that there is still HT remaining in agglomerated form which has not intercalated ASP molecules yet. For 10ASP10HT, a similar XRD spectrum is observed in Figure 5.6 (d). However, the lower intensity of the HT peaks at 2θ of 11.6° and 23.3° suggests its partial exfoliation. Therefore, two states of HT, namely an intercalated and an exfoliated one appear to be present in 10ASP10HT. Adding more ASP leads to a greater collapse of

the double-layer structure, and a less ordered arrangement which can be observed in the 30ASP10HT sample. The two characteristic peaks of HT completely disappear (Figure 5.6 (e)), suggesting an exfoliation state of the HT due to the collapse/separation of the layer structure to multiple platelets. There is no intercalation peak at a lower angle anymore; instead, crystalline peaks of ASP are present.

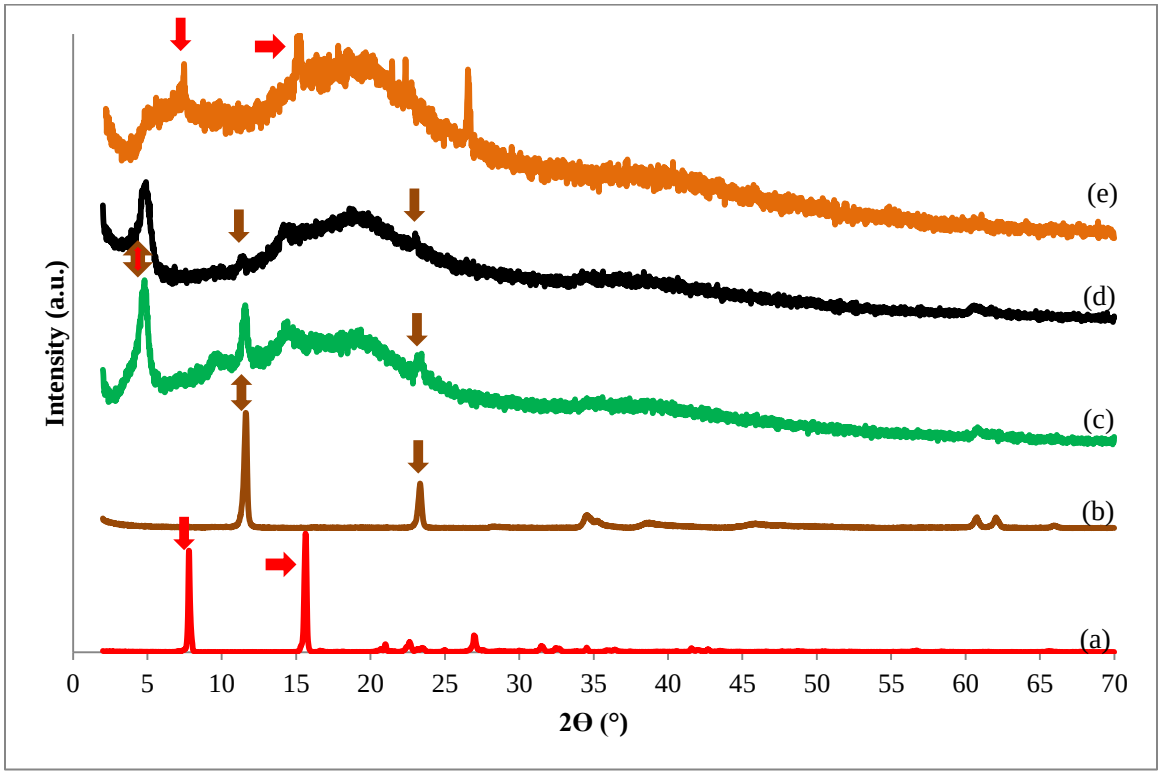

Fig 5.6 XRD spectra of (a) ASP, (b) HT, (C) 5ASP10HT, (d) 10ASP10HT, (e) 30ASP10HT.

5.3 FTIR Results

Figure 5.7 includes FTIR spectra of pristine Eudragit® L100-55, HT, TEC/ Eudragit® L100-55 and 10HT. Eudragit® L100-55 contains ester and carboxylic functional groups which correspond to the peaks at 1736 cm^{-1} and 1705 cm^{-1} due to the C=O vibrations of the esterified carboxylic group and carboxylic acid group, respectively. Additional ester vibration peaks are found at 1269 cm^{-1} and 1179 cm^{-1}. The peaks at 1396, 1449, and 1475 cm^{-1} are responsible for CH_x vibrations as per Evonik's literature. HT shows intense broad bands centered at 3500 cm^{-1} and 1638 cm^{-1} which are correlated with the -OH stretching modes of free and hydrogen-bonded hydroxyl groups in the hydroxide layer and interlayered water (Choy et al., 2004; Hernandez-Moreno et al., 1985). The band below 700 cm^{-1} is due to Mg/Al-OH stretching mode in the brucite-type layers (Arco et al., 2007; Aisawa et al., 2001; Pavia et al., 2009). The entrapped carbonate anions in HT's interlayer spacing correspond to a band at 1371 cm^{-1} due to asymmetric stretching of C=O (Ha and Xanthos, 2011; Kang et al., 2005). TEC/ Eudragit® L100-55, the processed polymer sample with only TEC, revealed a new intense sharp peak at 1401 cm^{-1} shifted from CH_x vibrations at 1396 cm^{-1}. The C=O vibration of the esterified carboxylic group still remained at 1735 cm^{-1} but with lower intensity. For the 10HT sample, the asymmetric stretching C=O band of the intercalated carbonate anions was superimposed by the CH_x vibrations of Eudragit® L100-55 peak at 1400 cm^{-1} whilst the -OH stretching modes of free and hydrogen-bonded hydroxyl group in the hydroxide layer and interlayered water are still found at 3000-3500 cm^{-1} and 1636 cm^{-1}, respectively.

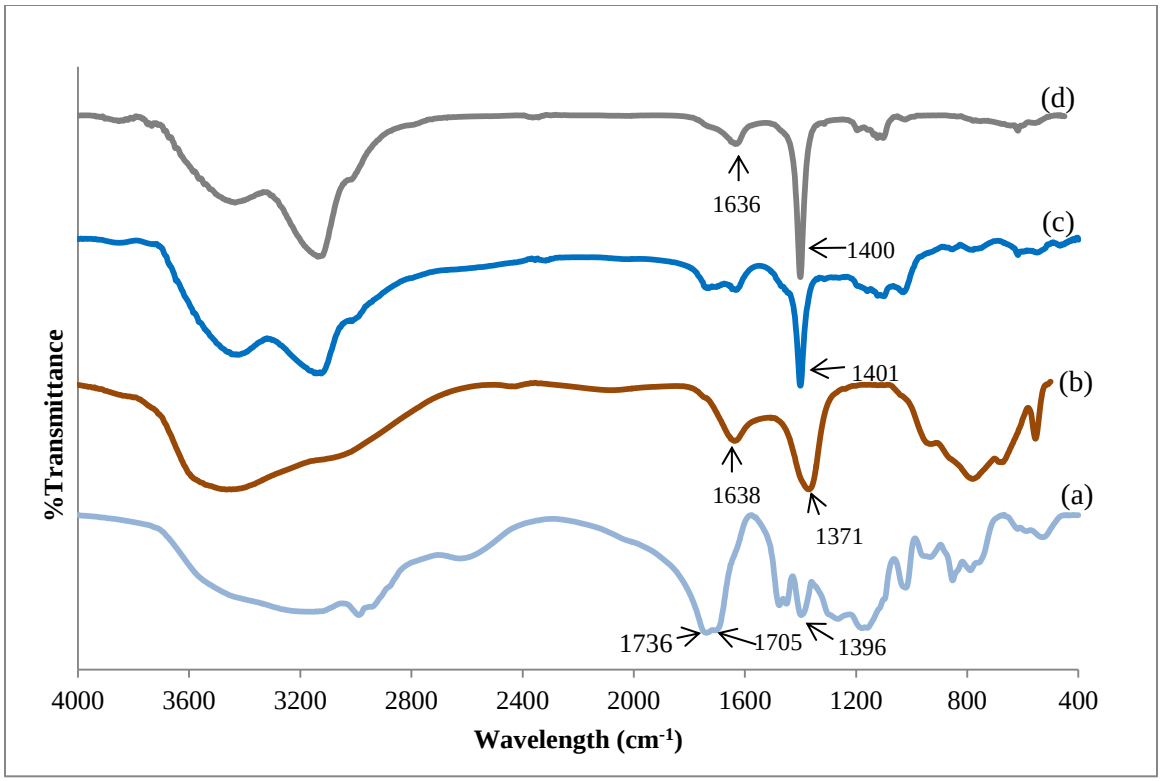

Figure 5.7 FTIR spectra of (a) Eudragit® L100-55, (b) HT, (c) TEC/EUL, (d) 10HT.

The FTIR spectra for ASP and the polymer nanocomposites are displayed in Figure 5.8 (400-4000 cm^{-1}) and Figure 5.9 (600-2000 cm^{-1}). For ASP, the peaks at 1755 cm^{-1} and 1692 cm^{-1} correspond to the C=O vibrations of the ester and the carboxylic acid groups, respectively, whereas the peak at 1606 cm^{-1} represents C=C in the benzene ring. The broad band in the range of 2500-3200 cm^{-1} is due to the OH vibrations of the carboxylic group (Rasool et al., 2010; Ajun et al., 2009; Olmsted III, 1998). All spectra of the polymer nanocomposites are dominated by -OH stretching at around 3500 cm^{-1} with the intense peak at 1400 cm^{-1} correlating with CH_x vibrations. Broad peaks observed at 1736 cm^{-1} in 5ASP10HT (Figure 5.9 (b)) are merged ester and carboxylic group peaks. Apparent splitting spikes are shown in 10ASP10HT and 30ASP10HT at 1753 cm^{-1} (C=O

of ester group) and 1692 cm^{-1} (C=O) of carboxylic group), respectively. This is evidence that ASP did not undergo hydrolysis during HMM.

Interestingly, there is a new peak of carboxylic acid salt shown at 1585 cm^{-1} in 10ASP10HT as illustrated in Figure 5.9 (c). It is attributed to the asymmetric carbonyl stretching vibration of carboxylic acid salt ($-COO^-$) (Socrates, 2001) or, more specifically to the magnesium carboxylate salt (Laskowska and Lipinska, 2012). Laskowska and Lipinska reported that absorption band of asymmetric carbonyl stretching of magnesium carboxylate salt at 1587 cm^{-1}. The presence of COO^- peaks in this region was also reported in ibuprofen-intercalated HT and mefenamic-intercalated HT (Arco et al., 2007; Ambrogi et al., 2001). Another absorption band is observed at 1025 cm^{-1} which is responsible to the Al-O-C group (Tunney and Detelier, 1994). According to the XRD results of 10ASP10HT, either ASP molecules or Eudragit® L100-55 polymer chains or both are intercalated into the HT layer. In the case of polymer chain-intercalated HT, the carboxylic groups of Eudragit® L100-55 are bonded to HT through Al-O-C bonding (1025 cm^{-1}) and Mg-O-C bonding (1585 cm^{-1}). For ASP molecules, the intercalation takes place through the similar Al-O-C and Mg-O-C bonding, resulting in the Al/Mg salt form of ASP. These two peaks (Al-O-C and Mg-O-C) should have also been present in 5ASP10HT (intercalated ASP); they did not, however, probably due to the lower ASP concentration. According to the FTIR spectra of 10ASP10HT, both carboxylic acid group (1692 cm^{-1}) and carboxylic acid salt (1585 and 1025 cm^{-1}) of ASP are present. This implies that there were 2 forms of ASP in the 10ASP10HT sample, i.e. free ASP and intercalated ASP. Based on the anionic exchange capacity of HT, the maximum amount of ASP that can be intercalated into HT is 6.12 g per 10 g of HT. This is in agreement

with the presence of intercalated and free ASP forms in 10ASP10HT as the FTIR spectra suggest. Unfortunately, the amounts of each ASP species cannot be quantified by FTIR spectroscopy.

The 30ASP10HT spectrum depicted in Figure 5.9 (d) also shows the band at 1024 cm^{-1} (Al-O-C) as observed in 10ASP10HT. However, the COO^- peak of 30ASP10HT is found at 1621 cm^{-1} vs. 1585 cm^{-1} for 10ASP10HT (The nearby peak located at 1606 cm^{-1} is corresponding to C=C of ASP's benzene ring). Carboxylic acid salts have a strong, characteristic band in the region 1540-1695 cm^{-1} due to the asymmetric stretching vibration of COO^- (Socrates, 2001) which depends on both the metal ion (Al and Mg in our case) and the organic portion of the salt. Other researchers suggested the band at 1612-1615 cm^{-1} corresponds to the carbonyl stretching vibrations of magnesium hydroxycarboxylate salt (Mandal, 2000; O'Keefe, 2004). It is inconclusive which element (Al or Mg) is responsible for the band at 1621 cm^{-1} for 30ASP10HT. 30ASP10HT's XRD spectrum suggests the exfoliation of HT. Therefore, this band at 1621 cm^{-1} is presumably due to the bonding between carboxylic group of ASP and/or Eudragit® L100-55 to either Mg or Al of HT. Since the 30ASP10HT spectrum also shows the peak of the ASP carboxylic group (1692 cm^{-1}), then, 30ASP10HT contains two forms of ASP, i.e. free ASP and bonded-ASP molecules with HT platelets.

Note that, Aluminum ASP (ASP-Al) and Magnesium ASP (ASP-Mg) are available in several forms. Mitra and Pitkin registered a patent for the production in the form of mono-hydroxy aluminum di-acetylsalicylate (Mitra and Pitkin, 1960). Aluminum ASP in which three anions of ASP are bonded to one Al cation (molecular formula: $C_{27}H_{21}AlO_{12}$, molecular weight = 564.43) is also commercially available (Chemical

Book, 2010). Magnesium aspirin (magnespirin) in which a magnesium cation is bonded to two anions of ASP is also available (PubChem). Table 5.2 summarizes the morphology of HT and ASP forms according to XRD and FTIR results.

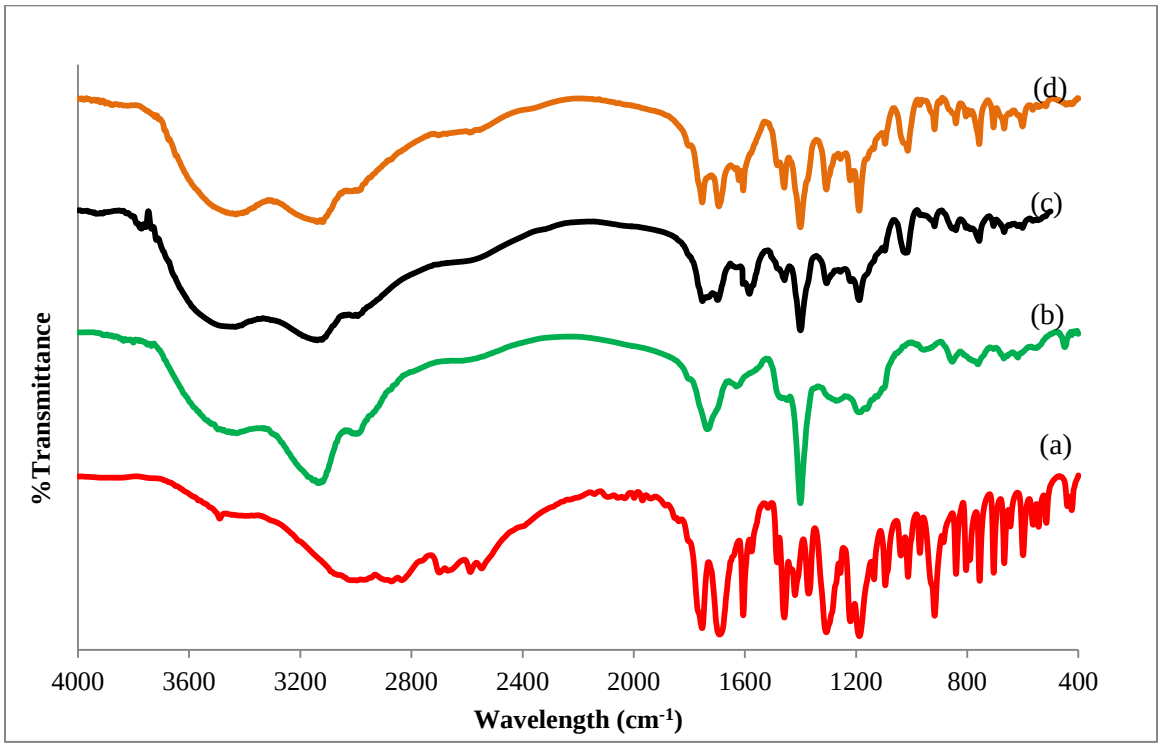

Figure 5.8 FTIR spectra of (a) ASP, (b) 5ASP10HT, (c) 10ASP10HT, (d) 30ASP10HT.

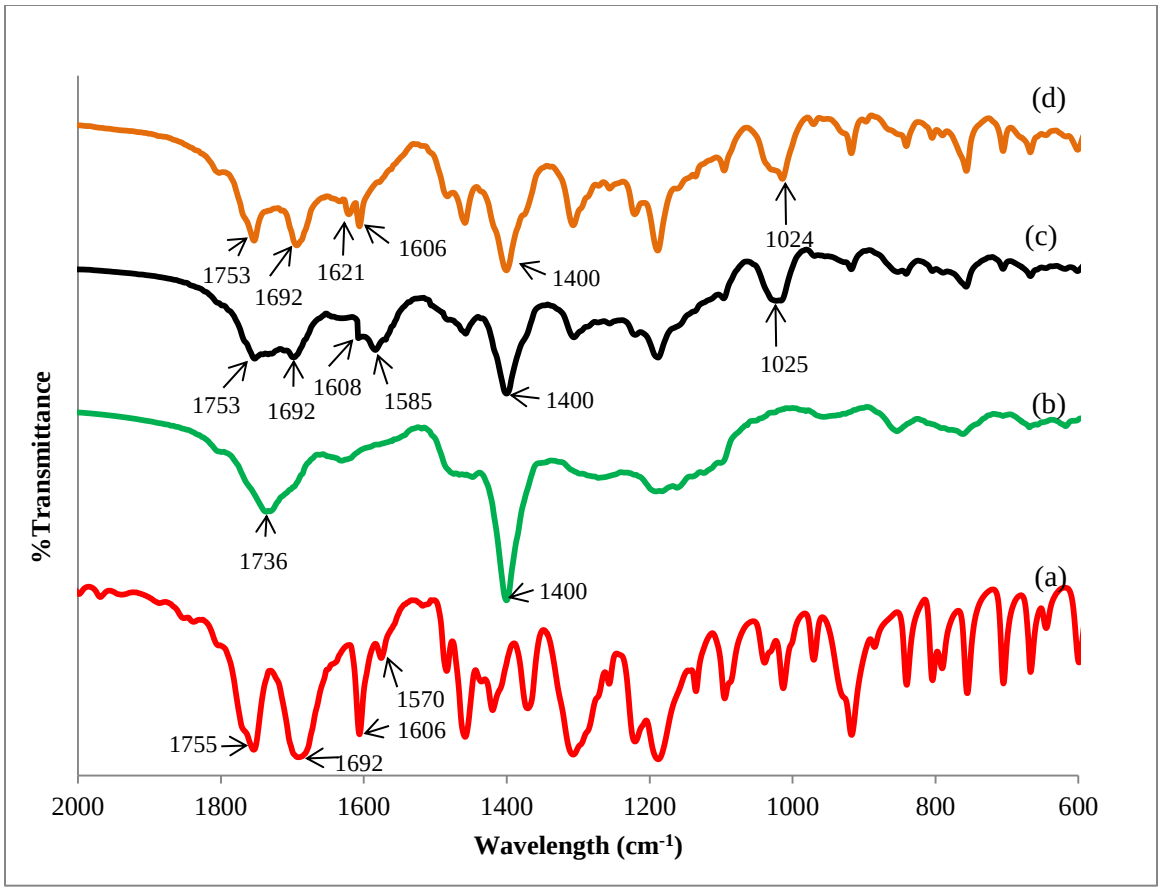

Figure 5.9 FTIR spectra (600-2000 cm^{-1}) of (a) ASP, (b) 5ASP10HT, (c) 10ASP10HT, (d) 30ASP10HT.

Table 5.2 Summary of HT Morphology and ASP Forms in the Polymer Nanocomposites

Sample	Form of ASP and HT	XRD	FTIR
10HT	Agglomerated HT	d_{001} = 11.6°	C=O band of CO_3^{2-} intercalated in HT was superimposed by the CH_x vibrations of Eudragit® L100-55 peak at 1400 cm^{-1}
5ASP10HT	Agglomerated HT	d_{001} = 11.6°	C=O band of CO_3^{2-} intercalated in HT was superimposed by the CH_x vibrations of Eudragit® L100-55 peak at 1400 cm^{-1}
	ASP-intercalated HT	d_{001} = 4.9°	Cannot be detected
10ASP10HT	ASP-intercalated HT	d_{001} = 4.9°	Carboxylic acid salt (Mg-O-C at 1585 cm^{-1} and Al-O-C at 1025 cm^{-1})
	Partial exfoliated HT	Lower intensity of d_{001} at 11.6° and 23.3°	Cannot be detected
	Free ASP	Cannot be detected	Carboxylic acid (1692 cm^{-1}) and ester (1753 cm^{-1})
30ASP10HT	Bonded-ASP with exfoliated HT	Disappearance of d_{001} at 11.6° and 23.3°	Carboxylic acid salt (1621 cm^{-1} and Al-O-C (1024 cm^{-1})
	Free ASP	Characteristic ASP peaks shown	Carboxylic acid (1692 cm^{-1}) and ester (1753 cm^{-1})

5.4 Glass Transition Temperature (T_g) Determination

T_g is an important property in polymer processing since it represents the transition temperature from glassy to rubbery state. Measured T_g values are shown in Figure 5.10. Pristine Eudragit® L100-55's T_g is determined to be 122°C, in agreement with Evonik's specifications. At a 1:4 ratio of TEC:Eudragit® L100-55, T_g is reduced by 20°C to 100.5°C. 10HT shows a slightly increased T_g by approximately 5°C since the agglomeration of HT has limited the free volume of the polymer chains, causing restriction of segmental chain motion. It is reported that the presence of intercalated and

exfoliated HT can increase T_g due to H-bonding and covalent bonding of the well dispersed filler and polymer chain (Nogueira et al., 2011). By adding ASP in the HT/Eudragit® L100-55 polymer matrix, T_g decreased with increasing ASP loading from 5% to 30%. The plasticizing effect of ASP to the TEC containing polymer by lowering T_g to 91.6°C at 30%w/w of ASP was shown in Chapter 4. Although nanocomposites with intercalated (10ASP10HT) and exfoliated (30ASP10HT) states of HT are obtained by HMM, the plasticizing effect of ASP still dominates by reducing the T_g. Note that processed 10ASP10HT has the highest standard error, possibly due to the presence of the two states of HT (intercalated and exfoliated).

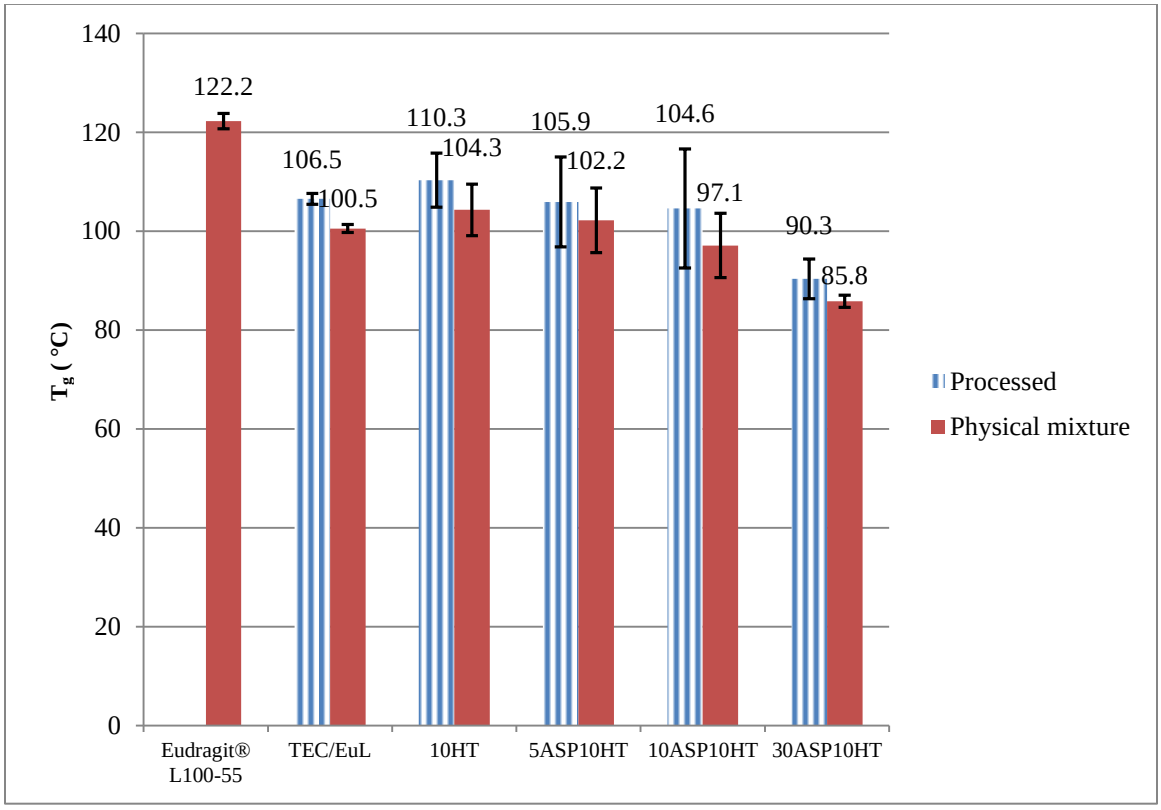

Figure 5.10 T_g of physical mixtures and hot-melt mixed samples. Comparison with pristine polymer.

5.5 SEM Results

Figure 5.11 shows ASP's oblong-shaped crystals with size ranging from 400 - 1000 μm. The ASP crystals were carbon-coated twice before conducting SEM due to their high charge, resulting in bright spots in the image. Pristine HT is shown in Figure 5.12 at two magnifications. A single platelet with approximately 150-300 nm in length can be observed in Figure 5.12 (a) whist various sizes of agglomeration formed by multiple platelets of HT with sizes up to 50 μm are shown in Figure 5.12 (b). The cross section of sample discs was examined in order to confirm different morphological features of HT as suggested by the XRD results. At the magnification of 500x (Figure 5.13 (b)), 5ASP10HT shows random sizes of HT ranging between 25–200 μm. The bright spots are presumably ASP molecules because the nanocomposite samples were carbon-coated once. EDX mapping of C and Mg atoms is illustrated in Figure 5.14. The size of HT sheets becomes smaller (25-100 μm) and more uniform as the ASP concentration is raised to 10%w/w as shown in Figure 5.15. Adding more ASP promoted the delamination of the HT agglomerates. The cross-sectional texture of the 30ASP10HT sample (Figure 5.16) is remarkably dissimilar from those of the 5ASP10HT and 10ASP10HT samples. The texture suggests the formation of a percolating network of ASP and HT platelets. EDX mapping in Figure 5.17 shows the distribution of Mg atoms (and that of HT particles) throughout the cross-sectional area.

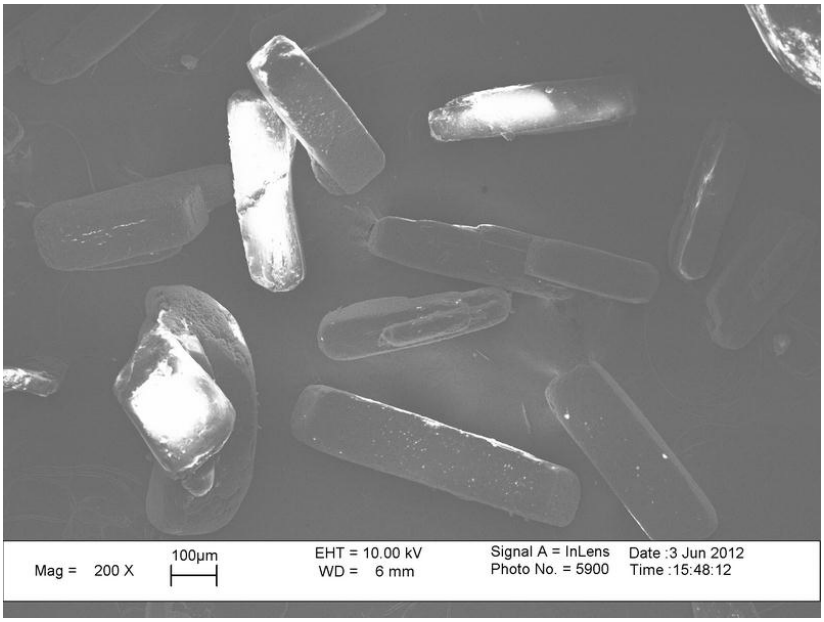

Figure 5.11 SEM of ASP crystals.

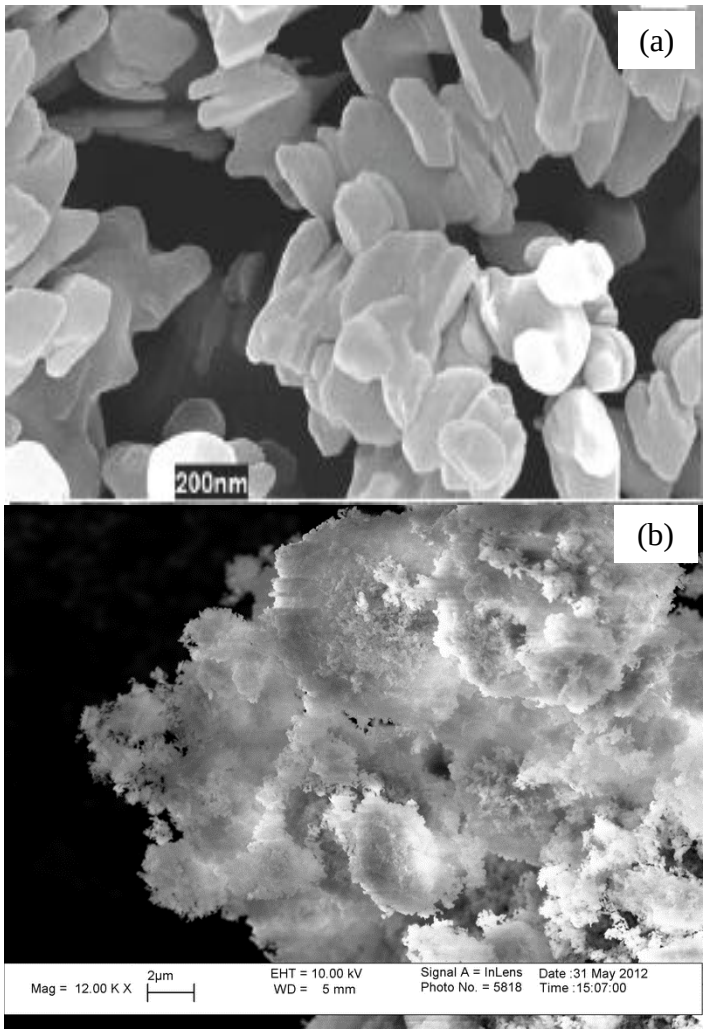

Figure 5.12 SEM of HT (a) single platelet (courtesy of Dr. T.G. Gopakumar, Polymer Processing Institute in Xanthos, 2010), (b) agglomeration observed at magnification 12 KX.

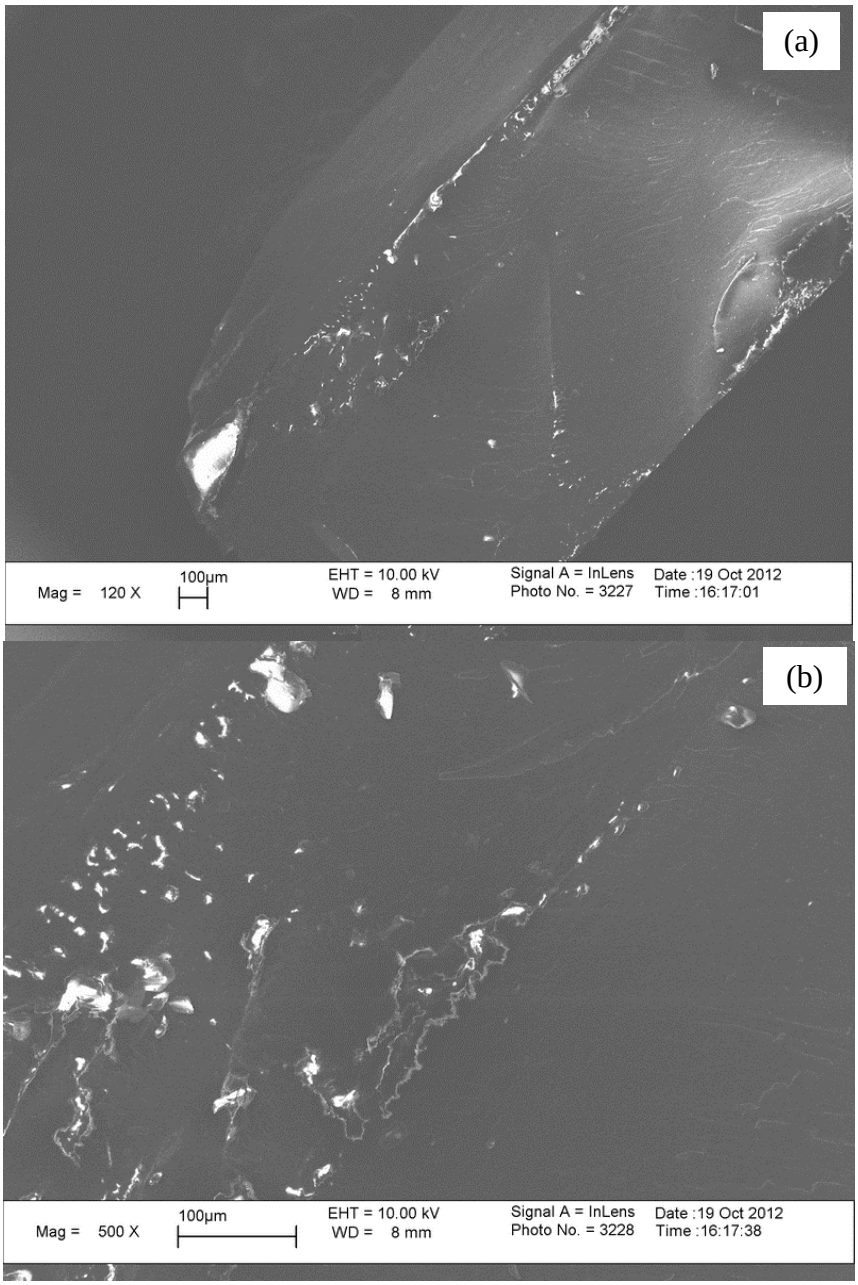

Figure 5.13 SEM of cross-section of 5ASP10HT (a) magnification 120X, (b) 500X.

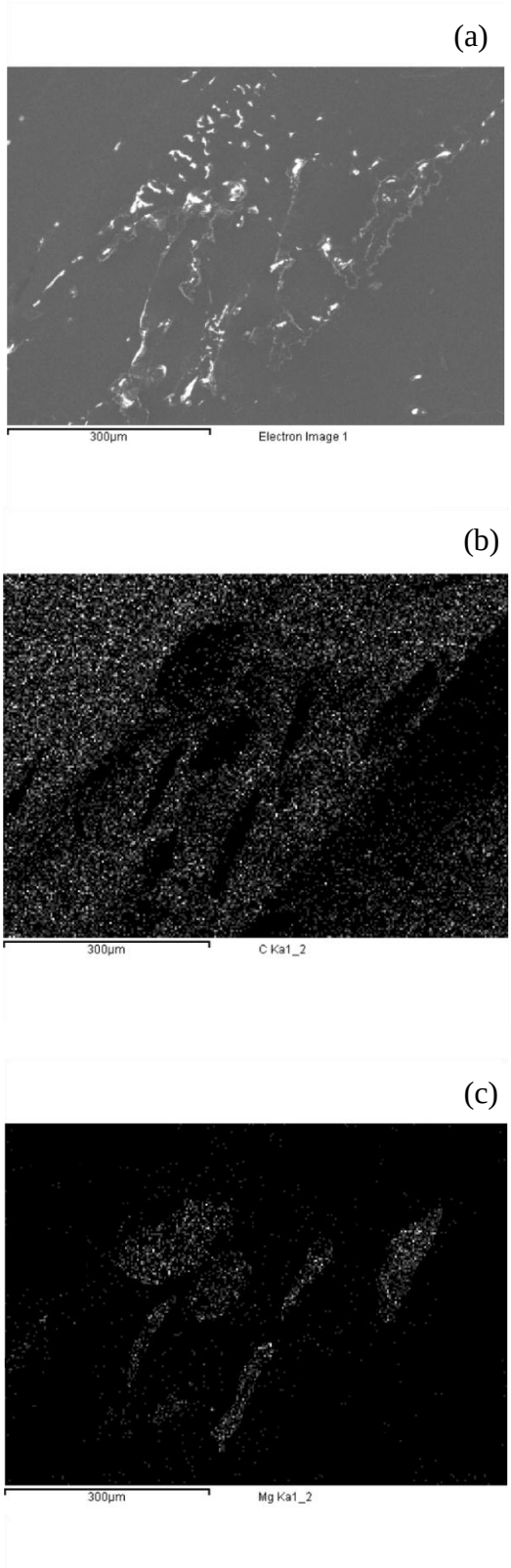

Figure 5.14 EDX Mapping of 5ASP10HT (b) Carbon, (c) Magnesium.

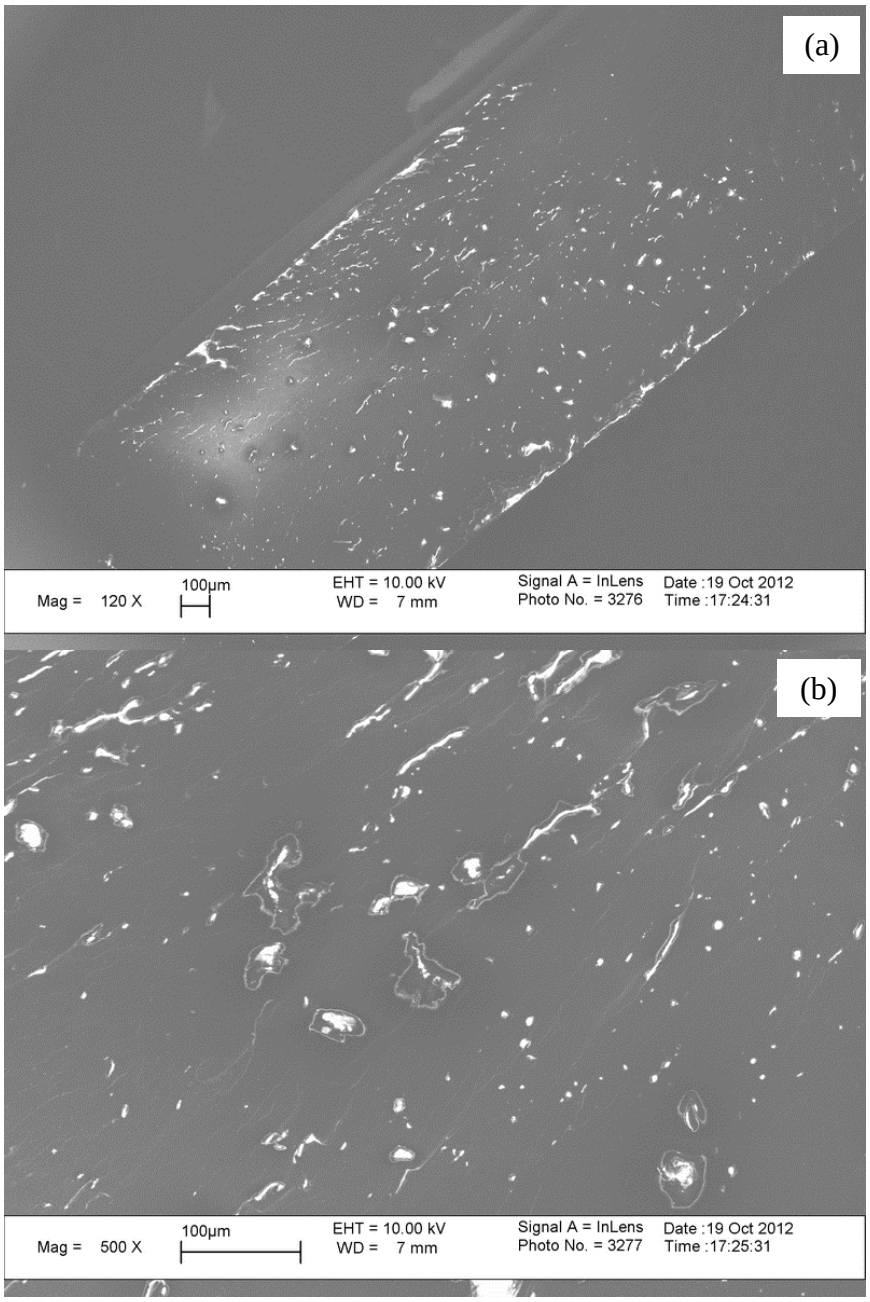

Figure 5.15 SEM of cross-section of 10ASP10HT (a) magnification 120X, (b) 500X.

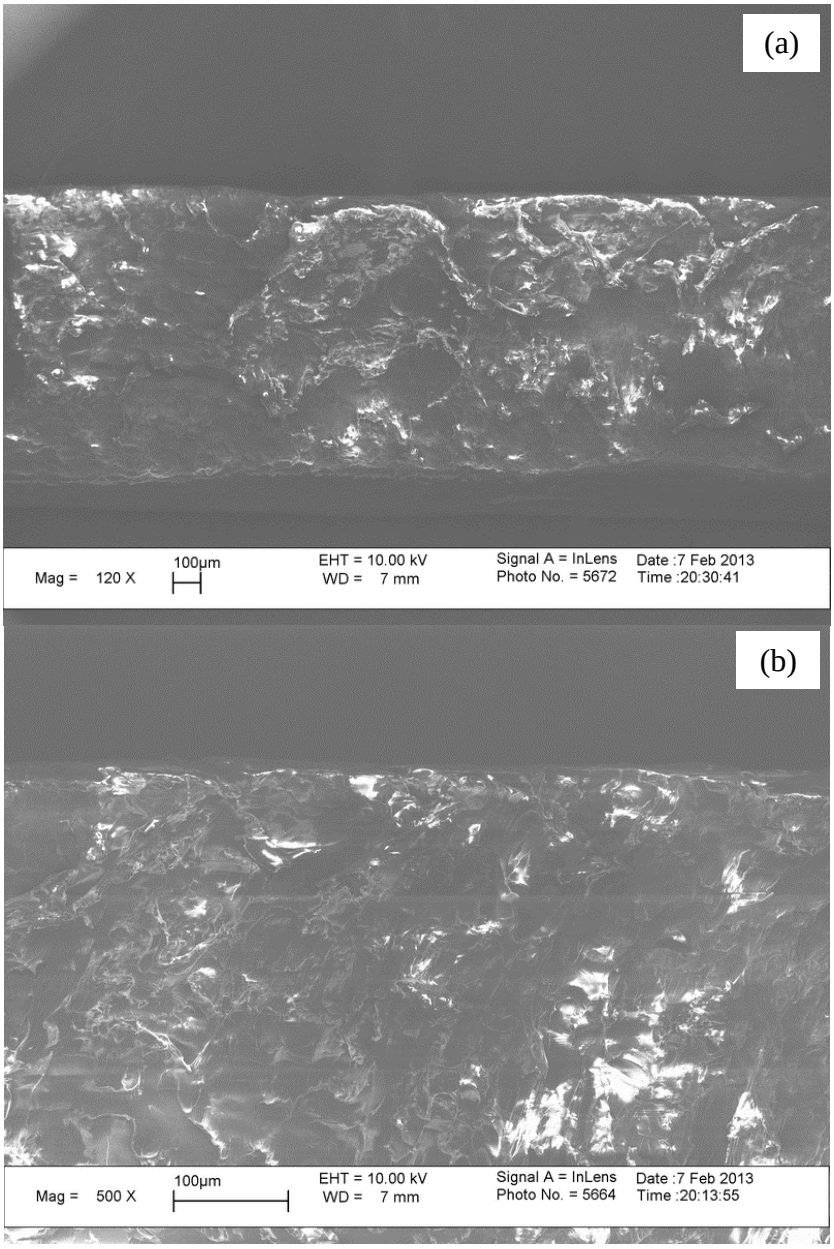

Figure 5.16 SEM of cross-section of 30ASP10HT (a) magnification 120X, (b) 500X.

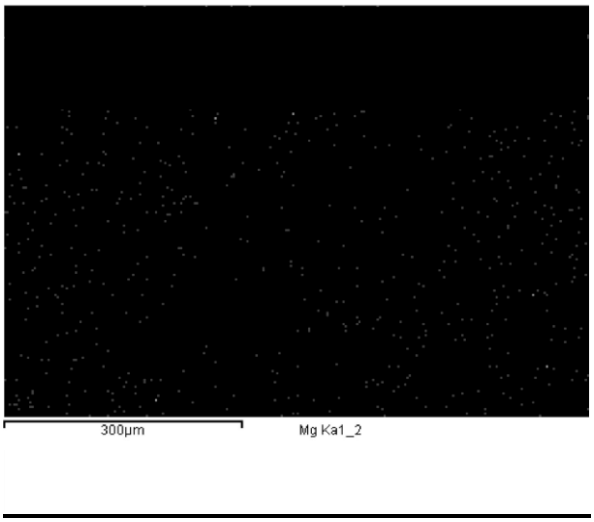

Figure 5.17 EDX Mg mapping of Figure 5.16 (b).

5.6 Dissolution Tests

The polymer nanocomposites containing 10% w/w of HT and various ASP concentrations showed a controlled-release ASP profile in the immediate-release tests in pH 7.4 medium; the extent of release inhibition strongly depends on the ASP concentration. The immediate-release test was performed in order to compare the ASP release profile with that of the delayed release, which involves two hours exposure in acidic conditions before returning to the pH 7.4 medium. In addition, the API release analysis using mathematical models is facilitated since the sample is tested under one pH condition and 100% of the API is still present in the sample at time t= 0. Figure 5.18 shows the dissolution profiles of the three nanocomposite formulations and that of ASP powder under the immediate release conditions of pH 7.4. For the 5ASP10HT sample, the ASP concentration reached approximately 95% over a period of six hours. The dissolution rate of 5ASP10HT is slightly slower compared to the ASP/Eudragit® L100-55 samples as reported in Chapter 4

in which 95% ASP release was reached over a period of four hours in all three formulations containing 10%-30% ASP. The release of ASP is retarded due to two reasons: Firstly, the presence of ASP intercalated HT slightly increases the nanocomposite tortuosity, resulting in longer time for the medium to reach the ASP However, according to SEM microphotographs, this effect may not be significant since the cross-section of 5ASP10HT at this HT concentration still shows a limited distribution of HT particles. The second mechanism which mainly contributes to the slower release of ASP is the intercalation of ASP into HT. Ion exchange between the phosphate ions in the pH 7.4 medium and the intercalated ASP must occur; then the ASP molecule is released from the HT and dissolves in the medium.

Remarkably, increasing the ASP concentration to 10% and 30% changes the ASP's release rate to about 90% over a 24 hours period and about 65% over a 48 hours period, respectively. Technically, prolonged-release as in this case is unnecessary for oral dosage forms due to the fact that the total gastrointestinal residence time is approximately 4-8 hours; it could be suitable, however, for implant or transdermal patch dosage forms requiring long term release over periods of days or weeks. The dramatic change of dissolution prolife for 10ASP10HT and 30ASP10HT is caused by the exfoliation of HT as confirmed by XRD results (partial exfoliation for 10ASP10HT and full exfoliation for 30ASP10HT).

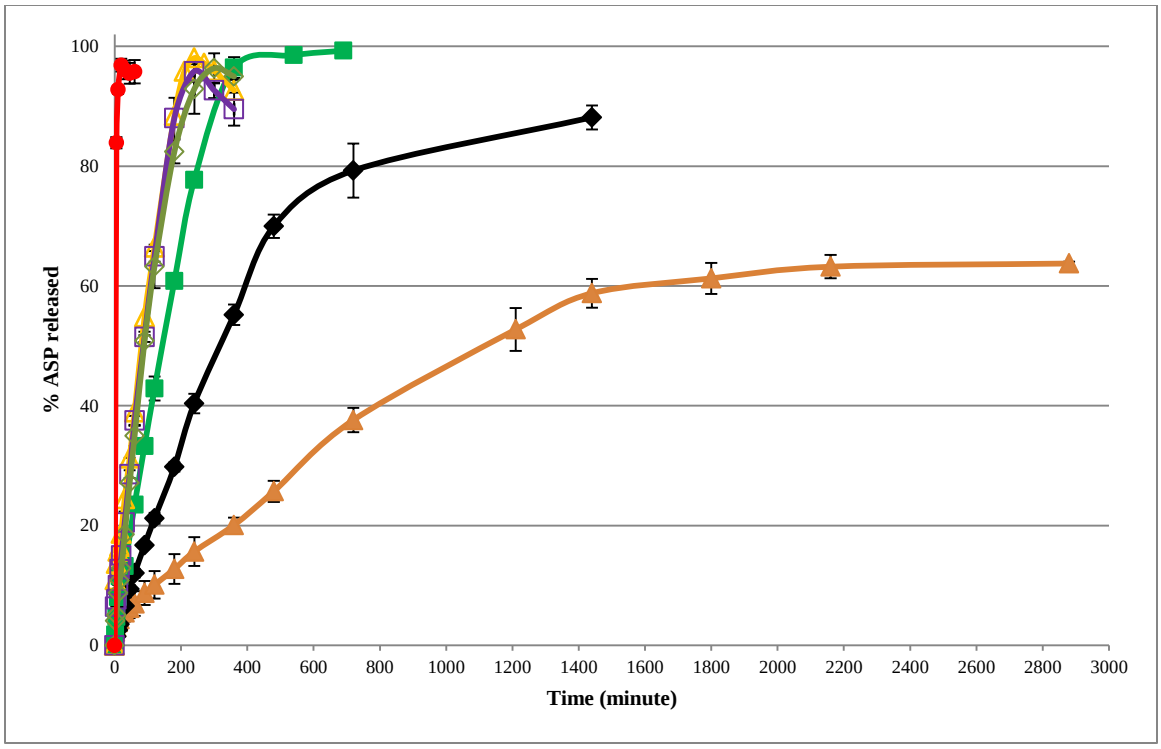

Figure 5.18 Immediate-release dissolution profiles (pH 7.4) (●) ASP, (◊) 10ASP, (□) 20ASP, (△) 30ASP, (■) 5ASP10HT, (♦) 10ASP10HT, (▲) 30ASP10HT.

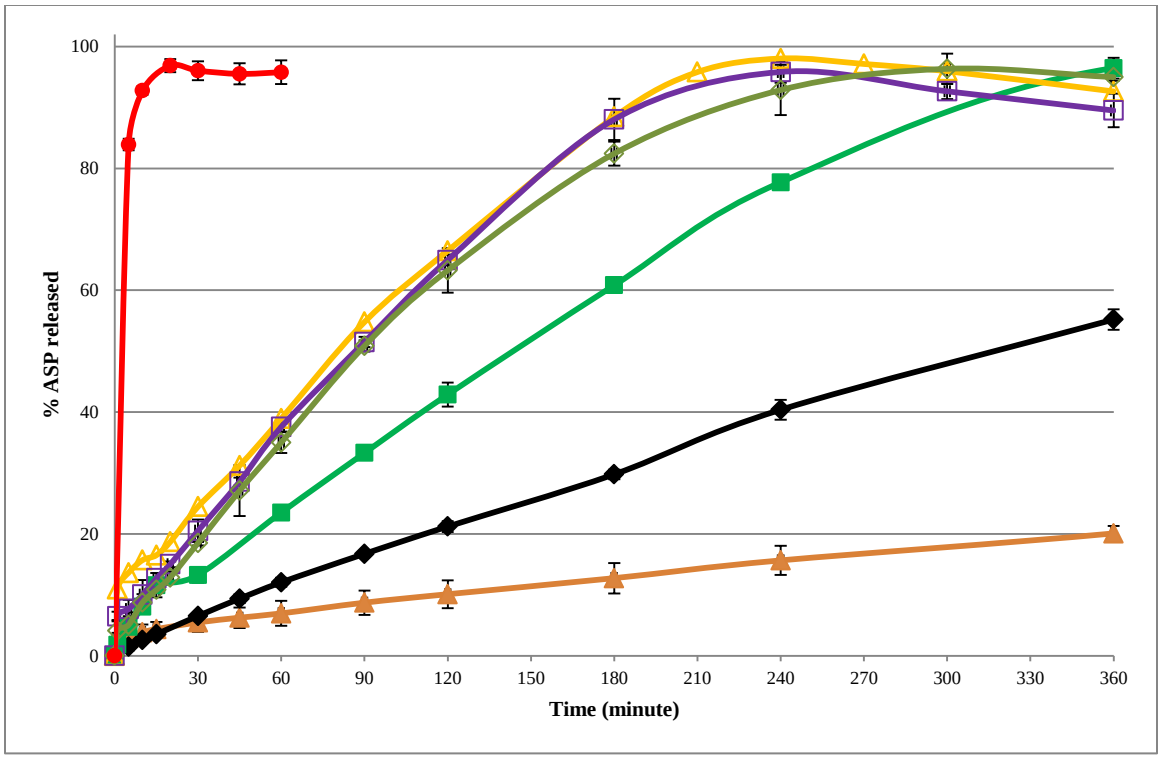

Figure 5.19 Immediate-release dissolution profiles (pH 7.4) in the first 6 hours of (●) ASP, (◊) 10ASP, (□) 20ASP, (△) 30ASP(■) 5ASP10HT, (♦) 10ASP10HT, (▲) 30ASP10HT.

Both 10ASP10HT and 30ASP10HT were not fully dissolved at the end of the dissolution test. A small fraction of the 10ASP10HT sample remained after undergoing 24 hours of dissolution while approximately 30-40% of the 30ASP10HT disc was left after about 48 hours.

An additional study was conducted by placing the 30ASP10HT samples in a beaker containing 1000 mL of pH 7.4 medium. A magnetic stirrer rotating at high speed was used to provide intensive mixing while the temperature was kept at 37°C. The time required for the discs to be fully dissolved was approximately 24 hours, resulting in a white turbid suspension. This study indicates that the solubility characteristics of the

polymer base, Eudragit® L100-55, are not altered and therefore, the change of the dissolution profile is due to the interaction between ASP and HT.

Polarized light microscopy images of the remaining 30ASP10HT disc after 48 hours of dissolution are shown in Figure 5.21. There is an opaque white layer adhering to the transparent layer of Eudragit® L100-55 (Figure 5.21 (a)) while this layer is illuminated in black color at 0° position (Figure 5.21 (b)). In the 0° position, ASP and HT are shown in black (Figure 5.20 (b) and (d)). Hence, this white layer is presumably a complex or salt of ASP-Al and ASP-Mg which is not dissolved within 48 hours under the standard experimental conditions.

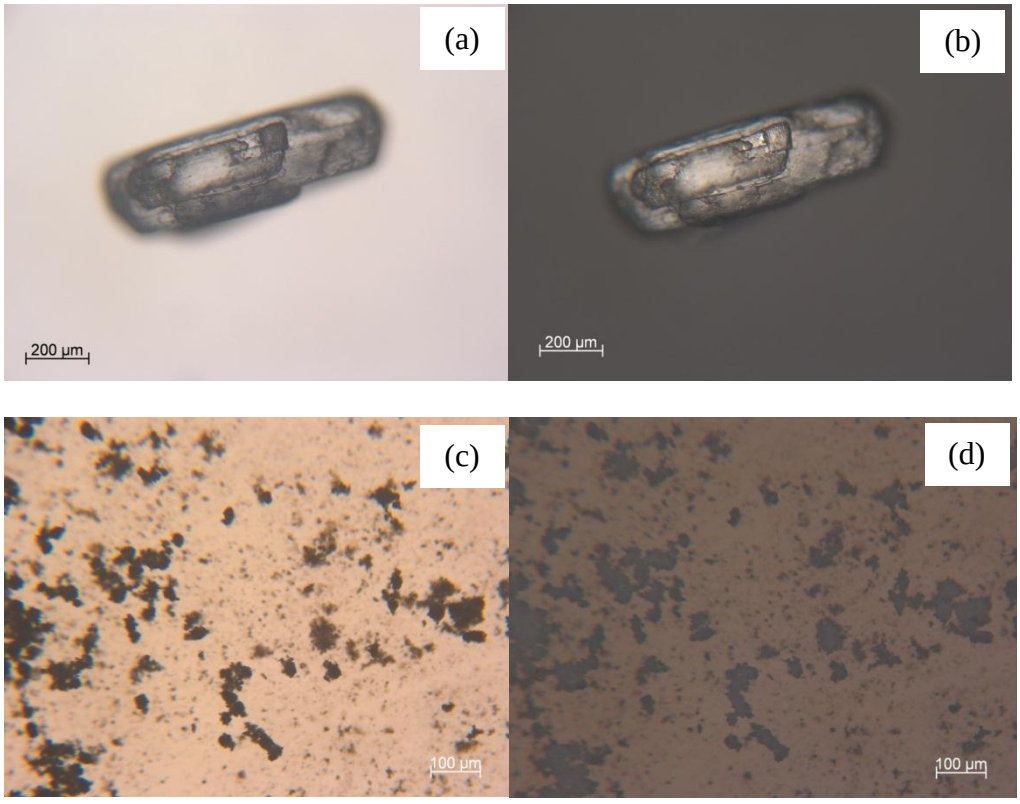

Figure 5.20 Polarized light microscopy of (a) ASP at 75° position (b) ASP at 0° position (c) HT at 75° position (d) HT at 0° position.

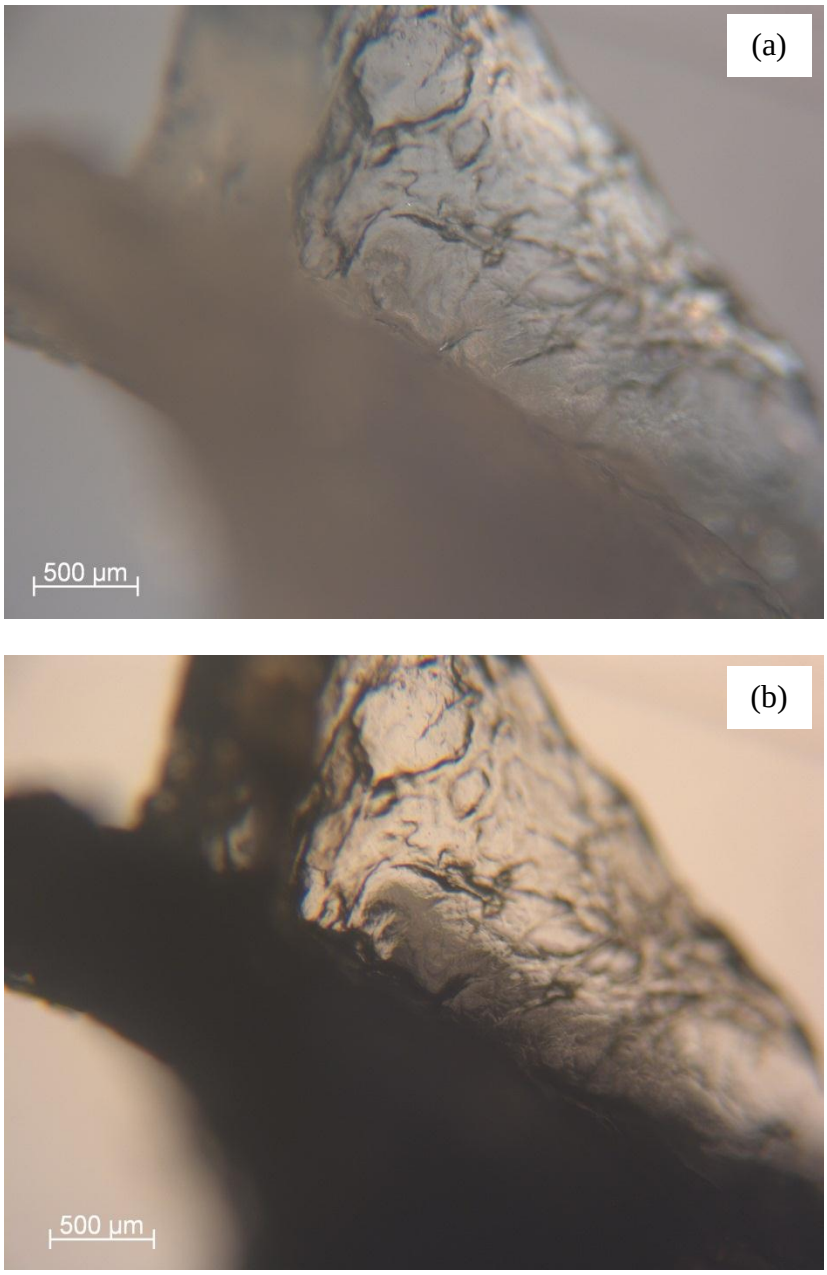

Figure 5.21 Polarized light microscopy of remaining 30ASP10HT after 48 hours of dissolution in pH 7.4 medium (a) 75° position (b) 0° position.

The heat flow of 30ASP10HT residue is measured using DSC from 25-500°C (Figure 5.22). Two broad endothermic peaks centered at approximately 200°C and 350°C could be the ASP-metal complex as observed in polarized light microscopy since HT also shows two endothermic peaks but at higher temperatures (270°C and 425°C).

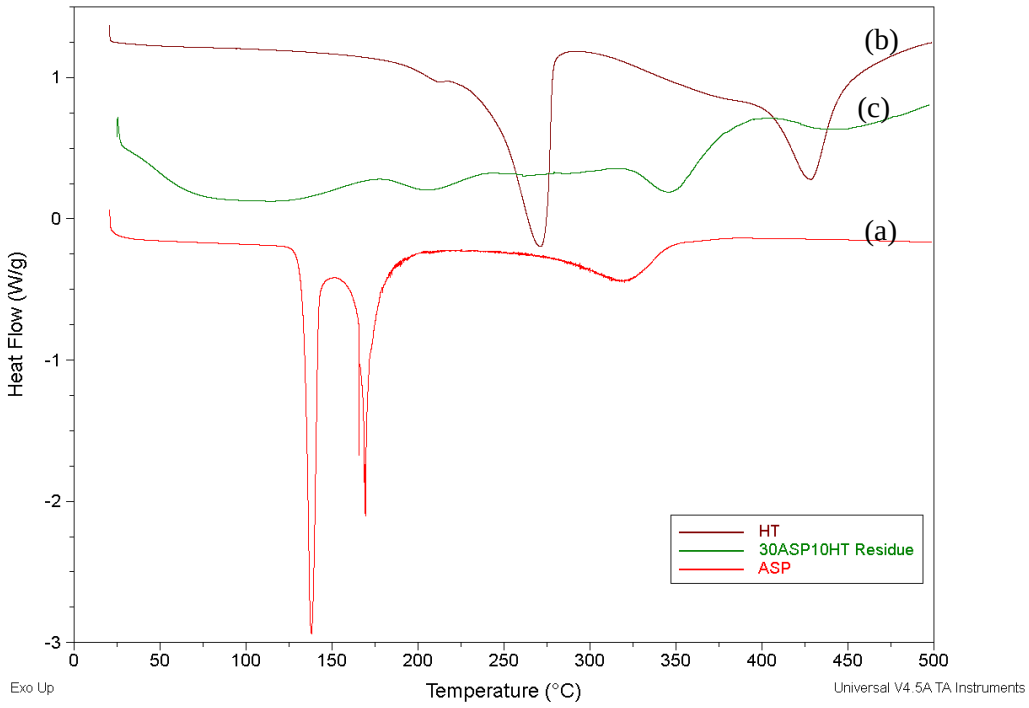

Figure 5.22 DSC heating results of (a) ASP, (b) HT, (c) 30ASP10HT residue.

The release of ASP from 10ASP10HT can be explained as follows: the exfoliated HT greatly increases the tortuosity which is observed in SEM images as more distribution of small HT particles throughout the cross-sectional area. Once the medium reaches the ASP-intercalated HT, ion-exchange and dissolution of ASP occur similarly to 5ASP10HT. The slower release of 10ASP10HT compared to 5ASP10HT is the result of the higher

degree of dispersion of the exfoliated HT. Note that 10ASP10HT also contains free ASP and the dissolution profile is controlled by the release of both free ASP and intercalated ASP, which, as mentioned earlier, cannot be quantitatively distinguished.

For 30ASP10HT, the higher HT degree of exfoliation is confirmed by XRD spectra and the percolating structure observed by SEM; this could be due to the formation of an ASP-metal salt as discussed in sections 5.1 and 5.3. The exfoliated HT greatly inhibits the diffusion of the medium to dissolve the free ASP; this results in approximately 65% ASP released over 48 hours. The remaining 35% ASP could be the ASP in the form of the ASP-metal complex which might require more than 48 hours to be released or a higher mixing intensity as shown by the magnetic stirrer study. Kaniwa and coworkers studied the bioavailability of aspirin vs. aspirin aluminum tablets (Kaniwa et al., 1981). The release rate of ASP from aspirin aluminum tablets was significantly slower than that of ASP tablets and the bioavailability was nearly 60% of that from ASP tablets. The authors conclude that the low bioavailability of ASP from aspirin aluminum tablets was caused by the slow release of ASP from the aluminum/ASP complex. The rate limiting step was the stage of release of free ASP from the metal complex.

The data in Table 5.3 are calculated using a curve fitting tool in MATLAB® with 95% confidence interval (CI) and R^2 greater than 0.99. Table 5.3 also provides information on Eudragit® L100-55 processed with only ASP as reported in Chapter 4 in order to compare the impact of added HT as a nanofiller. With only ASP in the polymer matrix (10-30%ASP), the exponent values in the Power Law Equation are between 0.5-1.0 indicating non-Fickian transport (Ritger and Peppas, 1987). At low ASP concentration, the n value of 0.86 is close to that of case II transport associated with polymer relaxation,

while at ASP loadings of 30% the n value of 0.59 is close to 0.5, associated with diffusion contribution. For polymer nanocomposites the exponent n values are also between 0.5-1.0 showing similar tendency of reduced n at higher ASP loadings. However, the rate constants responsible for diffusion (k_1) in the Peppas and Sahlin equation decrease with increasing ASP concentration in the polymer nanocomposites (Peppas and Sahlin, 1989). Since $k_1 = 4(D/\pi l^2)^{0.5}$ (Equation (4.2)), the decrease of k_1 indicates reduced diffusion coefficient, in other words, diffusion of the phosphate medium to the polymer nanocomposites samples while the ASP/Eudragit® L100-55 samples exhibit an opposite trend.

Ha and Xanthos reported values of n = 0.75 and 0.92 for the matrix of Eudragit® S100 containing 4%w/w diclofenac sodium and 10%w/w diclofenac/HT hybrid, respectively (Ha and Xanthos, 2011). The release mechanism for both samples was non-Fickian ($0.5 < n < 1.0$). However, the addition of the nanoclay hybrid has altered the release mechanism toward erosion. Yang and coworkers investigated the effect of nanoclay MMT on the property of acetaminophen-poly(ethylene glycol) matrix (Yang et al., 2010). The n value decreased form 1 for acetaminophen-poly(ethylene glycol) to about 0.7 for acetaminophen-MMT-poly(ethylene glycol), indicating that the drug release mechanism shifted from erosion dominant to anomalous.

Table 5.3 Calculated Model Parameters

Sample	Power law[1] $M_t/M_\infty = kt^n$	Peppas and Sahlin[2] $M_t/M_\infty = k_1t^{0.5} + k_2t$	
	n ± 95%CI	k_1 (%$min^{-0.5}$) ± 95%CI	k_2 (%$min^{-0.5}$) ± 95%CI
10ASP	0.86 ± 0.06	1.18 ± 0.44	0.43 ± 0.05
20ASP	0.78 ± 0.08	1.97 ± 0.63	0.36 ± 0.07
30ASP	0.59 ± 0.15	3.78 ± 1.66	0.18 ± 0.22
5ASP10HT	0.86 ± 0.09	1.44 ± 0.47	0.23 ± 0.04
10ASP10HT	0.78 ± 0.02	0.95 ± 0.13	0.13 ± 0.01
30ASP10HT	0.70 ± 0.04	0.71 ± 0.11	0.02 ± 0.01

[1] Ritger and Peppas, 1987
[2] Peppas and Sahlin, 1989

The delayed-release profile (Figure 5.23) is generated in order to investigate the effect of added HT to the nanocomposites integrity in acidic medium (stomach condition) and the change of the release profile once the pH is raised to 7.4 (small intestine condition). The HT is dissolved in acidic solution producing $MgCl_2$ and $AlCl_3$ (Ha, 2011). The dissolution of diclofenac/HT hybrid in pH 1.2 medium showed rapid release of diclofenac since the HT was quickly dissolved (Ha, 2011). Therefore, the dispersed HT in the nanocomposites might have an effect on the release profile when the composites are exposed to acidic conditions. All formulations met the USP32 delayed-release dissolution criteria since less than 10% ASP was released within two hours in the acid stage. In fact, the ASP released was found to be 3.0%, 6.2% and 6.1% for 5ASP10HT, 10ASP10HT and 30ASP10HT, respectively. After the pH was adjusted to pH 7.4, the dissolution profiles were similar to those of the immediate release study shown in Figure 5.18. Thus, the nanocomposites, in spite of the sensitivity of the hydrotalcite filler to low pH media, can withstand acidic conditions in the polymer used and maintain controlled release characteristics in the pH 7.4 medium.

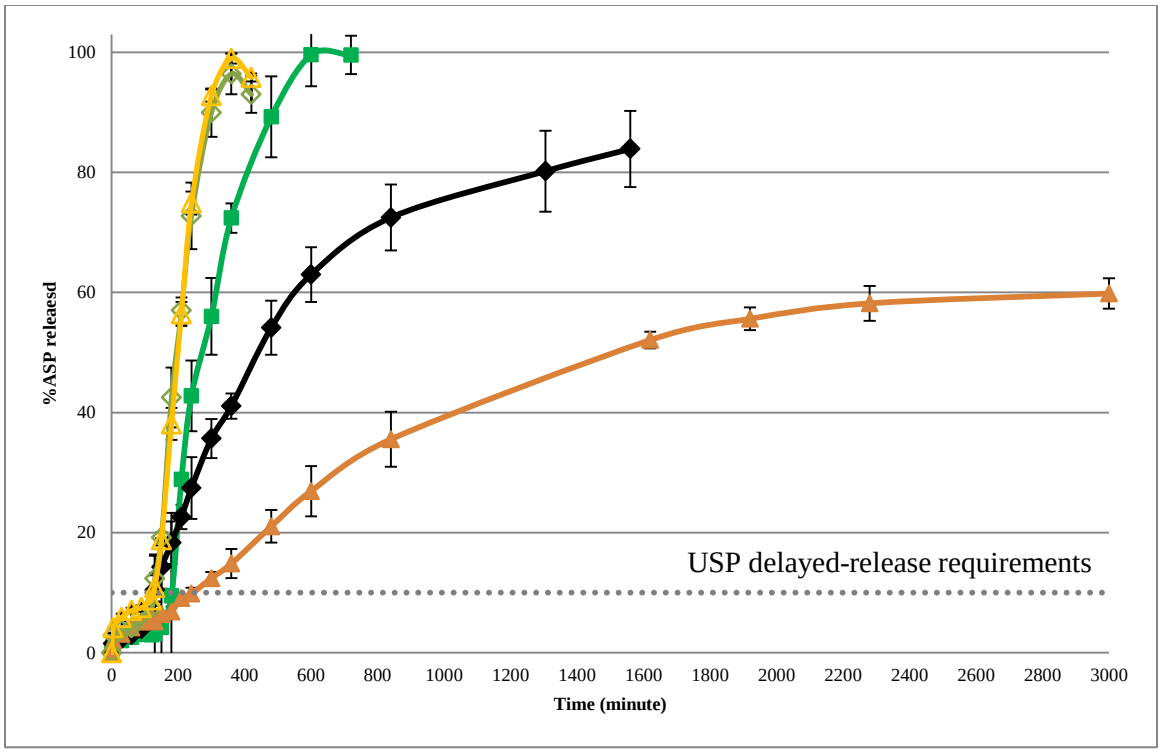

Figure 5.23 Delayed-release dissolution profile of (◊) 10ASP, (△) 30ASP(■) 5ASP10HT, (♦) 10ASP10HT, (▲) 30ASP10HT.

5.7 Rheological Results

Structural characterization and quantification of HT dispersion were investigated using rheological methods. The following points are worth mentioning when the nanocomposite samples were tested at 100°C: a) measurements are made above the T_g of most samples, b) ASP dissolves at elevated temperatures acting as a plasticizer, c) depending on the composition HT can exist in different degrees of agglomeration/exfoliation. As a result, viscosity measurements were performed at 80°C as shown in Figure 5.24. The viscosity is in the order of 30ASP10HT > 10ASP10HT > 5ASP10HT and as expected the degree of nanoclay dispersion had an effect on viscosity.

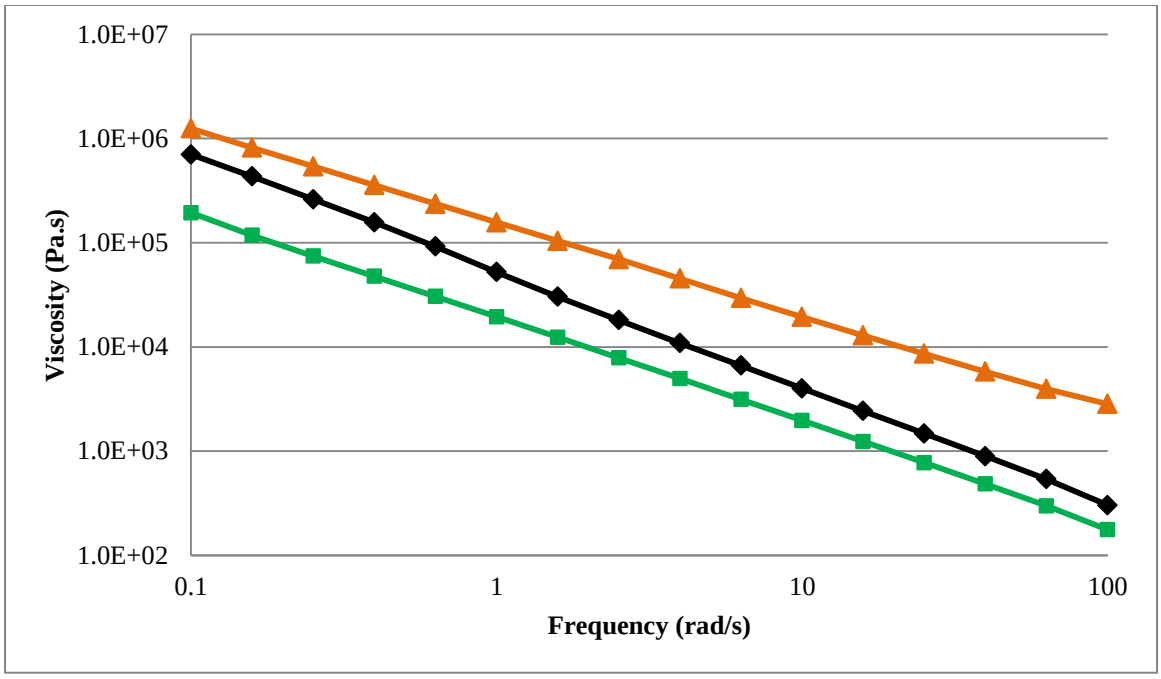

Figure 5.24 Viscosity vs. frequency curves measured at 80°C of (■) 5ASP10HT, (♦) 10ASP10HT, (▲) 30ASP10HT.

5.8 WVT Results

The permeability of the polymer can be altered by the presence of the nanoclays depending on their concentration, volume fraction, particle size, morphology, platelet orientation, etc. In general, adding impermeable nanoclays into the polymer results in decreased permeability due to an additional pathway (tortuosity) for solvents to pass through. The tortuosity can be further enhanced if nanoclays are fully dispersed to single platelets (exfoliation) compared to stacks of multiple platelets (agglomeration).

The barrier properties of the plasticized-polymer (without nanoclays) and polymer nanocomposites were tested using the ASTM E-96 standard water vapor method at room temperature. The measured weight loss of water from the sealed cup over a period of 168

hours (7 days) was plotted vs. time and the water vapor transmission rate (WVTR) was calculated from Equation (5.1).

$$WVTR = (G/t)/A \quad (5.1)$$

Where G is weight change from the straight line in g; t is time in hours; A is the test area (cup mouth area) in m^2. Note that, in this equation the sample thickness is not taken into account as suggested by ASTM E-96. Calculated WVTR values are shown in Tables 5.4 and 5.5.

Table 5.4 WVTR of Polymer Nanocomposites

Sample	Thickness	Slope	Cup mouth area	WVTR	Average WVTR	
	mm	g/hr	m^2	g/(hr.m^2)	g/(hr.m^2)	g/(d.m^2)
TEC/EUL	0.2634	0.0262	0.00181	14.486	13.823	331.74
	0.2146	0.0238	0.00181	13.159		
10HT	0.2547	0.0211	0.00181	11.666	11.279	270.70
	0.2355	0.0197	0.00181	10.892		
5ASP10HT	0.2479	0.0171	0.00181	9.455	9.842	236.20
	0.2974	0.0185	0.00181	10.229		
10ASP10HT	0.2273	0.0139	0.00181	7.685	7.519	180.47
	0.2758	0.0133	0.00181	7.354		
30ASP10HT	0.2147	0.0036	0.00181	1.990	2.101	50.42
	0.2687	0.0040	0.00181	2.212		

Table 5.5 Normalized WVTR of Polymer Nanocomposites

Sample	Thickness	WVTR	Normalized WVTR	Average normalized WVTR
	mm	g/(hr.m^2)	[g/(hr.m^2)]mm	[g/(hr.m^2)]mm
TEC/EUL	0.2634	14.486	3.816	3.320
	0.2146	13.159	2.824	
10HT	0.2547	11.666	2.971	2.768
	0.2355	10.892	2.565	
5ASP10HT	0.2479	9.455	2.344	2.693
	0.2974	10.229	3.042	
10ASP10HT	0.2273	7.685	1.747	1.887
	0.2758	7.354	2.028	
30ASP10HT	0.2147	1.990	0.427	0.511
	0.2687	2.212	0.594	

It is clear that the WVTR of the nanocomposites depends on the type of additive (HT vs. ASP/HT combinations) and the relative ratio of ASP/HT. It also appears that the system with the highest degree of HT exfoliation and slowest ASP release resulted in the lowest WVTR i.e. lowest permeability.

5.9 Mechanism of Intercalation and Exfoliation

The proposed mechanism taking place during the melt mixing in this study is illustrated in Figure 5.25. Without ASP in the formulation, HT is uniformly dispersed in the molten Eudragit® L100-55 during melt mixing in the batch mixer and present in an agglomerated form as the sample is cooled down to room temperature (Figure 5.25 (a)). The addition of ASP gradually changes the morphology of HT as a function of the ASP concentration. In the case of 5ASP10HT, ASP is first dissolved in the molten Eudragit® L100-55. Ion exchange then follows between the anionic ASP and the carbonate anions entrapped in HT's interlayer as a result of elevated temperatures and high shear. This is how the

intercalation process of ASP occurs as illustrated in Figure 5.24 (b). However, not all of HT molecules have intercalated ASP since the amount of ASP in the 5ASP10HT formulation is lower than the HT's AEC. Hence, there are HT particles left in a agglomerated phase.

Increasing the amount of ASP to 10% results in more ASP-intercalated HT molecules. Furthermore, exfoliated HT particles would have also been found in the 10ASP10HT sample. This could arise from the fact that the ratio of ASP to HT exceeds the AEC of HT (6.13 g of ASP to 10 g of HT). Since the mixing was carried out in the confined space of the batch mixer, therefore, there is a possibility that some HT molecules were continuously intercalating a higher amount of ASP during mixing. An excess ASP being forced to HT interlayer created unbalanced charge of MgAl(OH) positive layer, leading to the separation of HT layers.

When 30% ASP was mixed with 10%HT in the molten Eudragit® L100-55, a significant amount of ASP interacted with HT and resulted in much faster separation of the HT platelets compared to the other two formulations as shown in the onset of increasing torque after a certain mixing time. The amount of separated platelets is also higher than for 10ASP10HT. These exfoliated platelets bonded with ASP molecules through Al or Mg salts and formed a percolating network as the nanocomposites were cooled to room temperature, while the unbound ASP was recrystallized as regular ASP crystals.

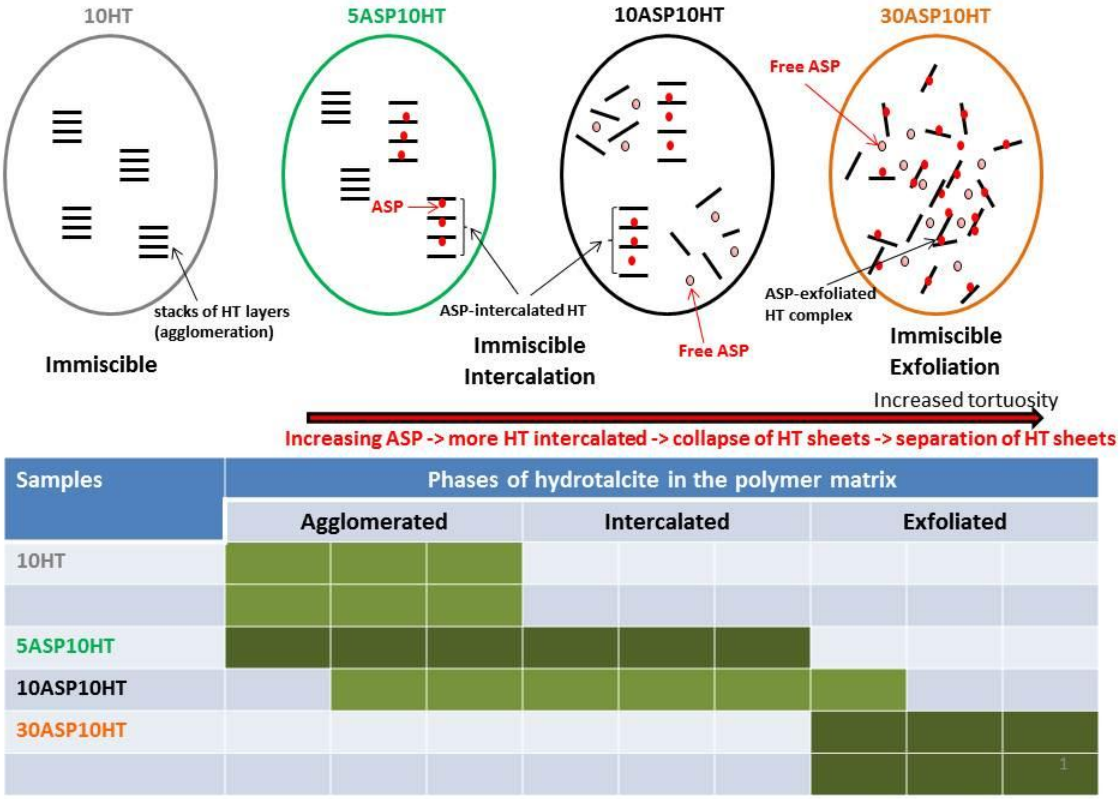

Figure 5.25 Proposed mechanism of intercalation and exfoliation in polymer nanocomposites prepared by hot-melt mixing with ASP and HT.

CHAPTER 6

API/ POLYMER MIXTURES: CAF/EUDRAGIT® L100-55

For CAF/Eudragit® L100-55, various CAF concentrations ranging from 10%-30%w/w are shown in Table 6.1.

Table 6.1 Sample Formulations Prepared by Hot-melt Mixing

System	Formulation	Component (%wt)		
		CAF	TEC	Eudragit® L100-55
API/plasticizer-polymer	10CAF	10	18	72
	20CAF	20	16	64
	30CAF	30	14	56

Solubility parameters obtained from the literature are shown in Table 6.2. The difference of solubility parameters among CAF, TEC and Eudragit® L100-55 shown in Table 6.2 is approximately 5.7-6.9, slightly close to maximum limit for a miscible system (difference in solubility parameter, 7.0).

Table 6.2 Solubility Parameters ($MPa^{1/2}$) for Components of Formulations

	CAFF	TEC	Eudragit® L100-55
Hildebrand[1]	26.8	22.2	21.1
Hansen[2]	25.6	20.9	22.3
Partial least square regression[3]	28.0	-	-
Experimental[4]	26.7	-	-

[1] Bustamante et al., 2011. Hildebrand solubility parameter to predict drug release from hydroxypropyl methylcellulose gels.
[2] Hansen, 2004. Polymer additives and solubility parameters.
[3] Tantishaiyakul et al., 2006. Prediction of solubility parameters using partial least square regression.
[4] Huu-Phuoc et al., 1986. Determination of partial solubility parameters of lactose by gas-solid chromatograph.

6.1 Mixing Process Monitoring

The evolution of torque for CAF/Eudragit® L100-55 is shown in Figure 6.1. Decreasing torque during mixing observed in Figure 6.1 indicated that CAF was dissolved in the molten Eudragit® L100-55 which was similar to the study of ASP/Eudragit® L100-55 system.

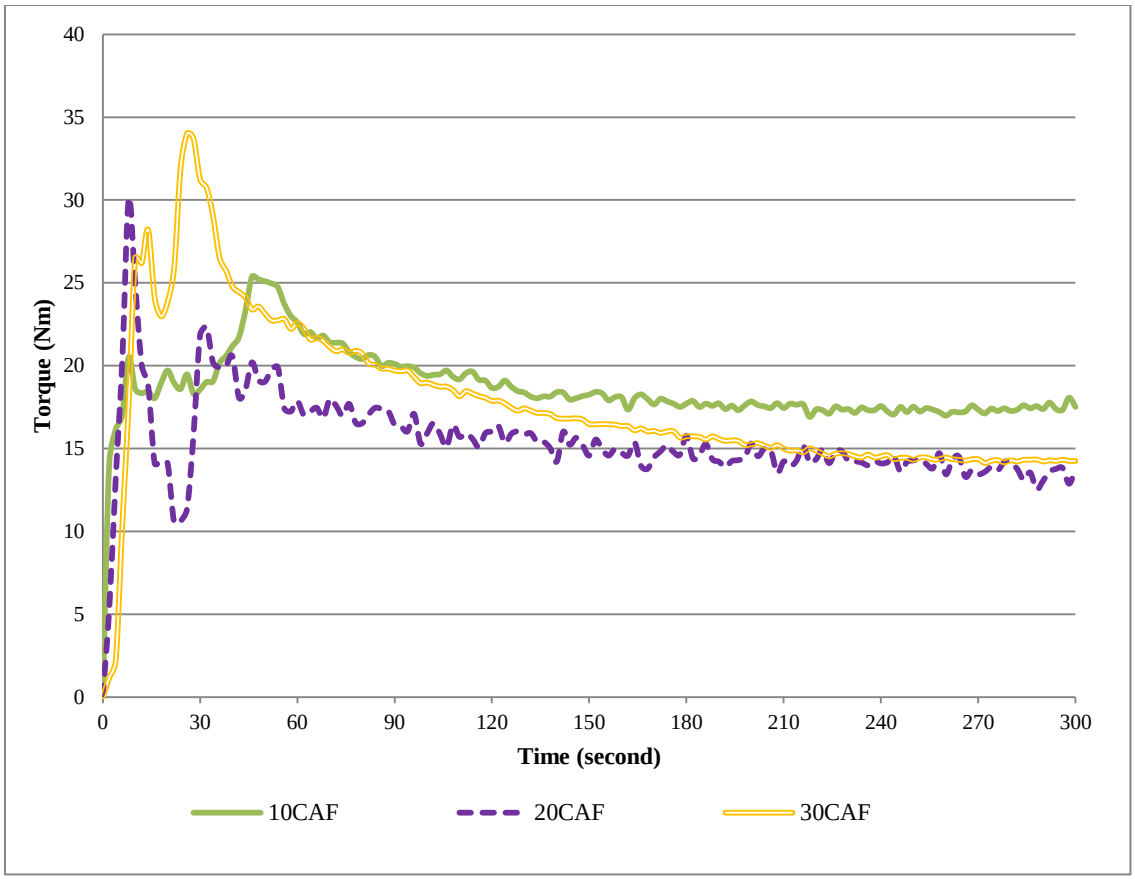

Figure 6.1 The evolution of torque of CAF/Eudragit® L100-55during melt mixing.

6.2 FTIR Results

The FTIR spectra of CAF, Eudragit® L100-55 are shown in Figure 6.2. CAF contains two carbonyl groups (>C=O) showing peaks between 1660-1700 cm^{-1} and one C=N with corresponding peaks in the range of 1640-1690 cm^{-1}. Hence, superimposed peaks are depicted at 1658 and 1701 cm^{-1} (Paradkar and Irudayaraj, 2002; Socrates, 2001). The peak at 1025 and 1359 cm^{-1} is attributed to the stretching mode of C-N. The C-H bond (stretching mode) of methyl group of the cyclic structure is shown at 2955 cm^{-1}. No new peaks are observed in the CAF/Eudragit® L100-55 samples while the intensity of the CH_x vibration attributed to the Eudragit® L100-55 shown at 1400 cm^{-1} decreased with increasing CAF loading. The characteristic peaks of CAF are clearly pronounced in 20CAF and 30CAF.

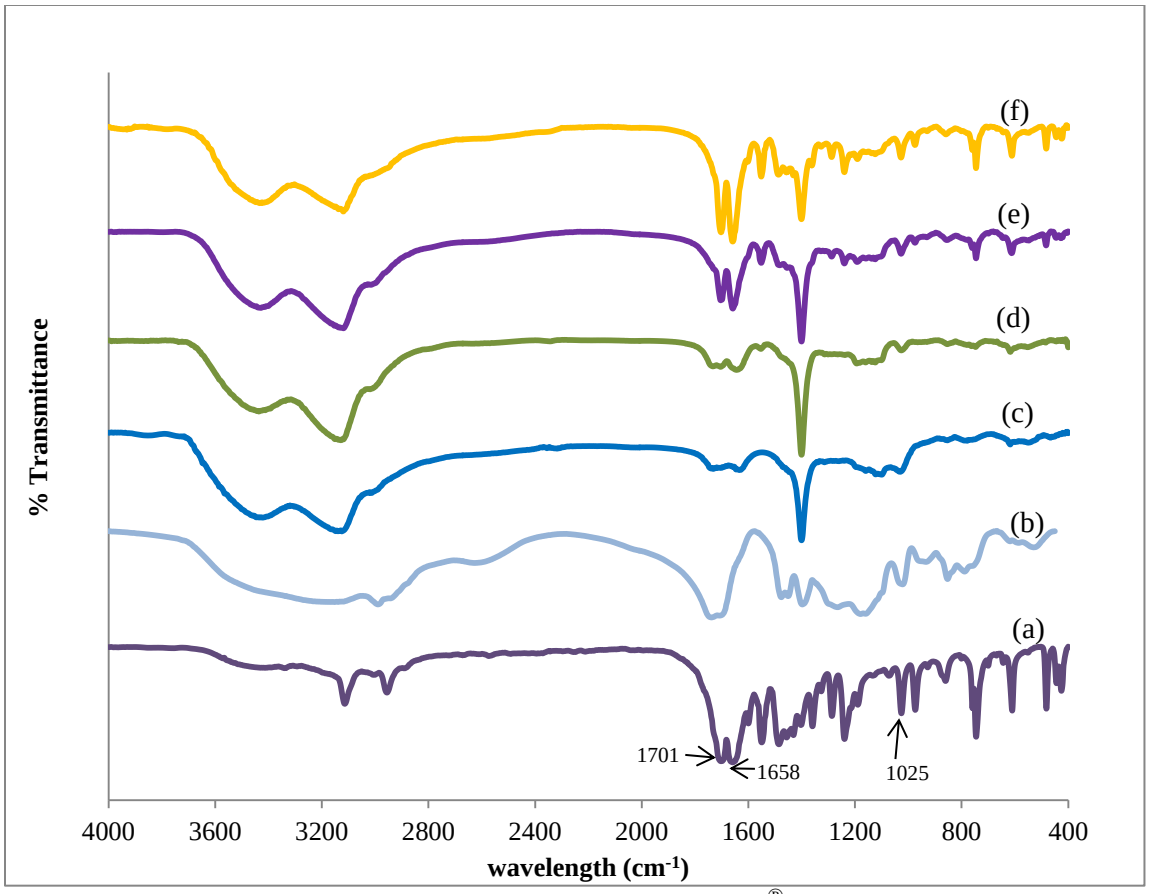

Figure 6.2 FTIR spectra of (a) CAF, (b) pristine Eudragit® L100-55, (c) TEC/EUL, (d) 10CAF, (e) 20CAF, (f) 30CAF.

6.3 XRD Results

From Figure 6.3 (a), CAF appears as a highly crystalline API like ASP due to the presence of several sharp peaks in the XRD spectrum. The processed samples (Figure 6.3 (d), (e) and (f)) also show strong peaks at the 2θ of the CAF's characteristic peaks, indicating that crystals of CAF are dispersed in the polymer matrix. Similarly to the ASP study CAF was dissolved in the Eudragit® L100-55 in the batch mixer and recrystallized at room temperature. Experimental results are quite in agreement with the miscibility with the polymer matrix predicted by solubility parameters.

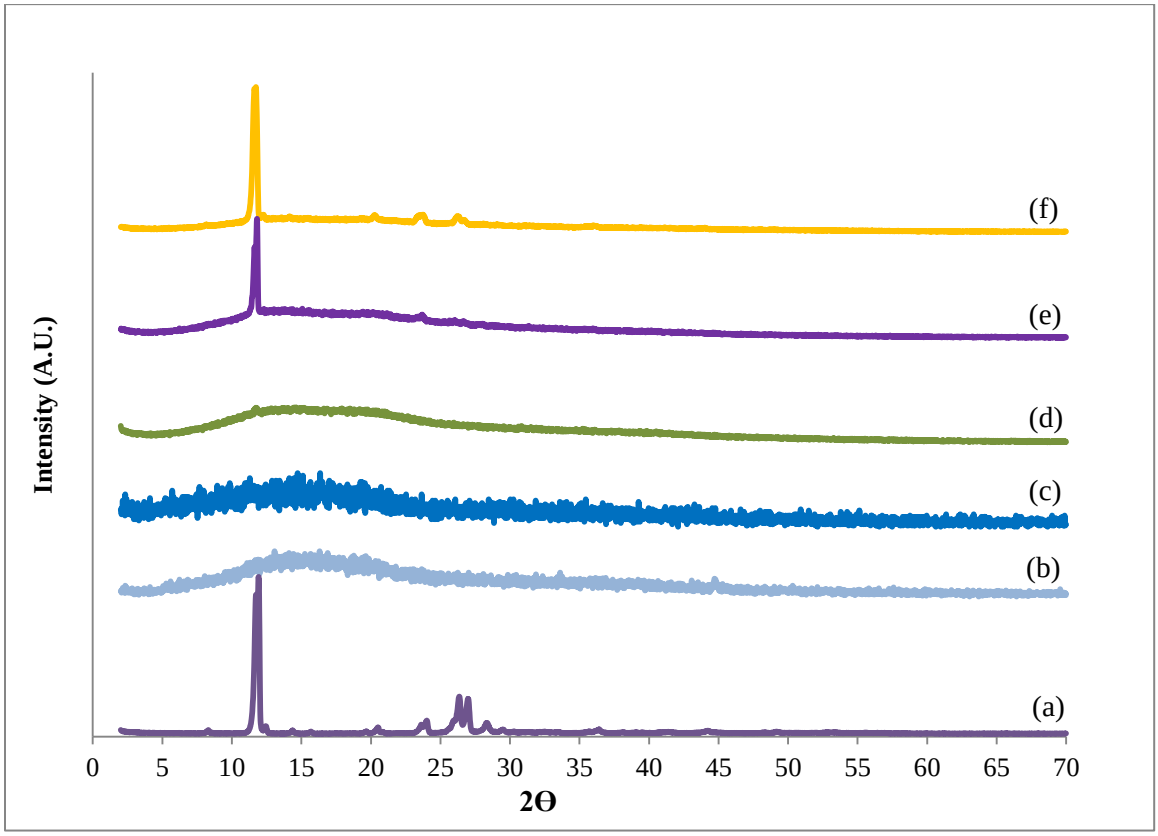

Figure 6.3 XRD spectra of (a) CAF, (b) pristine Eudragit® L100-55, (c) TEC/EUL, (d) 10CAF, (e) 20CAF, (f) 30CAF.

6.4 Dissolution Tests

The dissolution profile for CAF/Eudragit® L100-55 under pH 7.4 medium is shown in Figure 6.4. A sustained-release profile is obtained in the CAF/Eudragit® L100-55 system. After two hours of dissolution, CAF was released at 69.7%, 80.9% and 83.0% for 10CAF, 20CAF and 30CAF, respectively. In all formulations CAF release reached approximately 95% after three hours. Compared to ASP/Eudragit® L100-55 with identical API loading, ASP in all three concentrations (10%-30%) was released roughly 65% after two hours. CAF has higher solubility than ASP in pH 7.4, resulting in faster release rate. The curve fitting to power law and Pappas and Sahlin equations is shown table 6.3. The n values were between 0.5-1.0, indicating non-Fickian.

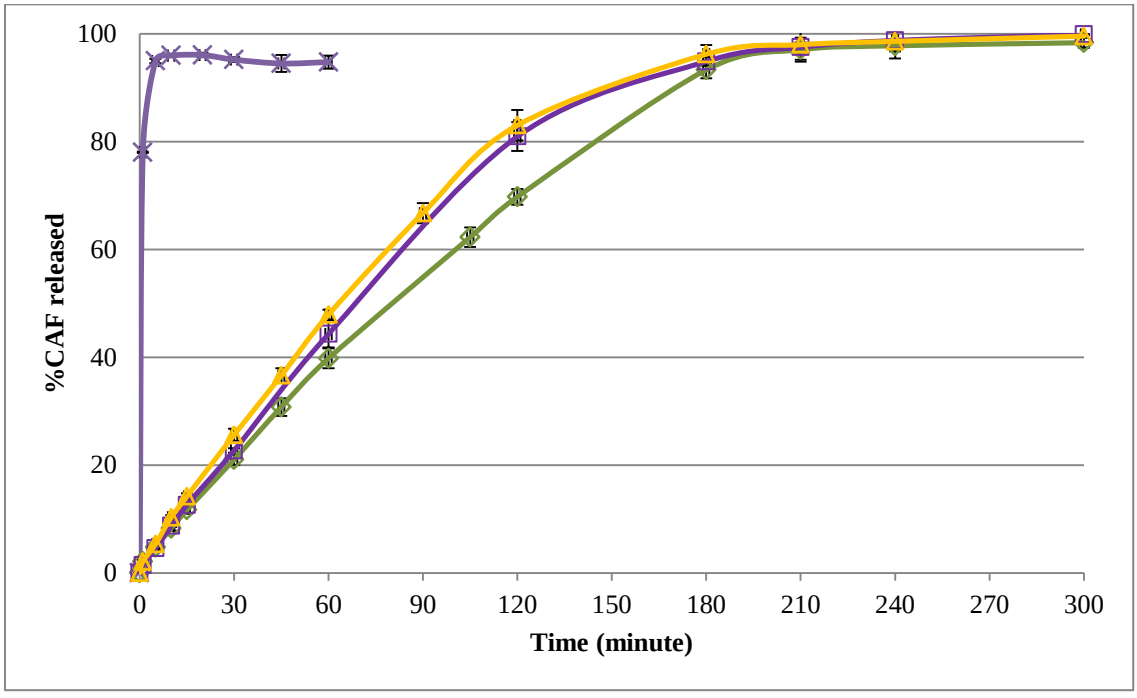

Figure 6.4 Immediate-release dissolution profiles (pH 7.4) of (x) CAF, (◊) 10CAF, (□) 20CAF, (△) 30CAF.

Table 6.3 Calculated Model Parameters

Sample	Power law[1] $M_t/M_\infty = kt^n$	Peppas and Sahlin[2] $M_t/M_\infty = k_1t^{0.5} + k_2t$	
	n ± 95%CI	k_1 (%min$^{-0.5}$) ± 95%CI	k_2 (%min$^{-0.5}$) ± 95%CI
10CAF	0.85 ± 0.03	1.31 ± 0.37	0.47 ± 0.05
20CAF	0.87 ± 0.03	1.11 ± 0.20	0.65 ± 0.03
30CAF	0.92 ± 0.04	0.65 ± 0.20	0.65 ± 0.03

[1] Ritger and Peppas, 1987
[2] Peppas and Sahlin, 1989

CHAPTER 7

API/NANOCLAY/POLYMER COMPOSITES: CAF/MMT/EULDRAGIT® L100-55

CAF loading in the polymer nanocomposites is varied from 5%-10%w/w while MMT was added at 10%w/w in all formulations. The TEC to Eudragit® L100-55 weight ratio was fixed at 1:4 in CAF/MMT/Eudragit® L100-55. The amount of CAF in the formulations was above CEC values of MMT which 1.80 g of CAF per 10 g of MMT (Appendix B).

Table 7.1 Sample Formulations Prepared by Hot-melt Mixing

System	Formulation	Components (%wt)			
		CAF	MMT	TEC	Eudragit® L100-55
Nanoclays/plasticizer -polymer	10MMT	-	10	18	72
API/nanoclays/ plasticizer-polymer	5CAF10MMT	5	10	17	68
	10CAF10MMT	10	10	16	64
	30CAF10MMT	30	10	12	48

7.1 Mixing Process Monitoring

The evolution of torque for CAF/MMT/Eudragit® L100-55 is demonstrated in Figure 7.1. In the presence of MMT, CAF/MMT/Eudragit® L100-55 samples also showed gradual decrease of torque toward the end of the mixing process. Therefore, it is suggested that no strong interactions occurred among CAF, MMT and Eudragit® L100-55. There was a human error when the 5CAF10MMT pre-mixed sample was added to the batch mixer, resulting in slightly slower feeding of the pre-mixed materials.

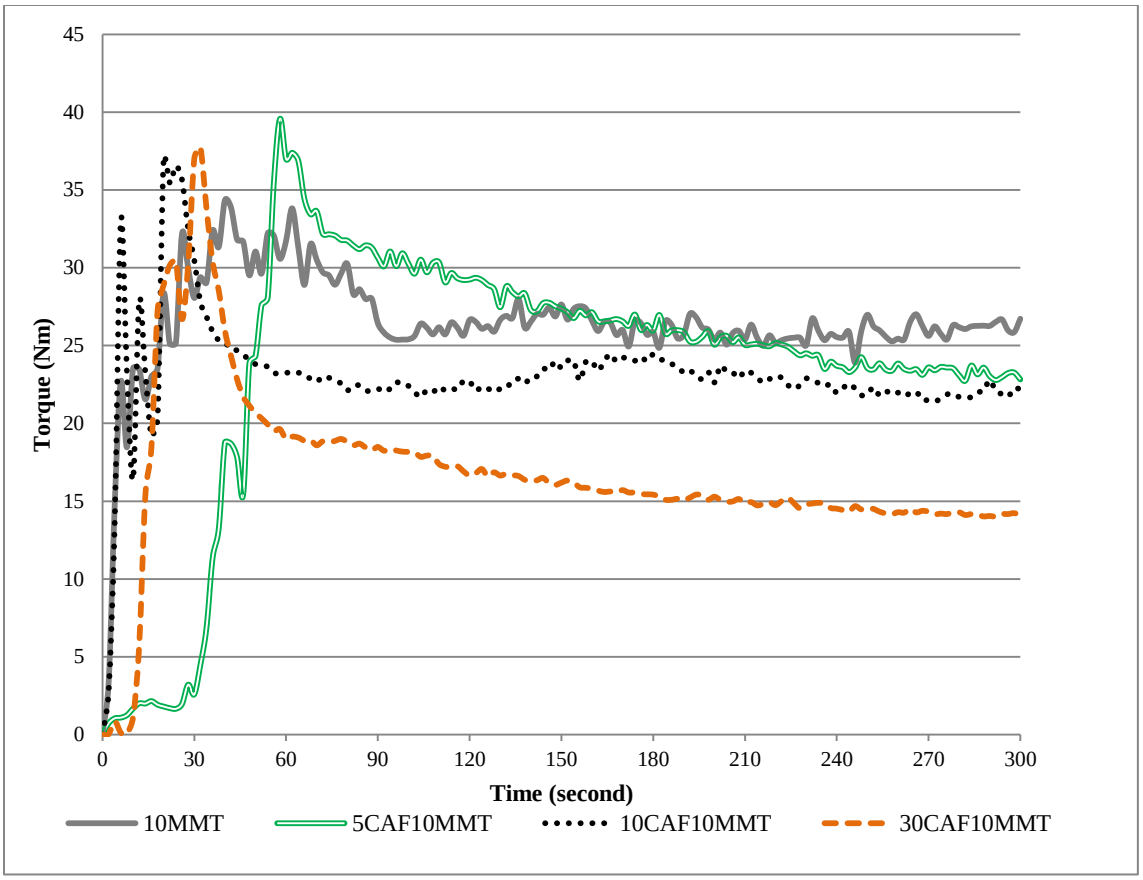

Figure 7.1 The evolution of torque of MMT/ Eudragit® L100-55 and CAF/MMT/Eudragit® L100-55 during melt mixing.

7.2 FTIR Results

Figure 7.2 contains FTIR spectra of MMT and CAF/MMT/Eudragit® L100-55 nanocomposites. For MMT, the peaks at 3632 and 3437 cm^{-1} are the stretching vibration of the O-H bonds in Al-OH and absorbed water in the interlayers. The Si-O stretching (in-plane) vibration and the Al-Al-OH bending vibration in the octahedral layer correspond to the peaks at 1026 and 917 cm^{-1}, respectively (Joshi et al., 2010). The Si-O bending vibration appears at 529 cm^{-1} (Fan, 2011). In Figure 7.2 (c), 10MMT shows MMT's peaks centered at 1027 and 463 cm^{-1} attributed to Si-O stretching (in-plane) vibration and Si-O bending vibration, respectively. The C=O vibration mode responsible

for the esterified group and the carboxylic group of Eudragit® L100-55 are observed at 1737 and 1703 cm^{-1}, respectively. The CH_x vibration of Eudragit® L100-55 still dominates at 1400 cm^{-1}. All CAF/MMT/Eudragit® L100-55 nanocomposites display both characteristic peaks of MMT and CAF at their original wavelengths. There are no new peaks in the nanocomposites, indicating no interactions among CAF, MMT and Eudragit® L100-55.

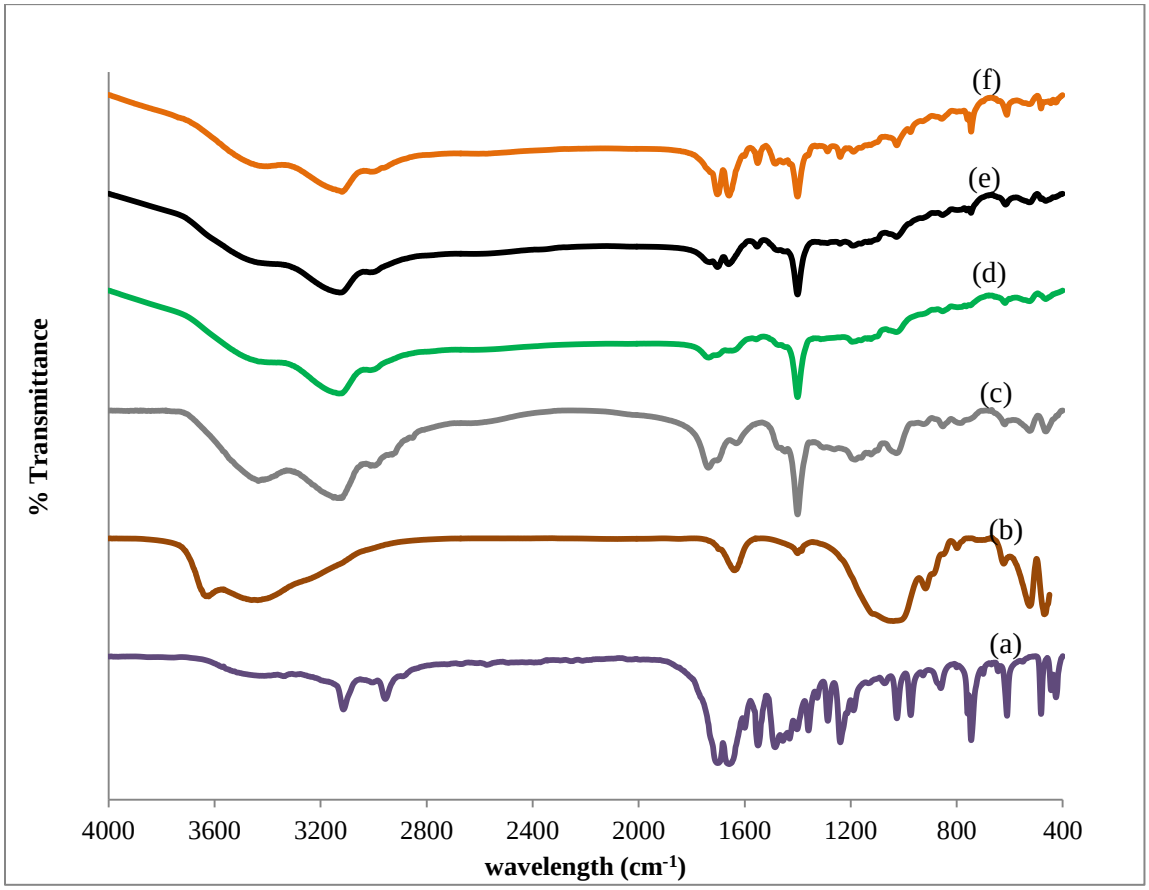

Figure 7.2 FTIR spectra of (a) CAF, (b) MMT, (c) 10MMT, (d) 5CAF10MMT, (e) 10CAF10MMT, (f) 30CAF10MMT.

7.3 XRD Results

XRD spectra of the polymer nanocomoposites are illustrated in Figure 7.3. Two sharp peaks of MMT as observed in Figure 7.3 (b) are associated with planes (001) and (002) (Patel et al., 2006). The strong peak around 7.50θ indicates that the original basal spacing (d_{001}) is 1.17 nm. In Figure 7.3 (c), 10MMT exhibits identical peaks as found in MMT which suggests that no interactions between polymer chain and MMT occur. This lack of change of the 10MMT basal space was similar to that of the 10HT in anionic system reported in Chapter 5. However, as the API is introduced to nanoclays/polymer, a difference is shown between the cationic polymer nanocomposites (CAF/MMT/Eudragit® L100-55) and the anionic nanocomposites (ASP/HT/Eudragit® L100-55). d_{001} of MMT located at 7.50θ is shown in all CAF/MMT/Eudragit® L100-55 nanocomposites (Figure 7.3 (d), (e) and (f)) without any shift of the 2θ angle whilst the characteristic peaks of CAF are found at the original 2θ angle except for 5CAFF10MMT due to the low concentration of CAF. The lack of change of the location of the MMT d_{001} implies that intercalation does not take place upon the addition of CAF to MMT/Eudragit® L100-55 which was not the case for the anionic nanocomposites systems. One plausible reason is that CAF is a weak base (pKa = 14.0), therefore CAF is less likely to be protonated. MMT processed with acetaminophen (pKa =9.51) and poly(ethylene glycol) in the identical batch mixer (50 rpm and 100°C for 6 minutes) also show gradual decreased torque toward the end of melt mixing; MMT in the processed sample was presence in agglomeration phase according to XRD spectrum (Yang et al., 2010). The intercalation of dapsone into MMT was successfully conducted by adding ionized dapsone solution into MMT suspension (Fan, 2011), resulting in the increase of the basal spacing of MMT.

Dapsone has two pKa values, 1.3 and 2.4 due to two ionizable amino groups (Fan, 2011). Hence, API's pKa might be a factor facilitating intercalation of MMT.

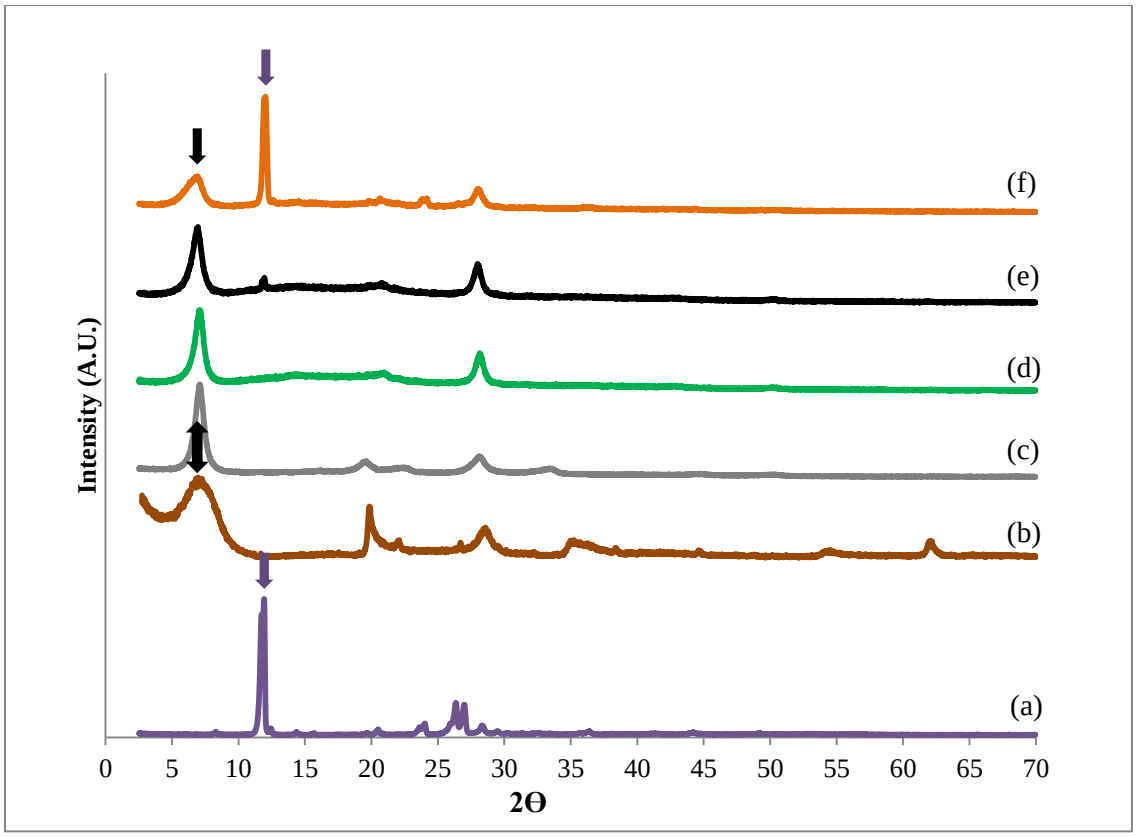

Figure 7.3 XRD spectra of (a) CAF, (b) MMT, (c) 10MMT, (d) 5CAF10MMT, (e) 10CAF10MMT, (f) 30CAF10MMT.

7.4 Dissolution Tests

In the presence of MMT, the release of CAFF was prolonged to a certain degree (Figure 7.4). After 3 hours, CAF release was found to be 77.2%, 79.9% and 83.2% for 5CAF10MMT, 10CAF10MMT and 30CAF10MMT, respectively. To achieve roughly 95% CAF release, all formulations required up to six hours of dissolution as compared to only three hours in the formulations without MMT.

Yang et al. studied the binary and ternary mixtures of acetaminophen (APAP), MMT (Closite® 15A and Closite® 30B) and poly(ethylene glycol) (PEO) prepared by hot-melt mixing using the batch mixer as used in this work (Yang et al., 2010). The complete release of APAP from the binary system (APAP/PEO) was roughly one hour while for the ternary system (APAP/MMT/PEO) was 6 hours. Furthermore, the contact angle of the dissolution medium on the surface of 10APAP is ten degrees smaller than 10APAP10Closite® 30B). Hence, it was suggested that the retardation in the release was possibly caused by the decrease of wettability in the presence of MMT.

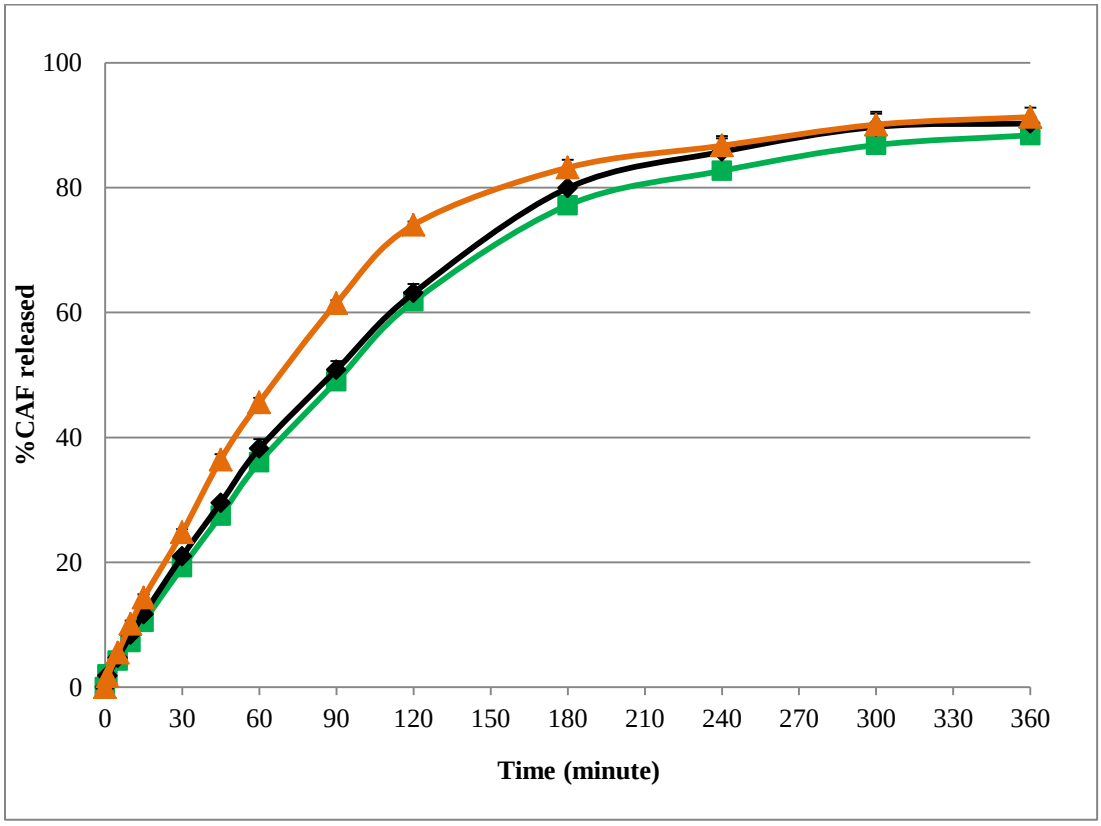

Figure 7.4 Immediate-release dissolution profiles (pH 7.4) of (■) 5CAF10MMT, (♦) 10CAF10MMT, (▲) 30CAF10MMT.

According to XRD results, the morphology of MMT in all CAF/MMT/Eudragit® L100-55 composites contains an agglomerated phase. In the presence of MMT for 90% release the dissolution time was extended from three hours (CAF/Eudragit® L100-55) to six hours (CAF/MMT/Eudragit® L100-55). Unlike the CAF/MMT/Eudragit® L100-55 system, ASP/HT/Eudragit® L100-55 samples contained HT with intercalation and exfoliation phases resulting in the tremendous prolonged-release of ASP from the nanocomposites. Table 7.2 compares the %API release vs. time for ASP/HT/Eudragit® L100-55 and CAF/MMT/Eudragit® L100-55.

Table 7.2 %API Release of Anionic and Cationic Polymer Nanocomposites

Sample	**Time (hour)**	**%API released (pH 7.4 medium)**			
		10ASP	**10ASP10HT**	**10CAF**	**10CAF10MMT**
10%API	0.5	18.5	6.5	21.0	21.0
	1	35.0	12.0	39.8	38.2
	2	63.2	21.2	69.7	63.1
	3	82.4	29.8	93.3	79.9
	4	92.9	40.4	97.8	85.7
	5	96.3	47.4	98.3	89.7
	6	95.0	55.2		93.3
	8		70.0		
	12		79.3		
	24		88.1		
Sample	**Time (hour)**	**30ASP**	**30ASP10HT**	**30CAF**	**30CAF10MMT**
30%API	0.5	24.5	5.5	25.6	24.8
	1	38.9	7.0	47.9	45.6
	2	66.5	10.1	83.0	74.0
	3	88.4	12.7	96.2	83.2
	4	98.0	15.7	98.6	86.7
	5	95.9	18.5	99.5	90.1
	6	92.6	20.1		94.3
	8		25.7		
	12		37.6		
	24		58.8		

The dissolution data are plotted to fit Power law and Peppas and Sahlin equations as shown in Table 7.3. According to power law equation, the n value of both CAF/Eudragit® L100 and CAF/MMT/Eudragit® L100 is between 0.5-1.0, indicating non-Fickian release mechanism.

Table 7.3 Calculated Model Parameters

Sample	Power law[1] $M_t/M_\infty = kt^n$	Peppas and Sahlin[2] $M_t/M_\infty = k_1t^{0.5} + k_2t$	
	n ± 95%CI	k_1 (%min$^{-0.5}$) ± 95%CI	k_2 (%min$^{-0.5}$) ± 95%CI
10CAF	0.85 ± 0.03	1.31 ± 0.37	0.47 ± 0.05
20CAF	0.87 ± 0.03	1.11 ± 0.20	0.65 ± 0.03
30CAF	0.92 ± 0.04	0.65 ± 0.20	0.65 ± 0.03
5CAF10MMT	0.83 ± 0.03	1.33 ± 0.38	0.40 ± 0.04
10CAF10MMT	0.83 ± 0.03	1.79 ± 0.48	0.50 ± 0.05
30CAF10MMT	0.81 ± 0.03	1.78 ± 0.57	0.50 ± 0.07

[1] Ritger and Peppas, 1987
[2] Peppas and Sahlin, 1989

CHAPTER 8

CONCLUDING REMARKS AND SUGGESTED FUTURE STUDIES

8.1 Summary

Four modified-release systems were investigated in this dissertation. All systems were prepared by HMM in the batch mixer. The carrier was poly(methacrylic acid-co-ethyl acrylate), Eudragit® 100-55 which is designed to be dissolved in water above pH 5.5. The first system discussed in Chapter 4 was the enteric matrix containing thermally-sensitive anionic API (ASP) while the second system reported in Chapter 5 was the polymer nanocomposite containing the same API but with the addition of anionic nanoclay (HT) in order to modify the API release from the original enteric matrix. The second API, CAF, representing a cationic API was investigated as the third system in Chapter 6. The fourth system included the addition of a cationic nanoclay (MMT) to the third system and was reported in Chapter 7.

For the first system, preliminary studies based on thermal analysis were used to determine the optimum processing conditions. Samples of the enteric matrix containing 10-30%w/w of ASP were successfully prepared without significant degradation of ASP. The ASP was recrystallized upon cooling to room temperature at all three concentrations, indicating an immiscible system even if a miscible system was suggested by applying solubility parameters estimation based on Hildebrand and Hansen methods. Therefore, these ASP-enteric matrix samples can be classified at room temperature as solid dispersions and, more specifically, glass suspensions in which a crystalline API is dispersed in the amorphous polymer. However, miscibility was apparent at high

temperatures where ASP acted as a plasticizer by reducing the T_g and melt viscosity of the matrix. The crystalline form of ASP in the matrix at room temperature was confirmed by XRD and SEM. Degree of crystallinity and ASP loading showed no significant impact on dissolution profiles for either immediate or delayed-release. In the delayed-dissolution test, an enteric property (resistance to acidic pH) was obtained and the sustained-release profile was exhibited as the pH value was raised to 7.4. The API release mechanism using power law was non-Fickian ($0.5<n<1.0$) and the tendency approached diffusion ($n=0.5$) with increasing ASP concentrations. The curved fitting to Peppas and Sahlin equation showed also higher diffusion coefficient at higher ASP loading. This enteric matrix would be suitable for low-dose ASP (60-81 mg) dosage form. With 30%w/w of ASP, the final enteric tablet (matrix) can be approximately 180-240 mg which is the size of regular tablets. Therefore, HMM can deliver an enteric dosage form by dispersing API in the enteric polymer; this technique allows fewer unit operations compared to the enteric-coated tablet process.

The second system can be considered as a polymer nanocomposite since the additional component was nanoclays typically employed in plastic-based materials. The dispersion of the impermeable nanoclays is expected to reduce the nanocomposite permeability. Limited dispersion of HT in Eudragit® 100-55 was found (no intercalation or exfoliation), suggesting poor chemical affinity between the polymer and the selected nanoclay or inadequate processing conditions. With the addition of ASP, HT dispersion was dramatically improved resulting in change of the HT morphology from agglomeration to exfoliation. From a polymer engineering perspective, ASP in this work can be considered as a compatibilizer and the modified morphology was greatly

dependent on the ASP concentrations. The intercalation of HT may occur by the insertion of both ASP molecules and Eudragit® L100-55 polymer chains. More than 1 phases of HT were apparent for the two lowest ASP concentrations (5% and 10%ASP) and reduced permeability was observed from both dissolution and water vapor transmission studies. The agglomerated HT and ASP-intercalated HT were found in 5ASP10HT, resulting in slightly prolonged release of ASP in the pH 7.4 dissolution test compared to ASP/Eudragit® L100-55 samples. 10ASP10HT also exhibited two phases but somewhat different from 5ASP10HT being ASP-intercalated HT and partially exfoliated HT. The partially exfoliated HT dispersed throughout the nanocomposite increased the tortuosity and thus significantly retarded permeation of pH 7.4 medium to penetrate and dissolve ASP molecules.

The highest ASP concentration (30%w/w) produced the lowest permeation as a result of the dispersion of exfoliated HT. This may also be related to the AEC of the HT. During HMM in the batch mixer, the amount of ASP above the HT's AEC (as for example, 30%ASP per 10%w/w HT) led to (a) the delamination of HT to individual HT platelets, (b) some ASP molecules to be bonded with these HT platelets and form ASP-Al and ASP -Mg salts and (c) recrystallization of the remaining ASP molecules as free ASP when the sample was cooled down. Hence, AEC is a factor that should be considered when the added component has a potential interaction with the nanoclay. According to the power law the API release mechanism was determined to be Non-Fickian However, the diffusion coefficient determined from the Peppas and Sahlin equation decreased with increasing ASP concentrations.

It is not always the case in which strong interactions between API and nanoclay occurs during melt mixing, resulting in the modification of the nanoclay's morphology (intercalation and exfoliation). 10%w/w MMT was processed with 10%w/w ASP under identical HMM conditions (Appendix C) without any dramatic increase of torque during the entire 5-minute mixing time. MMT was found in an agglomerated phase and the release profile of ASP was slightly prolonged compared to ASP/Eudragit® L100-55 samples but was not as long as for the ASP/HT/Eudragit® L100-55 samples.

In the third system, 10%-30%w/w of CAF was processed with plasticized Eudragit® L100-55 under identical conditions as for the first system. CAF in crystalline form was observed in the API/polymer blends after cooling; the calculated solubility parameters estimated by Hildebrand and Hansen methods suggest nearly immiscible system (difference in solubility parameters 5.7-6.9 $MPa^{1/2}$). The API release mechanism according to the power law was non-Fickian in all formulations ($0.5<n<1.0$). The release rate of CAF (CAF/Eudragit® L100-55) in pH 7.4 medium was slightly faster than ASP (ASP/Eudragit® L100-55) due its higher aqueous solubility.

The fourth system was classified as polymer nanocomposites as the second system but with a cationic API and an anionic nanoclay. All CAF concentrations in the formulation (10%-30% w/w CAF) exceeded the CEC of MMT (Appendix B). However, the melt mixing of CAF and MMT did not reveal strong interactions as those that occurred in the ASP/HT study. MMT was present in an agglomerated phase in the nanocomposites containing only MMT and all CAF concentrations (10%-30%w/w). The CAF release in the pH 7.4 medium from CAF/MMT/Eudragit® L100-55 was slightly slower compared to CAF/Eudragit® L100-55. Therefore, the agglomeration of MMT did

not significantly retard the release rate of CAF from CAF/MMT/Eudragit® L100-55 as well as the release of ASP from ASP/MMT/Eudragit® L100-55. The API release mechanism was also determined to be non-Fickian. The unchanged morphology of MMT could be due to the low affinity of CAF to MMT since CAF is a weak base (pKa of 14.0).

8.2 Future Studies

8.2.1 Extension of the ASP/HT/Eudragit® L100-55 Hot-Melt Mixing (HMM) System to Hot-Melt Extrusion (HME)

HMM provides information on processing parameters, for example, screw speed, torque, temperature, and residence time which can be used to provide useful data for a transition to an HME operation. For example, the HMM mixing time to reach a steady state of torque and temperature was approximately 120-150 s in all ASP/Eudragit® L100-55 formulations. This information might be used to estimate the minimum residence time for HME in order to ensure that the homogenous mixture (API and polymer in the rubber state) is obtained.

8.2.2 Polymer Nanocomposites with a Combination of Two APIs

ASP/Eudragit® L100-55 and CAF/Eudragit® L100-55 were studied individually. It would be of interest to investigate the combination of ASP and CAF in one polymer blend. ASP/CAF is commercially available in the market as tablets (Anacin®: 400 mg ASP and 32 mg CAF). Limited studies are conducted on a polymer matrix associated with HME/HMM and containing more than one API. Both ASP and CAF are present in crystalline forms in plasticized Eudragit® L100-55. However, the CAF has higher solubility than ASP in pH 7.4, therefore, the dissolution rate between ASP and CAF

might be different even if both API's are released from the polymer matrix in crystalline form. The addition of the nanoclays can also be included in an extended study containing a combination of APIs. The nanoclay should be selected carefully to avoid strong interaction among all components. MMT could be an appropriate candidate due to low ionic exchange capacity and demonstrated success in its processing with HME.

8.2.3 Polymer Nanocomposites Using Polymer without Carboxylic Groups

It is of interest that the carboxylic groups of Eudragit® L100-55 may react with Al and Mg in HT. A future investigation employing identical API and nanoclays i.e., ASP and HT, but a polymer without carboxylic groups such as Eudragit® E100 or Eudragit® E PO could confirm their role on the morphology and properties of the nanocomposites.

APPENDIX A

CALCULATION FOR ANION EXCHANGE CAPACITY (AEC)

AEC is calculated as follows:

Equivalent weight = formula weight divided by the total valence

$$mEq = \frac{\text{mg x valence}}{\text{atomic, molecular or formula weight}}$$

$$mg = \frac{\text{mEq x atomic, molecular or formula weight}}{\text{valence}}$$

$$Equiv\ Weight\ (g) = \frac{\text{atomic, molecular or formula weight}}{\text{valence}}$$

ASP's molecular weight = 180.15 g and has 1 valence at the carboxylic group.

$$ASP\ Equiv\ Weight\ (g) = \frac{180.15}{1}$$

$$ASP\ Equiv\ Weight\ (g) = 180.15\ \text{g}$$

$$ASP\ 1\ mEq\ = \frac{180.15\ \text{g}}{1000}$$

$$ASP\ 1\ mEq\ = 180.15\ \text{mg}$$

The reported AEC of HT is 3.4 mEq/g; 10 g of HT is equal to 34 mEq.

$$\frac{1\ mEq\ of\ ASP}{34\ mEq\ of\ ASP} = \frac{180.15\ \text{mg of ASP}}{x\ \text{mg of ASP}}$$

$$x\ = 6125.1\ \text{mg}$$

Since 34 mEq of ASP is equal to 6125.1 mg or 6.1251 g. Therefore, 10 g of HT can theoretically have an ion exchange with 6.1251g of ASP.

APPENDIX B

CALCULATION FOR CATIONIC EXCHANGE CAPACITY (CEC)

CEC is calculated as follows:

Equivalent weight = formula weight divided by the total valence

$$mEq = \frac{\text{mg x valence}}{\text{atomic, molecular or formula weight}}$$

$$mg = \frac{\text{mEq x atomic, molecular or formula weight}}{\text{valence}}$$

$$Equiv\ Weight\ (g) = \frac{\text{atomic, molecular or formula weight}}{\text{valence}}$$

CAF's molecular weight = 194.2 g and has 1 valence at the tertiary amine of the imidazole ring.

$$CAF\ Equiv\ Weight\ (g) = \frac{194.2}{1}$$

$$CAF\ Equiv\ Weight\ (g) = 194.2\ \text{g}$$

$$CAF\ 1\ mEq\ = \frac{194.2\ \text{g}}{1000}$$

$$CAF\ 1\ mEq\ = 194.2\ \text{mg}$$

The reported CEC of MMT is 0.926 mEq/g; 10 g of MMT is equal to 9.26 mEq.

$$\frac{1\ mEq\ of\ CAF}{9.26\ mEq\ of\ CAF} = \frac{194.2\ \text{mg of CAF}}{x\ \text{mg of CAF}}$$

$$x\ = 1798.3\ \text{mg}$$

Since 9.26 mEq of CAF is equal to 1798.3 mg or 1.7983 g. Therefore, 10 g of MMT can theoretically have an ion exchange with 1.7983 g of CAF.

APPENDIX C

API/NANOCLAY/POLYMER COMPOSITES: ASP/MMT/EUDRAGIT® L100-55

The formulation of ASP with cationic clays, MMT was prepared under similar hot-melt mixing condition (100°C for 5 minutes in the batch mixer). The formulation and characterization information are illustrated in this Appendix.

Table C.1 Sample formulations prepared by hot melt mixing

System	Formulation	Component (%wt)			
		ASP	MMT	TEC	Eudragit® L100-55
API-nanoclay-plasticizer-polymer	10ASP10MMT	10	10	16	64

In Figure C.1, torque gradually decreases suggesting the dissolution of ASP in the molten polymer and no strong interactions between ASP, MMT and Eudragit® L100-55.

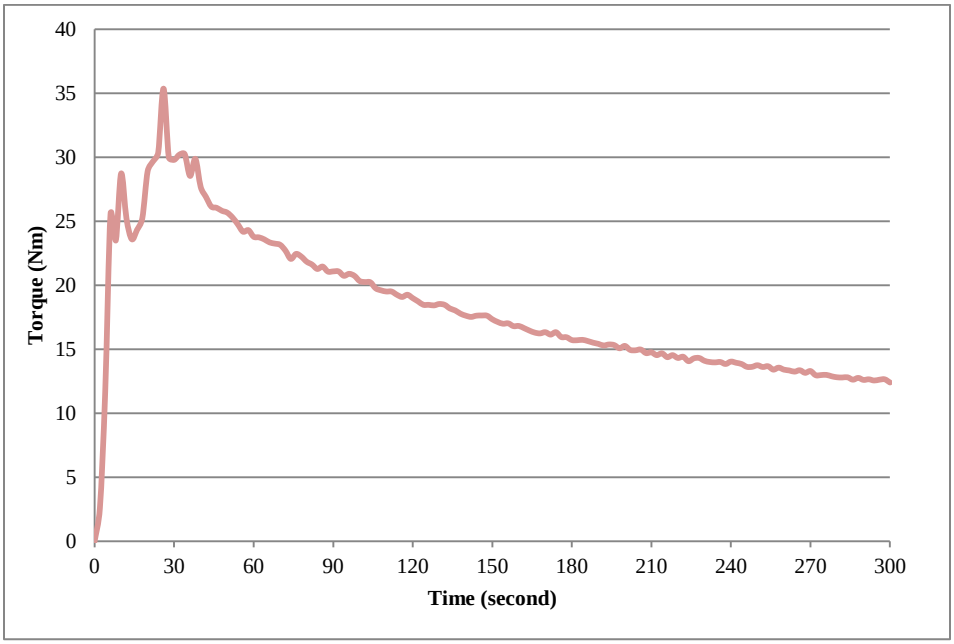

Figure C.1 The evolution of torque of 10ASP10MMT during melt mixing.

Figure C.2 (f) shows the XRD spectra of 10ASP10MMT. The MMT's peak is not shifted to lower angle, indicating no intercalation whereas the crystalline peaks of ASP are also shown at the original 2θ angle. Therefore, MMT is found in the agglomerated phase in the process sample.

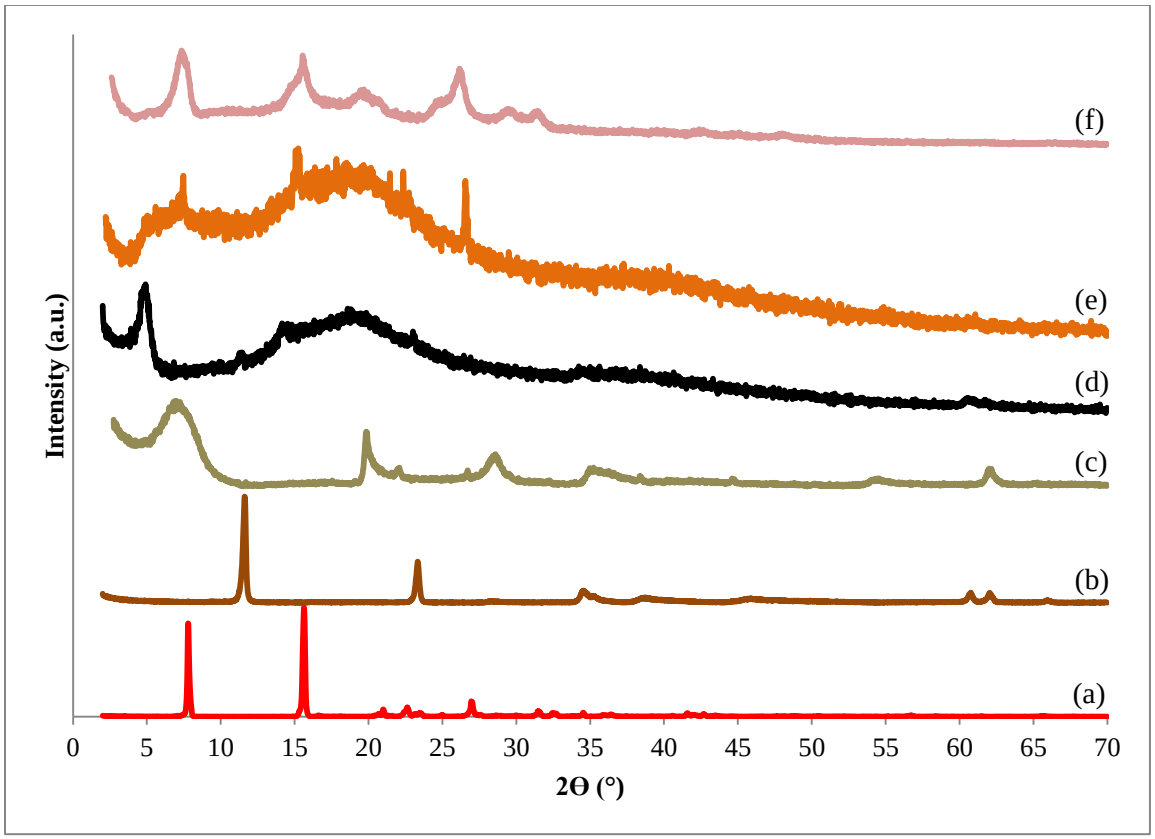

Figure C.2 XRD spectra of (a) ASP, (b) HT, (C) MMT, (d) 10ASP10HT, (e) 30ASP10HT, (f) 10ASP10MMT.

The release rate of ASP from 10ASP10MMT illustrated in Figure C.3 is slightly slower than ASP/Eudragit® L100-55 but still faster than ASP/HT/Eudragit® L100-55. This is due to the agglomeration of MMT which decreases the wettability of the polymer nancomposites. The degree of inhibited release rate caused by agglomeration of the MMT is much less than the impact of HT in the intercalation and exfoliation phases.

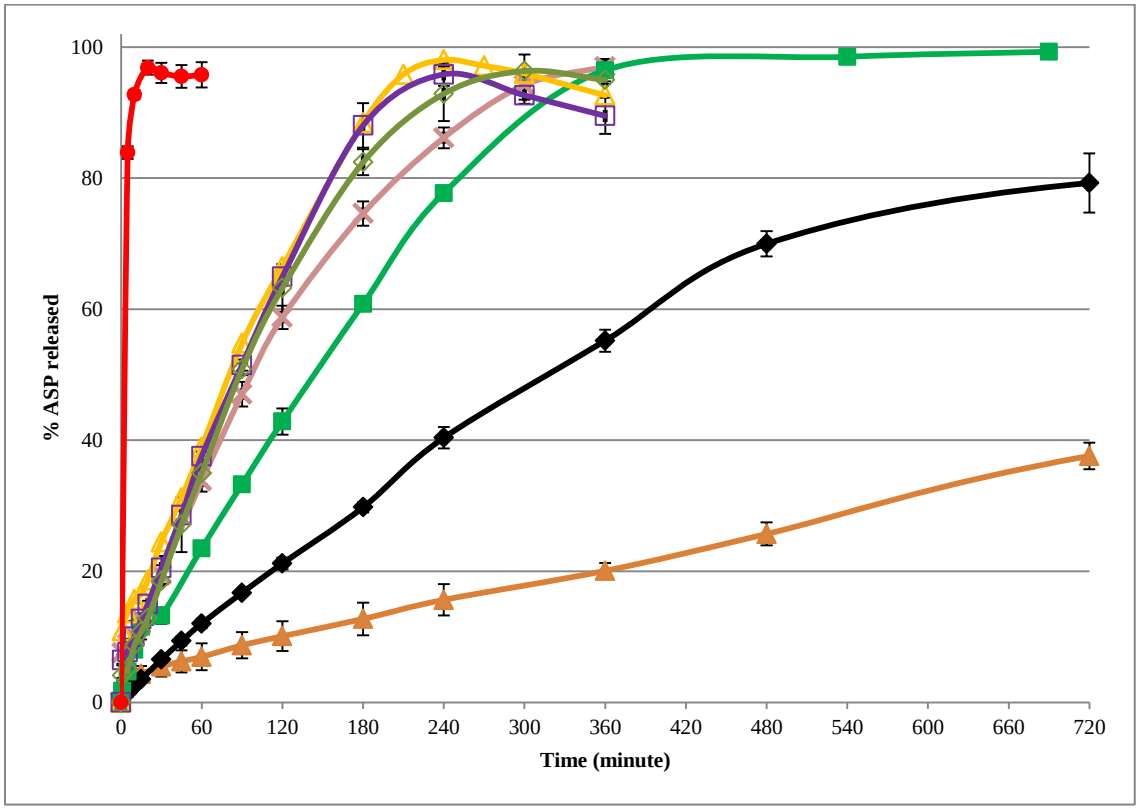

Figure C.3 Immediate-release dissolution profiles (pH 7.4) of (●) ASP, (◊) 10ASP, (□) 20ASP, (△) 30ASP(■) 5ASP10HT, (♦) 10ASP10HT, (▲) 30ASP10HT, (x) 10ASP10MMT

APPENDIX D

THERMAL STABILITY OF API/POLYMER MIXTURES AND API/NANOCLAY/POLYMER COMPOSITES

Figure D.1 shows the TGA results of physical mixtures and processed samples of TEC/EUL, 10ASP and 30ASP. The weight lost between physical mixture and processed samples of 10ASP and 30ASP is not significantly different.

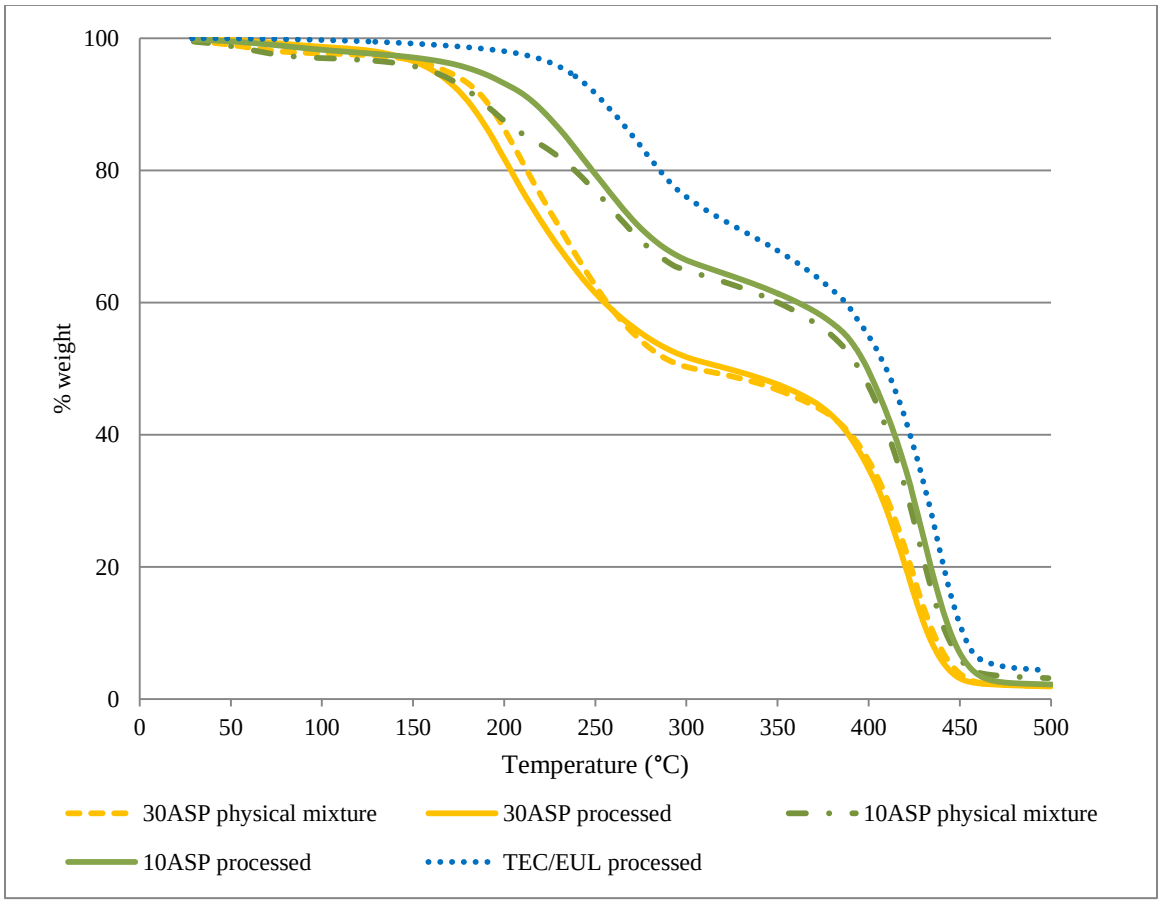

Figure D.1 TGA results of TEC/EUL, 10ASP and 30ASP. Comparison between physical mixture and processed samples.

Figure D.2 illustrates the weight loss of physical mixture and processed samples of 10ASP10HT. The processed 10ASP10HT shows significant improvement of thermal stability compared to the physical mixture. It can imply that there are strong interaction between ASP, HT and Eudragit® L100-55 or improved dispersion of HT which acts as a barrier to the increasing temperature during the test.

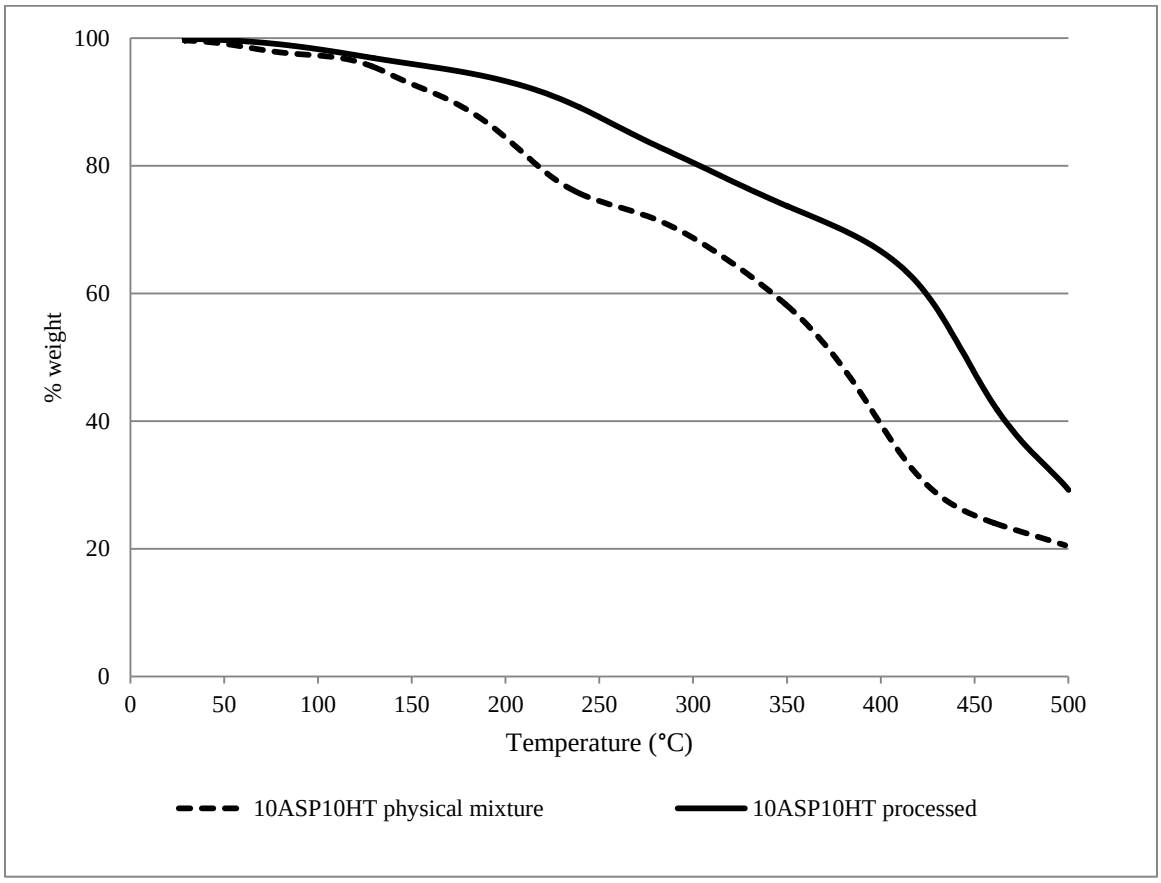

Figure D.2 TGA results of 10ASP10HT.

REFERENCES

Aisawa, S., Takahashi, S., Oggasawara, W., Umetsu, Y., Narita, E., 2001. Direct intercalation of amino acids into layered double hydroxides by coprecipitation. J. Solid State Chem. 162, 52-62.

Ajun, W., Yan, S., Li, G., Huili, L., 2009. Preparation of aspirin and probucol in combination loaded chitosan nanoparticles and in vitro release study. Carbohydr. Polym. 75, 566-574.

Alexandre, M., Dubois, P., 2000. Polymer-layered silicate nanocomposites: preparation, properties and uses of new class of materials. Mater. Sci. Eng., R 28, 1-63.

Allen, L.V., Popovich, N.G., Ansel, H.C., 2011. ANSEL's pharmaceutical dosage forms and drug delivery systems, ninth ed. Lippincott Williams & Wilkins, Philadelphia, PA.

Al-Taani, B.M., Tashtoush, B.M., 2003. Effect of microenvironment pH of swellable and erodable buffered matrices on the release characteristics of diclofenac sodium. AAPS PhamSciTech. 4, 1-6.

Ambrogi, V., Fardella, G. Grandolini, G., Perioli, L., 2001. Intercalation compounds of hydrotalcidte-like aninic clays with anti-inflammatory agents – I. Intercalation and in vitro release of ibuprofen. Int. J. Pharm. 220, 23-32.

Andrews, G.P., Jones, D.S., Diak, O.A., Mccoy, C.P., Watts, A.B., McGinity, J.W., 2008. The manufacture and characterisation of hot-melt extruded enteric tablets. Eur. J. Pharm. Biopharm. 69, 264–273.

Angiolillo, D.J., Guzman, L.A., Bass, T.A., 2008. Current antiplatelet therapies: benefits and limits. Am. Heart J. 156, 3s - 9s.

Arco, M.D., Fernandez, A., Martin, C., Sayalero, M.L., Rives, V., 2008. Solubility and release of fenamates intercalated in layered double hydroxides. Clay Miner. 43, 255-265.

Arco M.D., Martin, F.C., Rives, V., 2007. Intercalation of mefenamic and meclofenamic acid anions in hydrotalcite-like matrixes. Appl. Clay Sci. 36, 133-140.

Ardanuy, M., Velasco, J.I., Antunes, M., Rodriguez-Perez, M.A., De Saja, J.A., 2010. Structure and properties of polypropylene/hydrotalcite nanocomposites. Polym. Compos. 31, 870-878.

Bao, Y-Z., Huang, Z-M., Weng, Z-X., 2006. Preparation and characterization of poly(vinyl chloride)/ layered double hydroxides nanocomposites via in situ suspension polymerization. J. Appl. Polym. Sci. 102, 1471-1477.

Breitenbach, J., 2006. Melt extrusion can bring new benefits to HIV therapy: the example of Kaletra tablets. Am. J. Drug Deliv. 4, 61-64.

Brima, T.S., Hawk, G., Fujii, M., Gallaher, Jr., G.R., Kim, S., Townsend, IV, E.B., 2005. Hydrotalcites, synthesis, and uses. United States Patent: 6,846,870 B2.

Bruce, C., Fegely, K.A., Rajabi-Siahboomi, A.R., McGinity, J.W., 2007. Crystal growth formation in melt extrudates. Int. J. Pharm. 341, 162–172.

Budavari, S., O' Neil, M. J., Smith, A., Heckelman, P. E., Kinneary, J. F., 1996. The Merck Index, twelfth ed. Merck & Co., Inc, Whitehouse Station, NJ.

Bustamante, P, Navarro-Lupion, J, Pena, M.A., Escalera, B., 2011. Hildebrand solubility parameter to predict drug release from hydroxypropyl methycellulose gels. Int. J. Pharm. 414, 125-130.

Carja, G., Chiriac, H., Lupu, N., 2007. New magnetic organic-inorganic composites based on hydrotalcite-like anionic clays for drug delivery. J. Magn. Magn. Mater. 311, 26-30.

Carretero, M.I., Pozo, M., 2009. Clay and non-clay minerals in the pharmaceutical industry Part I. Excipients and medical applications. Appl. Clay Sci. 46, 73-80.

Carretero, M.I., Pozo, M., 2010. Clay and non-clay minerals in the pharmaceutical and cosmetic industres Part II. Active ingredients. Appl. Clay Sci. 47, 171-178.

Cayman Chemical, 2012. Product information: Aspirin (item no. 70260).

Chemical book, 2010. Aspirin aluminum. http://www.chemicalbook.com/ChemicalProductProperty_EN_CB8224497.htm

Cho, J.W., Paul, D.R., 2001. Nylon 6 nanocomposites by melt compounding. Polym. 42, 1083-1094

Choy, J.H., Jung, J.S., Oh, J.M., Park, M., Jeong, J.Y., Kang, Y.K., Han, O.J., 2004. Layered double hydroxide as an efficient drug reservoir for folate derivatives. Biomaterials 25, 3059-3064.

Chung, J. H-Y., Simmons, A., Zeng, Q., Poole-Warren, L.A., 2013. Effects of drug chemistry on the dispersion and release behavior of polyurethane organosilicate nanocomposites. Eur. Polym. J. 49, 652-663.

Clarke, E.G.C., Moffat, A.C., 1986. Clarke's isolation and identification of drugs: In pharmaceuticals, body fluids and post mortem material, second ed. The Pharmaceutical Press, London, UK.

Costa, P., Lobo, J.M.S., 2001. Modeling and comparison of dissolution profiles. Eur. J. Pharm. Sci. 13, 123-133

Costantino, U., Ambrogi, V., Nocchetti, M., Perioli, L., 2008. Hydrotalcite-like compounds: Versatile layered hosts of molecular anions with biological activity. Microporous Mesoporous Mater. 107, 149-160.

Crepaldi, E.L., Tronto, J., Cardoso, L.P., Valim, J.B., 2002. Sorption of terephthalate anions by calcined and uncalcined hydrotalcite-like compounds. Colloids Surf., A: Physicochem. Eng. Aspects 211, 103-114.

Crespo, I., Barriga, C., Rives, V., Ulibarri, M. A., 1997. Intercalation of iron hexacyano complexes in Zn,Al-hydrotalcite. Solid State Ionics 101, 729-735.

Dennis, H.R., Hunter, D.L., Chang, D., Kim, S., White, J.L., Cho, J.W., Paul, D.R., 2001. Effect of melt processing conditions on the extent of exfoliation in organoclay-based nanocomposites. Polym. 42, 9513-9522.

Dhirendra, K., Lewis, S., Udupa, N., Atin, K., 2009. Solid dispersions: A review. Pak. J. Pharm. Sci. 22, 234-246.

Drezdzon, M.A. 1988. Synthesis of isopolymetalate-pillared hydrotalcite via organic-anion-pillared precursors. Inorg. Chem. 27, 4628–4632.

Drits, V.A., Bookin, A.S., 2001. Crystal structure and X-ray identification of layered-double hydroxides, in: Rives, V. (Ed.), Layered Double Hydroxides: Present and Future. Nova Science Publishers, Inc., New York, NY, pp. 41-100.

Durmus, A., Kasgoz, A., Macosko, C.W., 2007. Linear low density polyethylene (LLDPE) / clay nanocomposites. Part I: Structural characterization and quantifying clay dispersion by melt rheology. Polym. 48, 4492 – 4502.

Egawa, H., Maeda, S., Yonemochi, E., Oguchi, T., Yamamoto, K., Nakai, Y., 1992. Solubility parameter and dissolution behavior of cephalexin powders with different crystallinity. Chem. Pharm. Bull. 40, 819-820.

El-Banna, H.M., Daabis, N.A., Abd El-Fattah S., 1978. Aspirin stability in solid dispersion binary systems. J. Pharm. Sci. 67, 1631-1633.

Erum, S., Hassan, F., Hasan, S.M.F., Jabeen, S., 2011. Formulation of aspirin tablets using fewer excipients by direct compression. Pak. J. Pharmacol. 28, 31-37.

Evonik Industries, 2011. Technical information: Eudragit® L100-55.

Fan J., 2011. Study of controlled release of Dapsone from modified montmorillonite and polymer matrices (MS Thesis). New Jersey Institute of Technology, Newark, NJ.

Fischer, H., 2003. Polymer nanocomposites: from fundamental research to specific applications. Mater. Sci. Eng., C 23, 763-772.

Florey, K., 1979. Analytical profiles of drug substance, Vol. 8. Academic Press, New York, NY.

Fornes, T.D., Yoon, P.J., Hunter, D.L., Keskkula, H., Paul, D.R., 2002. Effect of organoclay structure on nylon 6 nanocomposite morphology and properties. Polym. 43, 5915-5933.

Forster, A., Hempenstall, J., Rades, T., 2001. Characterization of glass solutions of poorly water-soluble drugs produced by melt extrusion with hydrophilic amorphous polymers. J. Pharm. Pharmacol. 53, 303-315.

Fukuoka, E., Makita M., Yamamura, S., 1987. Evaluation of crystalline orientation in tablets by X-ray diffraction methods. Chem. Pharm. Bull. 35, 1564-1570.

Giannelis, E.P., Krishnamoorti, R., Manias, E., 1999. Polymer-silica nanocomposites: model systems for confined polymers and polymer brushes. Adv. Polym. Sci. 118, 108-147.

Gopakumar, T.G., Patel, N.S., Xanthos, M., 2006. Effect of nanofillers on the properties of flexible protective polymer coatings. Polym. Compos. 27, 368-380.

Greenhalgh, D.J., Williams, A.C., Timmins, P., York, P., 1999. Solubility parameters as predictors of miscibility in solid dispersions. J. Pharm. Sci. 88, 1182–1190.

Guimaraes, J.L., Marangoni, R., Ramos, L.P., Wypych, F., 2000. Covalent grafting of ethylene glycol into the Zn-Al-CO_3 layered double hydroxide. J. Colloid Interface Sci. 227, 445-451.

Ha, J-U., 2011. Study of controlled release of active pharmaceutical ingredients from functionalized nanoclays and polymer matrices (PhD Dissertation). New Jersey Institute of Technology, Newark, NJ.

Ha, J-U., Xanthos, M., 2011. Drug release characteristic form nanoclay hybrids and their dispersion in organic polymers. Int. J. Pharm. 414, 321-331.

Hansen, C.M., 2007. Hansen solubility parameters: A user's handbook, second ed. CRC Press, Boca Raton, FL.

Hansen, C.M., 2004. Polymer additives and solubility parameters. Prog. Org. Coat. 51, 109-112.

Hernandez-Moreno, M.J., Ulibarri, M.A., Rendon, J.L., Serna, C.J., 1985. IR characteristics of hydrotalcite-like compounds. Phys. Chem. Miner. 12, 34–38.

Hong C., Wen-gong Z., 2010. Fluorescent drug-containing hydrotalcite-like compound for monitoring drug release. Microporous and Mesoporous Materials. doi:10.1016/j.micromeso.2010.10.041.

Huang, N.H., Wang, J.Q., 2009. A new route to prepare nanocomposites based on polyvinyl chloride and MgAl layered intercalated with laurylether phosphate. eXPRESS Polymer Letters 3, 595-604.

Hughey, J.R., Dinunzio, J.C., Bennett, R.C., Brough, C., Miller, D.A., Ma, H., Williams III, R.O., McGinity, J.W., 2010. Dissolution enhancement of a drug exhibiting thermal and acidic decomposition characteristics by fusion processing: a comparative study of hot melt extrusion and kinetisol® dispersing. AAPS PhamSciTech. 11, 760-774.

Huu-Phuoc, N., Nam-Tran, H., Buchmann, M., Kesselring, U.W., 1987. Experimentally optimized determination of the partial and total cohesion parameters of an insoluble polymer (microcrystalline cellulose) by gas solid chromatography. Int. J. Pharm. 34, 217-223.

Huu-Phuoc, N., Luu, R.P.T., Munafo, A., Ruelle, P., Nam-Tran, H., Buchmann, M., Kesslring, U.W., 1986. Determination of partial solubility parameters of lactose by gas-solid chromatograph. J. Pharm. Sci. 75, 68-72.

Jeon, I-Y., Baek, J-B., 2010. Nanocomposites derived from polymers and inorganic nanoparticles. Materials 3, 3654-3674.

Kang, M.R., Lim, H.M., Lee, S.C., Lee, Seung-Ho., Kim, K.J., 2004. Layered double hydroxide and its anion exchange capacity. Advances in Technology of Materials and Materials Processing 6, 218-223.

Kaniwa, N., Ogata, H., Aoyagi, N., Ejima, A., 1981. The bioavailabilities of aspirin from an aspirin aluminum and an aspirin tablets and the effects of food and aluminum hydroxide gel. J. Pharm. Dyn. 4, 860-864.

Kohan, M.I., 1973. Nylon Plastics. John Wiley & Sons, Inc. New York, NY.

Kojima, Y., Usuki, A., Kawasumi, M., Okada, A., Fukushima, Y., Karauchi, T., Kamigaito, O., 1993. Mechanical properties of nylon 6-clay hybrid. J. Mater. Res. 8, 1185-1189.

Kolter, K., Kari, M., Nalawade, S., Rottmann N., 2010. Hot-melt extrusion with BASF Pharma Polymers: Extrusion Compendium. BASF, Ludwigshafen, Germany.

Laskowska, A., Lipinska, M., 2012. Properties of carboxylated nitrile elastomer contained hydrotalcites with varying Mg/Al ratio. J. Eng. Technol. 2, 24-33.

Leeson, L.J., Mattocks, A.M., 1958. Decomposition of aspirin in the solid state. J. Am. Pharm. Assoc. 47, 329-333.

Linares, C.F., Brikgi, M., 2006. Interaction between antimicrobial drugs and antacid based on cancrinite-type zeolite. Microporous Mesoporous Mater. 96, 141-148.

Lipinski, C.A., 2001. Avoiding investment in doomed drugs, is poor solubility an industry wide problem? Curr. Drug Dis. 4, 17-19.

Liu, H., Wang, P., Zhang, X., Shen, F., Gogos, C.G., 2010. Effects of extrusion process parameters on the dissolution behavior of indomethacin in Eudragit® E PO solid dispersions. Int. J. Pharm. 383, 161-169.

Lund, W., 1994. The pharmaceutical CODEX: Principles and practice of pharmaceutics, twelfth ed. The Pharmaceutical Press, London, UK.

Mandal, U.K., 2000. Ionic elastomer based on carboxylated nitrile rubber: infrared spectral analysis. Polym. Intern. 49, 1653-1657.

Manzi-Nshuti, C., Chen, D., Su, S., Wilike, C.A., 2009. The effects of intralayer metal composition of layered double hydroxides on glass transition, dispersion, thermal and fire properties of their PMMA nanocomposites. Thermochim. Acta 495, 63-71.

Marangoni, R., Taviot-Gueho, C., Illaik, A., Wypych, F., Leroux, F., 2008. Organic inorganic dye filler for polymer: blue-coloured layered double hydroxides into polystyrene. J. Colloid Interface Sci. 326, 366-373.

Marchant, D., Jayaraman, K., 2002. Strategies for Optimizing Polypropylene-Clay Nanocomposite Structure. Ind. Eng. Chem. Res. 41, 6402-6408.

Martin, S.T., 2007. Rheology and torque rheometers, in: Ghebre-Sellassie, I., Martin C. (Eds.), Pharmaceutical Extrusion Technology. Informa Healthcare, New York, NY, pp. 135 – 151.

McGinity, J.W., Lach, J.L., 1976. In vitro adsorption of various pharmaceuticals to montmorillonite. J. Pharm. Sci. 65, 896-902.

McLellan, T.M., Kamimori, G.H., Voss, D.M., Bell, D.G., Cole, K.G., Johnson, D., 2005. Caffeine maintains vigilance and improves run times during night operations for special forces. Aviat. Space Environ. Med. 76, 647–654.

Mitaya, S., 1983. Anion-exchange properties of hydrotalcite-like compounds. Clays Clay Miner. 31, 305-311.

Mitra, A.K., Pitkin, C.G., 1960. Production of aluminum acetylsalicylate. United States Patent: 2,959,606.

Nalawade P., Aware, B., Kadam, V.J., Hirlekar, R.S., 2009. Layered double hydroxides: A review. J. Sci. Ind. Res. 68, 267-272

Nogueira, T., Botan, R., Wypych, F., Lona, L., 2012. Synthesis and characterization of LDHs/PMMA nanocomposites: Effect of two different intercalated anions on the mechanical and thermal properties. J. Appl. Polym. Sci. 274, 1764-1770.

Nogueira, T., Botan, R., Wypych, F., Lona, L., 2011. Study of thermal and mechanical properties of PMMA/LDHs nanocomposites obtained by in situ bulk polymerization. Composites Part A 42, 1025-1030.

O'Keefe, J.F., 2004. Identification of polymers by IR spectroscopy. Rubber World 230, 27-32.

Olmsted III, J., 1998. Synthesis of aspirin: A general chemistry experiment. J. Chem. Educ. 75, 1261-1263.

Paradkar, M.M., Irudayaraj, J., 2002. A rapid FTIR spectroscopic method for estimation of caffeine in soft drinks and total methylxanthines in tea and coffee. J. Food Sci. 67, 2507-2511.

Patel, H., Somani, R., Bajaj, H., Jasra, R., 2006. Nanoclays for polymer nanocomposites, paints, inks, greases and cosmetics formulations, drug delivery vehicle and waste water treatment. J. Mater. Sci. 29, 133-145.

Paul, D.R., Robeson, L.M., 2008. Polymer nanotechnology: Nanocomposites. Polym. 49, 3187-3204.

Pavia, D.L., Lampman, G.M., Kriz, G.S., Vyvyan, J.R., 2009. Introduction to Spectroscopy: a guide for students of organic chemistry, forth ed. Brooks/Cole Cengage Learning, Belmont, CA, USA

Peppas, N.A., 1985. Analysis of fickian and non-fickian drug release from polymers. Pharm. Acta Helv. 60, 110-111.

Peppas, N.A., Sahlin, J.J., 1989. A simple equation for the description of solute release III. Coupling of diffusion and relaxation. Int. J. Pharm. 57, 169–172.

Petereit, H-U., Weisbrod, W., 1999. Formulation and process considerations affecting the stability of solid dosage forms formulated with methacrylate copolymers. Eur. J. Pharm. Biopharm. 47, 15-25.

Pradhan, S., Costa, F.R., Wagenknecht, U., Jehnichen, D., Bhowmick, A.K., Heinrich, G., 2008. Elastomer/LDH nanocomposites: Synthesis and studies on nanoparticle dispersion, mechanical properties and interfacial adhesion. Eur. Polym. J. 44, 3122-3132.

PubChem. Magnespirin. http://pubchem.ncbi.nlm.nih.gov/summary/summary.cgi?cid=8591. (accessed in April 2013.

Rasool, B.K.A., Abu-Gharbieh, E. F., Al-Mahdy, J.J., Nessa, F., Ramzi, H.R., 2010. Preparation and characterization of aspirin-chitosan complex: An attempt for its solubility and stability improvement. J. Pharm. Res. 3, 1349-1354.

Rey-Mermet, C., Ruelle, P., Nam-Tran, H., Buchmann, M., Kesselring, U.W., 1991. Significance of partial and total cohesion parameters of pharmaceutical solids determined from solids dissolution calorimetric measurements. Pharm. Res. 8 636-642.

Rives, V., 2001. Layered Double Hydroxides: Present and Future. Nova Science Publishers, Inc., New York, NY.

Rosa, R., Leonelli, C., Villa, C., Priarone, G., 2013. Microwave-assisted melt reaction method for the intercalation of carboxylic acid anions into layered double hydroxides. J. Microwave Power Electromagn. Energy 47, 12-23.

Roy, A.D., Forano, C., Besse, J.P., 2001. Layered double hydroxides: Synthesis and post-synthetsis modification. In: Rives, V. (Ed.), Layered double hydroxides: Present and future. Novel Science Publishers, New York, NY, pp. 1-39.

Ritger, P., Peppas, N., 1987. A simple equation for description of solute release II. Fickian and anomalous release from swellable devices. J. Control. Release 5, 37–42.

Samaha, M.W., Naggar, V.F., 1990. Relationship between the solubility parameter and surface free energy of some solids. Drug Dev. Ind. Pharm. 16, 1135-1151.

Sasol, 2010. Product information: Hydrotalcite – Pural® MG 63 HT. http://www.sasolgermany.de/fileadmin/doc/alumina/PURAL_MG63HT.pdf

Sauer, D., 2008. An investigation of formulation factors and processing parameters for the powder-coating of tablets (dissertation). University of Texas, Austin, TX.

Schilling, S.U., Shah, N.H., Malick, A.W., McGinity J.W., 2010. Properties of melt extruded enteric matrix pellets. Eur. J. Pharm. Biopharm. 74, 352-361.

Sigma-Aldrich, 2013. Product information: Caffeine C0750.

Silva M. de A., E., Melo M. de A., D., De Moura de F.V., M., De Farias R.F., 2004. An investigation about the solid state thermal degradation of acetylsalicylic acid: polymer formation. Thermochim. Acta 414, 101–104.

Skalsky, B., Petereit, H-U., 2008. Chemistry and application properties of polymethacrylate systems, in: McGinity, J.W., Felton, L.A. (Eds.), Aqueous Polymeric Coating for Pharmaceutical Dosage Forms. Informa Healthcare, New York, NY, pp. 237-277.

Socrates, G., 2001. Infrared and raman characteristic group frequencies: Tables and charts, third ed. John Wiley & Sons, Ltd., West Sussex, England.

Tan, D., Zhao, B., Moochhala, S., Yang,Y-Y., 2006. Sustained-release of caffeine from a polymeric tablet matrix: An in vitro and pharmacokinetic study. Mater. Sci. Eng., B 132, 143-146.

Tantishaiyakul, V., Worakul, N., Wongpoowarak, W., 2006. Prediction of solubility parameters using partial least square regression. Int. J. Pharm. 325, 8-14.

Terife, G., Wang, P., Faridi, N., Gogos, C.G., 2012. Hot melt mixing and foaming of Soluplus® and indomethacin. Polym. Eng. Sci. 52, 1629-1639.

Toraishi, T., Nagasaki, S., Tanaka, S., 2002. Uptake mechanism of IO_3^- to NO_3^- hydrotalcite. Radiochim.Acta 90, 671-675.

Troy, D.B., 2006. Remington: The science and practice of pharmacy, twenty-first ed. Lippincott Williams & Wilkins, Philadelphia, PA.

Tunney, J.J., Detellier, C., 1994. Preparation and characterization of two distinct ethylene glycol derivatives of kaolinite. Clays Clay Miner. 42, 552-560.

Turk, M., Lietzow R., 2008. Formation and stabilization of submicron particles via rapid expansion process. J. Supercrit. Fluids 45, 346-355.

Usuki, A., Kojima, Y., Kawasumi, M., Okada, A., Fukushima, Y., Kuauchi, T., Kamigaito, O., 1993. Synthesis of nylon 6-clay hybrid. J. Mater. Res. 8, 1179-1993.

Wai, K.N., DeKay, H.G., Banker, G.S., 1966. Applications of the monmorillonites in tablet making. J. Pharm. Sci. 55, 1244-1248.

Wang, G., Wang, C., Chen, C., 2006. The disorderly exfoliated LDHs/PMMA nanocomposites synthesized by in situ bulk polymerization: the effects of LDH-U on thermal and mechanical properties. Polym. Degrad. Stab. 91, 2443-2450.

Xanthos, M., 2010. Functional fillers for plastics, second ed. Wiley-VCH, Weinheim, Germany.

Xu, A.S., Macdonald, J.M., Labotka, R.J., London, R.E., 1999. NMR study of the sites of human hemoglobin acetylated by aspirin. Biochim. Biophys. Acta 1432, 333-349.

Yang, M., Wang, P., Huang, C.-Y., Ku, M.S., Liu, H., Gogos, C., 2011. Solid dispersion of acetaminophen and poly(ethylene oxide) prepared by hot-melt mixing. Int. J. Pharm. 395, 53–61.

Yap, S.F., Adams, M.J., Seville, J.P.K., Zhang, Z., 2008. Single and bulk compression of pharmaceutical excipients: Evaluation of mechanical properties. Power Technol. 185, 1-10.

Zhao, H., Chen, Bl, Lin, Y., Chen, J., Fan, J. Peng, X-F., 2012. The effect of nanoclay on the rheological property and melt strength of polypropylene/polyamide-6 blend. ANTEC, 2012 (Orlando, FL).

Zhao, J., 2003. Rheological characterization of polystyrene–clay nanocomposites as the relate to the degree of exfoliation and dispersion. ANTEC, 2003 (Chicago, IL).

Zhao, J., Alexander, B.M., Harris, J.D., 2005. Rheological characterization of polystyrene–clay nanocomposites to compare the degree of exfoliation and dispersion. Polym. 45, 8641-8660.